Investigations of the Long Term Catalytic Activity and Stability of Zeolite-based Catalysts in the Conversion of Methanol-to-Hydrocarbons.

Dissertation for the degree of Philosophiae Doctor

Daniel Rojo Gama

DEPARTMENT OF CHEMISTRY

Faculty of Mathematics and Natural Sciences

UNIVERSITY OF OSLO

May 2017

© Daniel Rojo Gama, 2017

Series of dissertations submitted to the
Faculty of Mathematics and Natural Sciences, University of Oslo
No. 1888

ISSN 1501-7710

All rights reserved. No part of this publication may be
reproduced or transmitted, in any form or by any means, without permission.

Cover: Hanne Baadsgaard Utigard.
Print production: Reprosentralen, University of Oslo.

Preface

This Thesis is submitted in candidacy for the PhD degree from the Faculty of Mathematics and Natural Sciences, University of Oslo (UiO). The work presented in this Thesis has been carried out mainly at the Department of Chemistry (UiO) and at Haldor Topsøe A/S from August 2014 to May 2017 with the economic support of The European Research Council under the European Industrial Doctorate (EID) - Marie Curie Actions: "ZeoMorph" Project.

Professor Stian Svelle (UiO) has been my principal supervisor. Further supervision from the University of Oslo has been provided by Professor Unni Olsbye. Dr. Pablo Beato has been my main supervisor at Haldor Topsøe A/S, the industrial partner of the project.

The work performed during these three years of research has been focused on the investigation of the long-term catalytic activity and stability on different zeolite-based catalysts during the conversion of methanol-to-hydrocarbons. In addition to the present Thesis, the manuscripts published in international journals are included as appendices.

Among all the popular proverbs that are found in Spanish language, my favorite one can be translated as "Gratitude is the sign of noble souls". Therefore, I would like to take this opportunity to express my sincere gratitude to all the people who have contributed in the completion of my PhD. Firstly; I am grateful to Professor Stian Svelle, Professor Unni Olsbye and Dr. Pablo Beato for having given me the opportunity to work with you for the last three years.

Professor Stian Svelle is greatly acknowledged for the close guidance, everlasting patience, stimulating discussions and good collaboration during the course of this work. I would like to thank to Dr. Pablo Beato for the fruitful scientific discussions we had during my period at Haldor Topsøe. Professor Unni Olsbye is acknowledged for having shared with me her inspiration, knowledge and commitment to science.

I am deeply grateful to all the colleagues at Catalysis Group because you have contributed to make a very pleasant working environment. Special thanks go to my colleagues in the "ZeoMorph" project: Juan, Kasia, Andrea and Malte. It has been a pleasure to have inspiring scientific discussions with you over the last three years. I would also like to thank to Pablo

del Campo and Irene Pinilla for the training sessions you provided me at the beginning of my PhD. I really appreciate the time you two and Michael spent in reading the preliminary versions of this Thesis and the valuable feedback you gave. I am also grateful to Peter and Renato, colleagues at Haldor Topsøe, for contributing to the nice atmosphere we had there.

I would like to thank Francesca Bonino and Silvia Bordiga for the guidance and support you gave me while my stay in Turin. Special thanks go to Matteo Signorile for the help with the UV-Raman measurements, even when you were finishing your Thesis.

Dimitri, Lars, David and Georgios, or in other words, the ESRF team are thanked for the enjoyable days, and nights, of hard work we had in our visit to the Synchrotron in Grenoble, which made that experience unique and extremely valuable.

I am deeply grateful to my parents and sister for their daily encouragement and support, despite being some thousands of kilometers away. A substantial piece of this work belongs to you because you have taught me to work hard and to pursue the goal without giving up.

Finally, I want to profoundly thank my girlfriend, Irene. She has been my main support during these three years. You have walked with me hand-by-hand this journey, which has not always been the most pleasant path to walk. I am extremely grateful for your support during these years giving me the strength and determination to complete the PhD. Thank you very much for letting me leaning on you and for having helped me to grow as scientist and as human being.

List of abbreviations

MTH	Methanol-to-Hydrocarbons
E_a	Activation Energy
IUPAC	International Union of Pure and Applied Chemistry
IZA	International Zeolite Association
SDA	Structure Directing Agents
EFAL	Extra-Framework Aluminium Species
FCC	Fluid Catalytic Cracking
MTG	Methanol-to-Gasoline
Bpd	Barrel-per-Day
DME	Dimethyl ether
TIGAS	Topsøe Integrated Gasoline Synthesis
MTO	Methanol-to-Olefins
MTP	Methanol-to-Propene
MOGD	Mobil-Olefin-to-Gasoline-and-Distillate
HCP	Hydrocarbon Pool
MAS-NMR	Magnetic Angle Spinning Nuclear Magnetic Resonance
PMB	Polymethylbenzene
PFR	Plug Flow Reactor
CSTR	Continuous Stirred-Tank Reactor
TGA	Thermogravimetric Analysis
FTIR	Fourier Transformed Infrared Spectroscopy
UV-Vis	Ultraviolet-Visible
NMR	Nuclear Magnetic Resonance
EPR	Electron Paramagnetic Resonance
XRD	X-Ray Diffraction
LDI-TOF-MS	Laser Desorption Ionization-Time of Flight-Mass Spectrometry
TEOM	Tapered Element Oscillating Microbalance

W/F	Contact time
τ_0	Applied contact time
τ_{crit}	Critical contact time
$t_{1/2}$	Time to reach 50% MeOH conversion
MP-AES	Microwave Plasma Atomic Emission Spectrometry
SEM	Scanning Electron Microscopy
EDS	Energy Dispersive Spectroscopy
BET	Brunauer–Emmett–Teller
MCT	Mercury Cadmium Telluride
BAS	Brønsted Acid Sites
LAS	Lewis Acid Sites
a.u.	Arbitrary Units
IMEC	Integrated Molar Extinction Coefficient
CCD	Charge-Coupled Device
GC-MS	Gas Chromatography-Mass Spectrometry
GC	Gas Chromatography
WHSV	Weight Hourly Space Velocity
TOS	Time-on-Stream
FID	Flame Ionization Detector
PFD	Process Flow Diagram
HXRD	High Energy X-Ray Diffraction
O.D.	Outer Diameter
I.D.	Inner Diameter
ESRF	European Synchrotron Radiation Facility
HTI	Hydrogen Transfer Index
TOF	Turnover Frequency
TPD	Temperature Programmed Desorption
TPO	Temperature Programmed Oxidation

Table of contents

List of publications

Paper I: *Structure-deactivation relationships in zeolites during the methanol-to-hydrocarbons reaction: quantitative assessments of the coke content*. Daniel Rojo-Gama, Matteo Signorile, Francesca Bonino, Silvia Bordiga, Unni Olsbye, Karl Peter Lillerud, Pablo Beato, Stian Svelle. *Journal of Catalysis* ***2017****, 351, 33-48*

Paper II: *Time- and space-resolved study of the Methanol to Hydrocarbons (MTH) reaction - influence of zeolite topology on axial deactivation patterns.* Daniel Rojo-Gama, Samaneh Etemadi, Eliot Kirby, Karl Petter Lillerud, Pablo Beato, Stian Svelle, Unni Olsbye. *Faraday Discuss.*, ***2017****, 197, 421–446*

Paper III: *Influence of the crystal morphology of ZSM-5 on the conversion of Methanol-to-Hydrocarbons reaction at industrial relevant conditions.* Daniel Rojo-Gama, Unni Olsbye, Karl Petter Lillerud, Pablo Beato Stian Svelle. (In preparation)

Paper IV: *A straightforward descriptor for the deactivation of zeolite catalyst H-ZSM-5.* Daniel Rojo-Gama, Malte Nielsen, David Wragg, Hanne Falsig, Lars F. Lundegaard, Pablo Beato, Rasmus Yding Brogaard, Karl Petter Lillerud, Unni Olsbye, Stian Svelle. (Submitted)

Author's contribution

Paper I: The author characterized fresh and partially deactivated samples, with the exception of the UV-Raman experiments. The author performed all the catalytic tests and he contributed in the planning of the experiments, interpretation of the results and preparation of the manuscript.

Paper II: The author characterized the samples and performed approximately two thirds of the catalytic experiments. Further contribution by the author was done by planning the experiments, interpretation of the results and preparation of the manuscript.

Paper III: The author performed the basic characterization of the materials, the catalytic tests and characterization of the deactivated samples. Author also was involved in the preparation of the manuscript.

Paper IV: The author carried out the experimental part of the work (i.e, characterization of the samples, catalytic reactions, and post-reaction characterization). The author further contributed to the analysis and interpretation of the results, and preparation of the manuscript.

Related papers not included in this Thesis

- *Conversion of methanol to hydrocarbons over zeolite ZSM-23: Exceptional effects of particle size on catalyst lifetime*. A. Molino, K.A. Lukaszuk, Daniel Rojo-Gama, K.P. Lillerud, U. Olsbye, S, Bordiga, S. Svelle, P. Beato. (*ChemComm DOI: 10.1039/C6CC10118F*).

- *Zeolite morphology and catalyst performance: Conversion of Methanol to Hydrocarbons over Offretite*. K.A. Lukaszuk, D. Rojo-Gama, Sigurd Øien-Ødegaard, Gloria Berlier, Silvia Bordiga, Karl Petter Lillerud, Unni Olsbye, Pablo Beato, Lars Fahl Lundegaard, Stian Svelle. (Submitted to *Catalysis Science and Technology*).

- *Fossil Fuels: The Effect of Zeolite Catalyst Particle Morphology on Catalyst Performance in the Conversion of Methanol to Hydrocarbons.* Katarzyna Anna Łukaszuk, Pablo del Campo Huertas, Andrea Molino, Malte Nielsen, Daniel Rojo-Gama, Juan Salvador Martinez-Espin, Karl Petter Lillerud, Unni Olsbye, Silvia Bordiga, Pablo Beato and Stian Svelle. In book: Nanotechnology for Energy Sustainability, Chapter: Chapter 1, Publisher: Wiley-WCH, *DOI: 10.1002/9783527696109.ch1*

Conference contributions

I. *Quantitative studies on zeolite deactivation by coke in the methanol-to-hydrocarbon process.* D. Rojo-Gama, P. Beato, K.P. Lillerud, U. Olsbye, S. Svelle. 15th Norwegian Catalysis Symposium, Bergen, Norway, 2015/12/03-05 (**Oral presentation**)

II. *Zeolite deactivation by coking in the Methanol to Hydrocarbons process.* D. Rojo-Gama, M. Signorile, F. Bonino, S. Bordiga, U. Olsbye, K.P. Lillerud P. Beato, S. Svelle. 11th Natural Gas Conversion Symposium, Tromsø, Norway, 2016/06/05-09 (**Poster presentation**).

III. *Spatiotemporal study on the deactivation of zeolites by coking in the Methanol to Hydrocarbon Process.* D. Rojo-Gama, S. Svelle, P. Beato, K.P. Lillerud, U. Olsbye. 17th Nordic Symposium on Catalysis, Lund, Sweden, 2016/06/14-16 (**Poster presentation**).

Patent application

1. *New ZSM-23 catalyst for the Conversion of Oxygenates to Olefins with improved resistance towards deactivation.* A. Molino, K.A. Lukaszuk, D. Rojo-Gama, S. Svelle, P. Beato. *Danish Patent Office*. Reference number 00578 DK, Copenhagen, Denmark, 2016/09/30

1. Introduction

The first chapter introduces the topics and materials relevant for this Thesis. Firstly, catalysis is briefly described. Secondly, an overview of zeolites with special attention to their structure and properties as acid catalysts is provided. Finally, in the last part of this section, the structures of the zeolites used in this work are described and the motivation and scope of the thesis is presented.

1.1. Catalysis

Chemical industries are nowadays challenged not only by the continuous increase in global population, which has to be supplied with the demands required, but also by the limited availability of natural resources. In this line, the primary goals of chemical industries are the production of high quality products at a low cost while minimizing the environmental side-effects. Thus, efficiency is a key parameter to maximize in chemical processes.

Catalysis is a field that has substantially improved the efficiency of chemical processes and that has helped chemical industries to supply high quality products at reasonable costs with a limited amount of natural resources. The importance of catalysis is such, that currently, approximately 85-90 % of all petro-chemical products are obtained via catalytic processes [1]. It is therefore reasonable that since the mid-19th century, when the first studies of catalysis were reported [2], a great effort has been made in this field to understand and improve the catalytic processes with the ultimate goal of designing catalysts that provide very high selectivity to the desired products with minimum by-product formation.

The transformation of certain reactants to specific products under a chemical reaction requires that reactants overcome an energy barrier. Catalysts are substances that without being consumed accelerate the kinetics of a chemical reaction by decreasing the energy barrier, called Activation Energy (E_a). It is worth highlighting that catalysts change neither the thermodynamics nor the equilibrium concentration of the chemical species at any time during the reaction. In other words, the energy difference between reactants and products is kept constant. However, catalysts lead the reaction through a less energetically-demanding path. Figure 1.1 shows the potential energy diagrams of a catalyzed and of a non-catalyzed

reaction. As observed in Figure 1.1, the catalyzed reaction, represented by the dashed line, proceeds at a much lower energy barrier [1].

Despite the fact that the reaction path of the non-catalyzed reaction is less complex than that of the catalyzed, the latter results in a significant decrease in activation energies. For a catalytic reaction to happen, three consecutive steps have to take place. First, reactants are to adsorb and stabilize on the catalysts' surface. Second, reactants are transformed into products on the surface of the catalysts. Finally, products have to desorb from the surface. In a catalyzed reaction the number of collisions between molecules and the probability of a favorable orientation for the reaction to occur increase, which provide a lower energy barrier. As a consequence, the catalytic reaction is more favorable to happen.

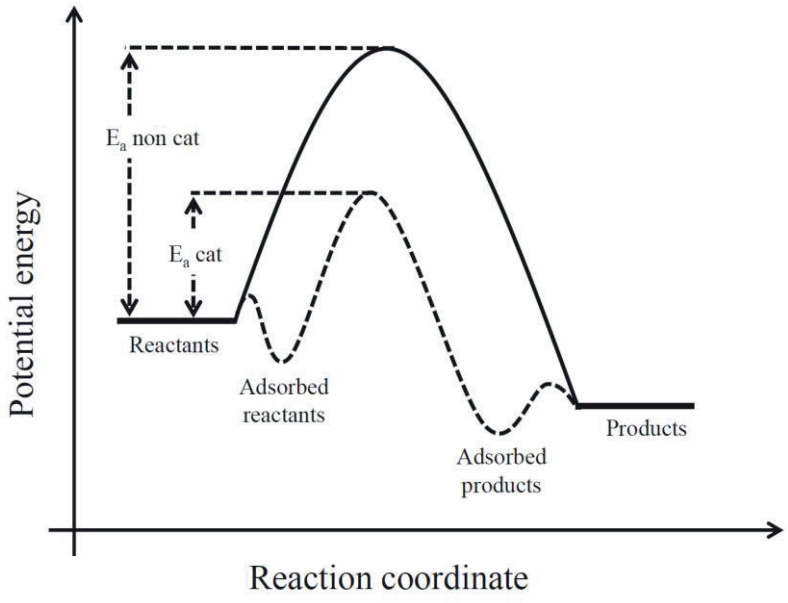

Figure 1.1 Potential energy diagram of a non-catalyzed (solid line) and of an heterogeneous catalyzed reaction (dashed line). Adapted from [1].

Depending on the nature and phase of the catalyst, the field of catalysis can be sub-categorized into three different groups: homogenous, heterogeneous and bio-catalysis. Bio-catalysis takes place in biological processes and it implies the use of natural catalysts such as enzymes. In homogeneous catalysis, reactants, products and catalysts are in the same phase, usually in liquid. This fact makes homogeneous catalysis more limited due to the need of additional separation and purification steps. In contrast, in heterogeneous catalysis, catalysts

are in a different phase than that of the reactants and products. Commonly, reactants and products are gases or liquids whereas the catalyst is in solid phase.

The work presented in this Thesis deals entirely with heterogeneous catalysis. Particularly the conversion of methanol-to-hydrocarbons has been chosen as the target reaction to study, which is catalyzed by zeolites, a special type of acid solid catalysts.

1.2. Zeolites: Structure and properties

Zeolites are a very attractive class of materials owing to their high surface to volume ratio and high thermal stability [3]. Zeolites are microporous crystalline aluminosilicates that belong to the class of tectosilicates, meaning that they are built from tetrahedral TO_4 units, where T can either be Si or Al. These primary tetrahedral units are arranged into a three-dimensional structure by sharing the oxygen corner atoms in the TO_4 units, resulting in a framework with nanometer-sized channels and cages (Figure 1.2) that provide them with high porosity and a large surface area [4].

Porous materials are classified according to their pore size in three different categories. It is possible to distinguish between microporous, mesoporous and macroporous materials when the pore dimensions are smaller than 20 Å, between 20 and 500 Å and larger than 500 Å, respectively. Since the dimensions of zeolite channels, cages and intersections generally do not exceed 20 Å, The International Association of Pure and Applied Chemistry (IUPAC) classify zeolites as microporous materials [5].

The chemical formula of zeolites is determined by the composition of the unit cell. Typically, the empirical formula of a zeolite in the as-synthesized form is as follows: $[xM_{2/n}O{\cdot}xAl_2O_3{\cdot}ySiO_2{\cdot}wH_2O]$ [6]. *M* corresponds either to the cation with valence *n* of a chemical element which belongs to the group IA or IIA, or to an organic cation; *(x + y)* is the number of tetrahedrons per unit cell, and *w* refers to the number of moles of water contained in the zeolite voids.

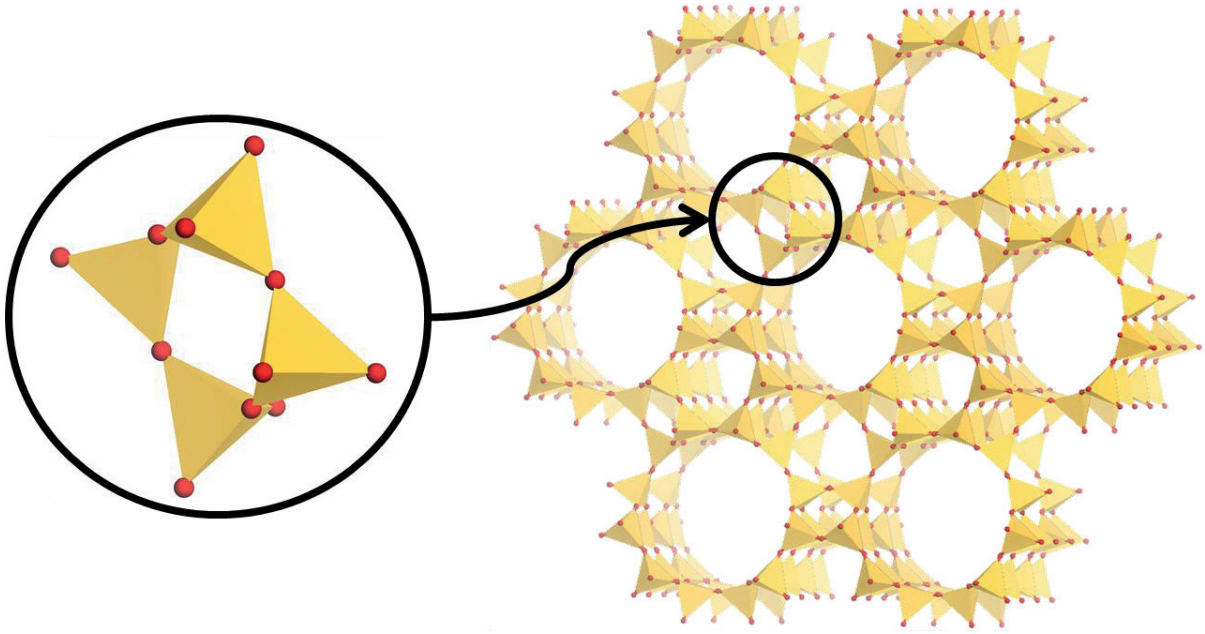

Figure 1.2. Representation of a zeolite structure where the tetrahedral building units are linked by oxygen corner sharing giving rise to a three dimensional framework.

Zeolites normally follow the Löwenstein´s rule, which establishes that two Al atoms cannot share the same O atom. This limitation implies that the Si/Al ratio in the zeolite cannot be lower than one, meaning that most of T atoms in the structure are silicon. As a consequence, zeolites can be referred as silicates with a number of silicon atoms substituted by aluminium atoms. The increase in the number of Al atoms relative to the Si T-atoms in a zeolite also influences the hydrophobicity of the material, being zeolites with low Si/Al ratios, i.e. high amount of Al, strongly hydrophilic [7].

The discovery of zeolites happened in 1756 by the Swedish scientist Axel Fredrik Cronstedt. He named this mineral as "zeolite" according to the Greek terms "*zein*" and "*lithos*", which mean boiling stone, because the newly discovered material released steam and water upon heating [3, 8]. After the discovery of the material, the scientific interest in zeolites was sparse for 200 years [9]. However, the synthesis of zeolites using low-temperature methods, reported by Barrer and Milton during the 1940s' and 50s' [10-13] was a key step to increase the interest in zeolites owing to the easiness of the synthesis procedure. This made accessible a type of material with powerful features such as catalytic, ion exchange, adsorption and molecular sieving properties [14, 15]. Such combination of properties has made zeolites a very relevant type of materials for industrial and commercial applications

within catalysis, ion-exchange and sorption processes. As a result, several million tons of zeolites are consumed on an annual basis [10, 16].

Nowadays, more than 230 different types of zeolites, with different topologies (channels and cavities dimensions and interconnections), are registered in the database of The International Zeolite Association (IZA) [17]. Among such a large number of reported zeolites, approximately one fifth of them can be found in nature and the rest are synthetically made in laboratories. Additionally, theoretical studies show that there are millions of possibilities to build up these type of structures, but only up to 450000 are likely to be stable considering the lattice energies [18]. New frameworks are continuously being discovered; however, some of the new zeolite structures require sophisticated synthesis conditions to crystalize and expensive Structure Directing Agents (SDA), which may prevent them from being industrially applied.

The pore size of a zeolite can be described by the number of T-atoms that form the entrance (ring-size) to the interior of the crystal. According to this classification, zeolites are traditionally classified into small, medium and large pore structures having 8, 10, 12 T-atoms, respectively [18]. In recent years, materials containing pores with 14 or more T-atoms, which are described as ultra-large pore size zeolites, have also been discovered [18-20].
Zeolites can be further classified attending to the dimensions in which their pores are distributed. Channels may be uniform or non-uniform and they may intersect with other channels. Thus, zeolites can have one-dimensional pore system, such as ZSM-12 (MTW) and ZSM-22 (TON), two-dimensional pore structures, like in MCM-22 (MWW), or a three-dimensional pore system, as it is the case of ZSM-5 (MFI) or zeolite-Y (FAU). Some examples of how TO_4 tetrahedra can assemble to generate structures with different pore sizes and geometries are shown in Figure 1.3

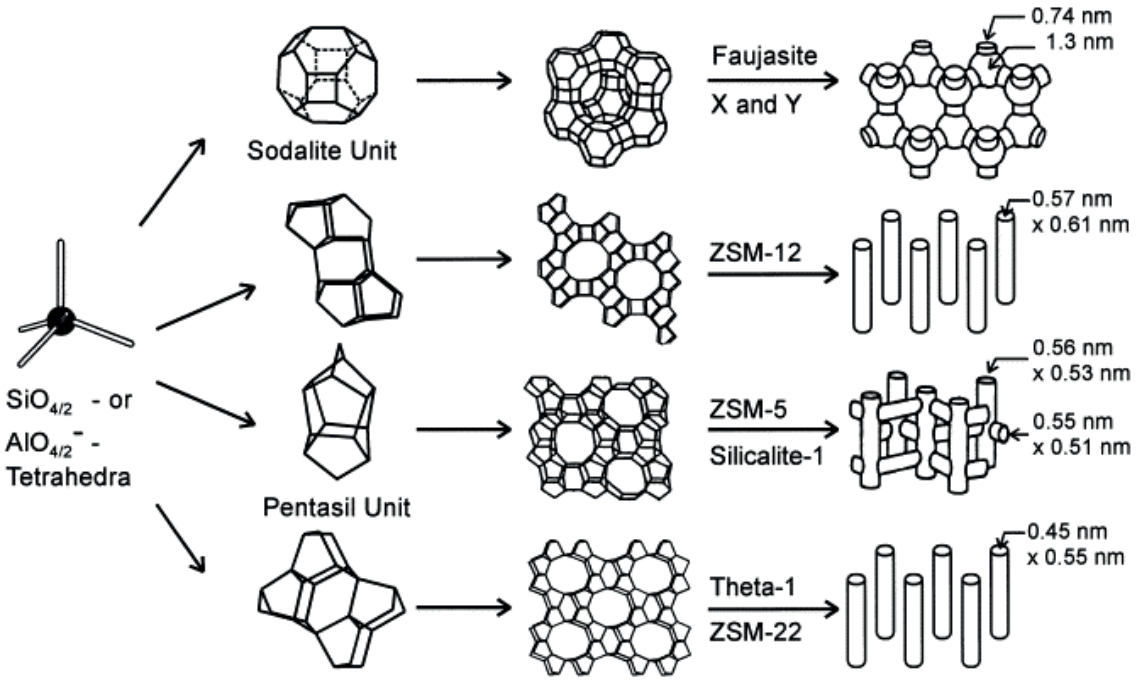

Figure 1.3. Example of how TO4 tetrahedra can assemble in different ways generating four different structures. Adapted from [11].

Generally speaking, zeolites contain silicon, aluminium and oxygen atoms. However, it is also possible to synthesize materials with similar structures to zeolites, but with different chemical composition. These materials are regarded as zeotypes and display slight different properties than zeolites. In the case of AlPO materials, the T positions of the tetrahedra are occupied by Al or P. Besides, other elements such as Be, Ga, B, Ti, Co, Mn, etc can be introduced in the framework by iso-morphous substitution [21-26]. The elements introduced in the structure need to have a tetrahedral TO_4 configuration and a suitable size to be isomorphically replaced [25]. The silicoaluminophosphate (SAPO), formed by the incorporation of Si in an AlPO framework, is the most common zeotype used in industrial applications, and thus, this material has been extensively investigated during the last decades [27].

1.3. Zeolite as acid catalysts

Silicate materials, those which only contain SiO_4 tetrahedra in their structure, are highly hydrophobic, electrically neutral and do not work as active catalysts because its surface is homopolar, with no active sites (i.e. specific locations on the surface of the catalyst where the chemical reaction takes place) able to donate or attract protons and/or electrons during the chemical reaction. In order for a zeolite to be catalytically active, it must have active sites, which are created when a Si atom is isomorphically substituted by an Al atom in the zeolite framework. Such exchange generates a negative charge in the lattice that must be balanced to assure electron neutrality in the system. As previously highlighted, zeolites are excellent materials for ion-exchange applications. Thus, in the case of natural zeolites, the cations balancing the charge in the structure are typically alkali or earth alkali metal ions such as K^+, Na^+, Ca^{2+} or Mg^{2+}. These ions, however, do not provide zeolites with the sufficient acidity to use them as acid catalysts.

The negative charge can also be balanced by protons, which are bound to the O atom connected to Si and Al neighbor atoms forming a bridged hydroxyl group, more commonly referred as bridging Brønsted acid site (-Si (OH)Al-) [28] (Figure 1.4). The Brønsted acid sites confer zeolites with sufficient acid strength and are the responsible of the catalytic properties exhibited by zeolites.

By definition, a Brønsted acid site works both as a proton donor and as an active center in acid catalyzed reactions. However, it is important to bear in mind that, among various parameters, the strength of the acid sites is dependent on the topology of the material as well as the framework composition [29]. The total acid site density increases concomitantly with the number of Al atoms located in the zeolite framework, which give rise to Brønsted acidity. On an ideal zeolite, the acid site density is equal to the number of substituted framework atoms (with respect to an electronically neutral material). It is customary to report the molar ratio between silicon and aluminium (Si/Al) or their corresponding oxides (SiO_2/Al_2O_3), being this value inversely proportional to the acid site density of the material.

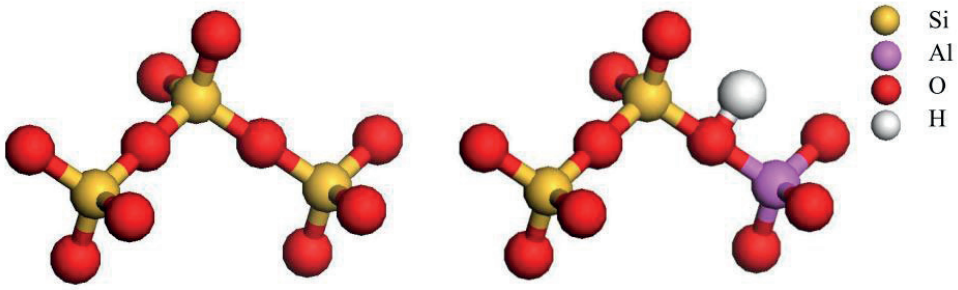

Figure 1.4. Example showing the formation of a Brønsted acid site. Left) Three $[SiO_4]^{4-}$ tetrahedral connected through oxygen bridge. Right) One $[SiO_4]^{4-}$ tetrahedron is replaced by a $[AlO_4]^{5-}$ and the negative charge is compensated by a proton.

In addition to the framework Al species, some Al atoms can also be located on extra-framework positions i.e. extra-framework aluminium species (EFAL). The nature of these EFAL species remains unclear, and different authors have identified EFAL species as Al^{3+}, AlO^{+}, $[Al(OH)]^{2+}$ or $[Al(OH)_2]^{+}$ cations [29-33]. Moreover, it is reported that EFAL species are formed upon post-synthetic treatments or during zeolite activation [30]. When EFAL species are in the form of Al^{3+}, they display a high Lewis acid character, i.e. they can accept a pair of electrons from the reaction substrate. Such Lewis sites, which can also be introduced by ion-exchange with polyvalent cations [16], may affect the total acid strength when interacting with surrounding Brønsted sites, eventually influencing the catalytic properties of the zeolites [34, 35].

When zeolites are used as solid catalysts, they display the advantage of straightforward separation from the reactants and/or products, which is inherent to heterogeneous catalyzed processes. However, two additional properties of zeolites set the difference from other (amorphous) solid acid catalysts: well-defined active sites and shape selectivity. The former has been discussed on previous paragraphs, whereas the latter is introduced at this point.

The pore sizes of the zeolites are in the range of the molecular diameters of organic compounds and only molecules possessing smaller free-diameter than the zeolite pores can get access to the interior of the zeolite crystals. Owing to the ability to sort molecules depending on the size, zeolites are often regarded as molecular sieves [3]. By engineering selectively the zeolite framework and thus, the pore size, the zeolite structure sorts out molecules attending to their size, allowing only certain molecules to enter the pores, to get

out of the pore and to form certain reaction intermediates inside the pores, thereby affecting the product selectivity.

The shape selectivity concept was firstly described by Weisz and Frilette during the 1960s' [36] as follows, "the chemical transformation of molecules solely depends on the space offered by the zeolite" [4]. It is described based on mass transfer limitations and it is possible to distinguish three different types of shape selectivity:

a) **Reactant shape selectivity** is depicted in Figure 1.5 a). This phenomenon takes place when molecules bigger than the zeolite pore openings are prevented from reaching the active sites in the zeolite crystal [37, 38]. Only molecules with smaller size than the pore openings will get into the active sites and further react.

b) **Transition state shape selectivity** is exemplified in Figure 1.5 b). This type of shape selectivity states that products of reactions will only be formed from reaction intermediates whose size fits in the zeolite pores and whose orientation is favorable for the reaction to occur [37, 38]

c) **Product shape selectivity** is shown in Figure 1.5 c). It occurs when only certain products of reaction which are smaller than the pore size can diffuse out of the zeolite structure [37, 38]. Products which are bigger than the dimensions of the pore must undergo further cracking or isomerization reactions to yield molecules with sizes that can exit the crystal.

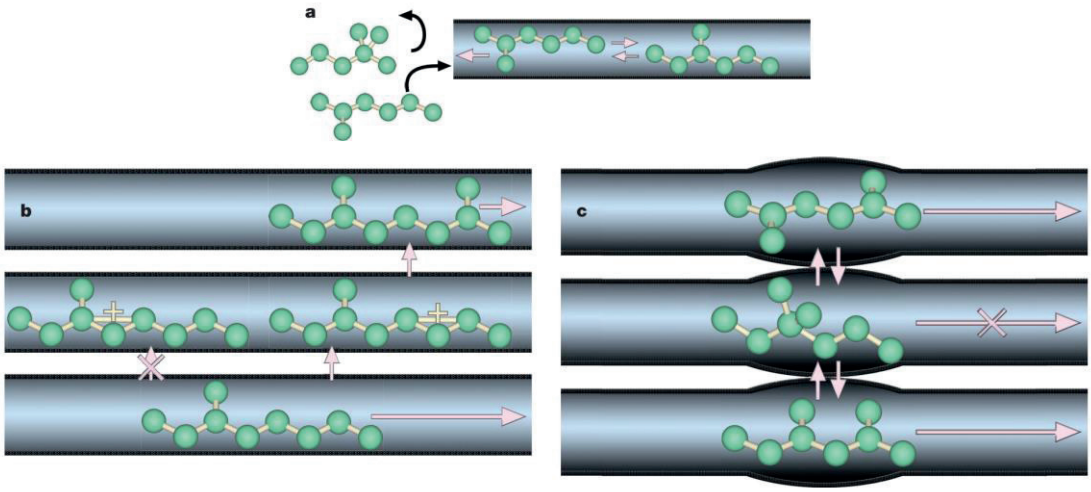

Figure 1.5. Scheme of the different types of shape selectivity. a) Reactant shape selectivity where molecules that are too large, cannot enter the zeolite pores. b) Transition state shape selectivity states that molecules and transition state that are too large to fit in the pores will not be formed and c) Product shape selectivity, where only the molecules formed that fit in the zeolite pores will get out of the pore. Adapted from [4]

Owing to the aforementioned reasons: high thermal stability, high surface to volume ratio, shape selectivity and possibility of controlling the acidic properties, zeolites are one of the most currently employed catalysts on heterogeneous catalyzed processes such as oil conversion, production of chemicals and fine chemicals and upgrading of natural gas, coal or biomass [39-42]. To exemplify the large number of applications of zeolites, a very brief overview of the most important breakthroughs in the zeolite field is provided below.

As previously said, Barrer and Milton [13, 43-46] during 1940s' and 1950s' reported for the first time the synthesis of zeolites using low-temperature hydrothermal methods. This approach boosted the interest in both zeolite synthesis and their application, resulting in the commercialization of adsorbents based on zeolites A and X in 1948 [25]. At that time, researches at Union Carbide envisaged the potentialities of zeolites as catalyst by functionalizing their structure [47]. Resulting from this thorough and fundamental research, an important breakthrough in zeolite catalysis took place in 1964 by the introduction of zeolite Y as commercial Fluid Catalytic Cracking (FCC) catalyst by Mobil (nowadays ExxonMobil) [48]. Later, researchers from Mobil were able to synthesize ZSM-5 zeolites, which were used as FCC cracking additive to enhance the cracking activity of linear with respect to branched olefins in the gasoline range, thereby increasing the octane number in the final product.

An important development in the field of zeolite catalysis, which is very relevant for this Thesis, was carried out by researchers at Mobil when, in 1977, Chang and co-workers discovered that acidic zeolite catalysts selectively converted methanol and other oxygenated compounds into a mixture of hydrocarbon compounds: paraffins, aromatics, naphthenes and olefins [49]. Owing to the oil crises in 1973 and 1979, an extensive development of the Methanol-to-Gasoline (MTG) process was performed and different bench-scale and pilot-plan demonstrations were initiated [50].

Since the conversion of methanol-to-hydrocarbons (MTH) is the principal reaction investigated during this work, a dedicated chapter on this Thesis (Chapter 2) focuses on different aspects of the Methanol-to-Hydrocarbons reaction.

1.4. Catalysts relevant to this work

The influence of the zeolite topology on the deactivation was set as one of the main goals to look into during this work. Therefore, especial efforts were put in selecting zeolites with substantial structural differences that could provide a comprehensive insight into the role of zeolite structure as one of the key parameters influencing the loss of activity and stability during the conversion of methanol-to-hydrocarbons. In the following paragraphs, a detailed description of the zeolite structures most relevant to this Thesis is presented. All the materials are assigned with a three capital letters code, according to the rules set by IZA [17].

1.4.1. Mordenite (MOR)

Mordenite has 12- and 8-membered ring channels distributed parallel to the c-axis, as displayed in Figure 1.6. Typical channel dimensions are 6.5 Å x 7.0 Å and 5.7 Å x 2.6 Å for the 12- and 8-membered rings, respectively [17]. These systems are connected by 8-ring channels parallel to the b-axis which are not accessible to any diffusing species. The perpendicular eight-ring channels are very tortuous, leading to the so-called side pockets to the 12 rings. Thus, molecules are unlikely to pass through the eight rings because of steric limitations. In conclusion, Mordenite is in real terms, a one-dimensional 12-ring system.

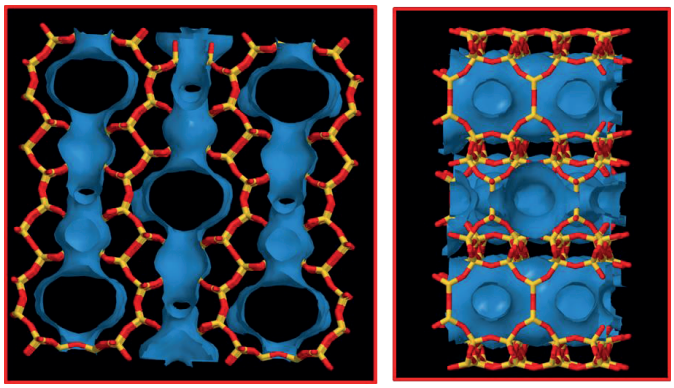

Figure 1.6. Illustration of the Mordenite (MOR) topology. The pore system is highlighted in blue.[17]

1.4.2. Zeolite ZSM-22 (TON)

ZSM-22 is a one-dimensional medium pore size zeolite. The 10-ring channels of the material are elliptical, with dimensions 5.7 Å × 4.6 Å and slightly zigzagged in shape. The maximum diameter of a sphere that can be included in the channels of ZSM-22 is 5.71 Å. This zeolite has a framework density of 19.2 T-atoms per 1000 $Å^3$, displaying orthorhombic symmetry and lattice constants a = 13.9 Å, b = 17.4 Å and c = 5.0 Å [17, 51]. The illustration of the pore system in ZSM-22 can be observed in Figure 1.7.

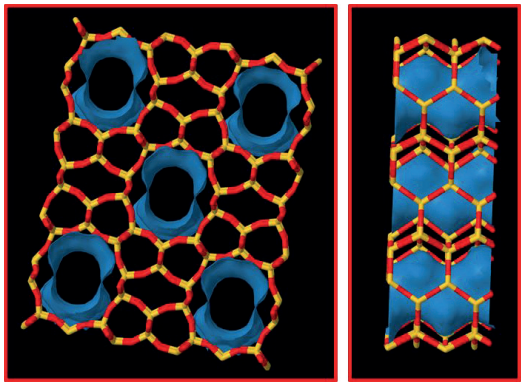

Figure 1.7. Schematic representation of the structure and channel system of ZSM-22 zeolite (TON)[17]

1.4.3. Zeolite ZSM-5 (MFI)

This particular zeolite, which is known for being largely applied in different industrial processes, is a three-dimensional medium pore size zeolite made from interconnecting straight and sinusoidal 10-ring channels, as shown in Figure 1.8. The straight channels have

dimensions of 5.1 × 5.5 Å and the sinusoidal channels are 5.3 Å × 5.6 Å in size. The maximum diameter of a sphere that can be fitted in the channels of ZSM-5 is 6.36 Å [17].

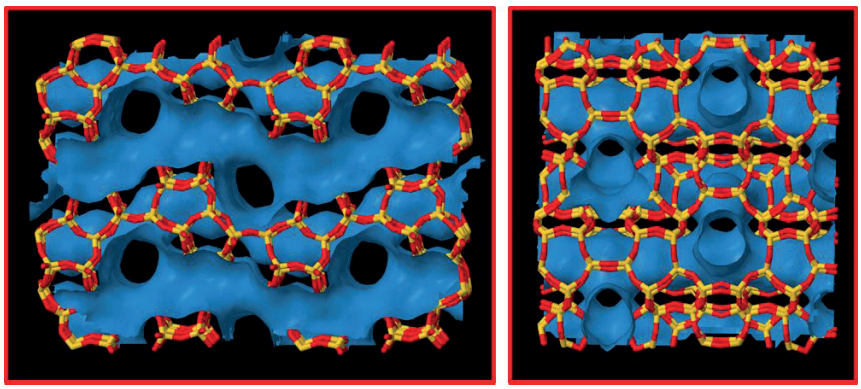

Figure 1.8 Illustration of the MFI topology. Straight (left) and sinusoidal (right) l channels are highlighted in blue

1.4.4. Beta (BEA)

Beta zeolite is a disordered structure made of three intergrown polymorphs A, B, and C [52], that results in a three-dimensional 12-ring channel system, which is displayed in Figure 1.9. Polymorphs are individually ordered, but the stacking produce a disordered structure along the c-axis. All the polymorphs have two channel systems linear, mutually orthogonal and perpendicular to the c-axis, and topologically identical. These two linear channels intersect producing a third channel system, parallel to the c-axis and with sinusoidal shape. Linear channels have the dimensions 6.6 Å x 7.7 Å. The third channel, highly tortuous, is smaller with dimensions of 5.6 Å x 5.6 Å [17].

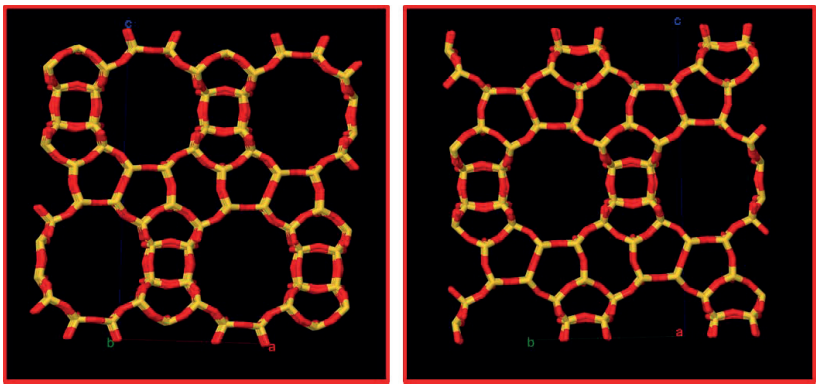

Figure 1.9 Illustration of the BEA topology [17]

1.4.5. Zeotype SAPO-34 (CHA)

SAPO-34 is a silicoaluminophosphate (SAPO) material with chabazite topology (CHA) having a three dimensional small pore structure. The pore system in SAPO-34 is formed by large cages made of 12-ring openings that are connected by 8-ring windows of 3.8 Å × 3.8 Å dimensions, as shown in Figure 1.10. The maximum diameter of a sphere that can be included in the cages of SAPO-34 is 7.37 Å [18].

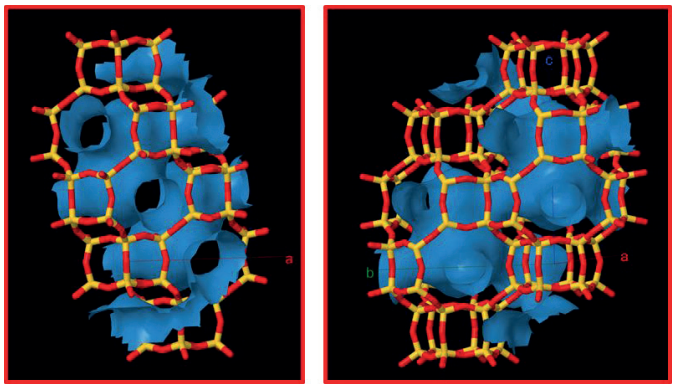

Figure 1.10 Illustration of the pore system and cages in CHA structure [17]

1.5. Motivation and scope of the work

Even though zeolites are the preferred acid catalysts for converting methanol into hydrocarbons, the main drawback that zeolites display is that their catalytic activity decreases with time owing to the deposition of non-volatile species, which remain trapped in the channels and cavities of the catalysts, preventing the reaction from proceeding.

Despite the numerous and detailed studies focused on zeolite deactivation during the MTH process published during the last years, which with no doubt have substantially contributed to elucidate the mechanism of coke formation, there are still some interesting questions related to zeolite deactivation which are worth being addressed and that we would like to investigate.

The first goal is to study in detail the role of zeolite topology in the deactivation. We do not aim at screening all the zeolite structures currently available. Instead, we want to investigate and quantitatively assess the nature and content of the deactivating species in some of the most efficient catalyst used for converting methanol into hydrocarbons. In addition, we want to evaluate the application of a theoretical deactivation model, which was proposed for a particular zeolite strucutre, to a larger number of frameworks to evaluate if a mathematical model can reasonably predict the parameters governing the deactivation regardless of the zeolite topology employed.

Keeping with the influence of zeolite pore structure on the deactivation, among the vast number of publications focused on the catalyst deactivation, only a handful of works have studied the loss of catalytic activity axially along the catalyst bed, and to the best of our knowledge only the catalyst with the largest industrial interest, H-ZSM-5 and H-SAPO-34, have been subjected to this type of investigations. Therefore, to shed some light and gain more insight into the axial mode of deactivation along the catalyst bed, we aim at performing spatial- and temporal- deactivation studies over zeolites with varying pore size and structure.

So, the research questions that are to be addressed can be stated as: How does the zeolite topology influence the nature, evolution and accumulation of deactivating species during the MTH process? How accurate is the application of the deactivation model propsed for ZSM-5

to other zeolites with different topology? How does the pore size influence the axial mode of deactivation?

In addition to the influence of zeolite topology on the deactivation, we also want to look into the role of particle morphology on the deactivation of ZSM-5, the most applied catalyst at industrial scale for the conversion of methanol to hydrocarbons. In recent years, studies investigating this effect have been published. However, in this work, and differently from previous contributions, the MTH process will be performed using reactions conditions similar to those used at industrial scale. Therefore, the research question we want to address is: How does the particle morphology of ZSM-5 catalysts influence the deactivation during the MTH reaction evaluated at industrial relevant conditions?

Finally, the last objective set for this thesis is a bit different from the previous ones. In this case we will not look at the influence of any paremeter in the deactivation. Rather, we want to elucidate if the modifications that the zeolite strucutre undergoes during the formation and accumulation of hydrocarbon residues can be used to directly evaluate the degree of deactivation of a zeolite. Since this is a novel approach, it was decided to use a single zeolite catalyst i.e. ZSM-5 for being the archetype catalyst used in the MTH process. Therefore, the research question to be answered could be stated as: Can the changes observed in the zeolite strucutre during the formation of coke be used to evaluate the degree of deactivation over ZSM-5 catalysts?

2. Methanol-to-Hydrocarbons (MTH)

2.1 Historical development of the Methanol-to-Hydrocarbons (MTH) technology.

From an historical point of view, 1973 was the year when the first oil crisis took place. As a consequence, the price of the crude oil increased sharply. Figure 2.1 shows the evolution of the price of crude oil from 1968 to 2016 [53]. Resulting from this steep increase in the oil price during the beginning of 1970's, intensive research plans with the aim of developing new processes that could reduce the dependency of the society on crude oil were established in certain chemical companies.

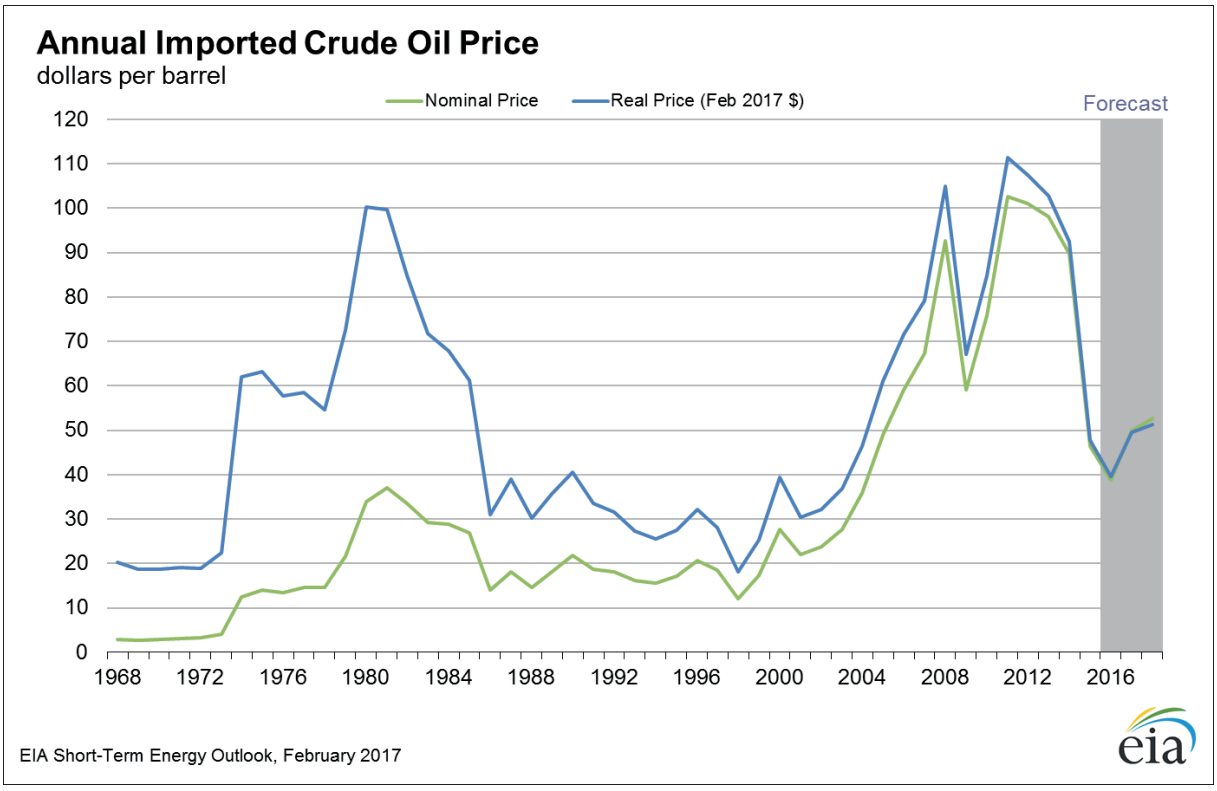

Figure 2.1 Evolution of the crude oil barrel price ($/barrel) from 1968 to today [53].

After patenting the process in 1976 [54], Chang and Silvestri, researches at Mobil (today ExxonMobil) provided in 1977 the first experimental evidence on how methanol and other oxygenated compounds were transformed into a mixture of hydrocarbons using acidic zeolites as catalysts [49]. They showed that over H-ZSM-5, hydrocarbons in the gasoline

range (C_4-C_{10}) were formed provided that sufficient contact time between methanol and the zeolitic catalysts was applied.

The discovery of the Methanol-to-Hydrocarbons reaction triggered a vast interest in the process from both, academia and industry, which lasts until today [27, 50]. Owing to the second oil crisis (1979) and the subsequent increase in crude oil (Figure 2.1), special efforts were devoted to the scale-up and commercialization of the MTH process. Demonstration plants were built in Paulsboro (New Jersey) in 1978 [55], and in Wesseling (Germany) between 1981-1984 with a production of 4 and 100 barrel-per-day (bpd), respectively. Finally, in 1985 Mobil commercialized the Methanol-to-Gasoline (MTG) process in New Zealand with a production of 14,500 bpd. This plant used natural gas as raw material, which was subsequently converted into methanol via synthesis gas over $Cu/ZnO/Al_2O_3$ catalysts [56-58]. Despite the fast growing industrial interest in the MTH reaction, the drop in crude oil prices made the process no longer profitable, which led to a shutdown of the plant in New Zealand in the mid-1990's [56].

Even though the profitability of MTH process is primarily dependent on the price of crude oil, other industries (apart from Mobil) invested significantly in the methanol-to-hydrocarbons process. As a result, Haldor Topsøe A/S filled a patent in 1984 [59] where they developed and demonstrated on a pilot scale the Topsøe Integrated Gasoline Synthesis (TIGAS) process [60]. Similarly to the Mobil's MTG, the TIGAS process relied on the use of H-ZSM-5 catalyst. However, the peculiarity of the TIGAS was that the synthesis of methanol and dimethyl ether (DME) is merged in a single reactor at high pressures and moderate temperatures, thereby increasing the conversion of syngas to high octane gasoline products. Nevertheless, the TIGAS process was no further developed on those days due to the low prices of oil, which made the TIGAS process uneconomical.

Some years later, efforts were devoted to the production of light olefins (ethene and propene) using the same reaction scheme as in the MTG process. The main difference was that instead of using H-ZSM-5 as acid catalyst, researches from Union Carbide (nowadays UOP) synthesized a new silicoaluminophosphate, H-SAPO-34, with chabazite structure (CHA) in which the large cavities are connected by narrow 8-ring windows, thereby improving significantly the selectivity towards ethene and propene rather than to higher hydrocarbons

in the gasoline range. However, opposite to the long lifetime of the H-ZSM-5 catalyst, the deactivation of H-SAPO-34 was relatively rapid, requiring regular regenerations to burn off the coke deposits that deactivate the catalyst. Resulting from such process optimization, UOP/Norsk Hydro developed the Methanol-to-Olefins (MTO) technology which was scaled up in a demo plant in 1995 using a low pressure fluidized-bed reactor that allowed efficient temperature control and catalyst regeneration simultaneously [61].

In parallel to the development of the UOP/Norsk Hydro MTO technology, Lurgi attempted and succeeded in the development of a process that maximized the selectivity of propene, i.e. the Methanol-to-Propene (MTP) process, using H-ZSM-5 catalysts, which was also demonstrated in a demo plant [62]. The MTP is characterized for operating at high temperatures (460-480 °C) and atmospheric pressures using a parallel-fix bed reactor with intermediate feed injection between beds, enabling intermittent regeneration. Besides, undesired products such as ethene and butenes are recycled to the conversion step, increasing the selectivity towards the primary product: propene [50]. Mobil further developed its original MTG technology into the Mobil-Olefin-to-Gasoline-and-Distillate (MOGD) Process. In this case, a fluidized-bed reactor working at low pressures and high temperatures enabled the production of light olefins as primary and gasoline as secondary products using H-ZSM-5 as the catalyst of the process [50]. Besides, the concept was additionally extended by designing a gasoline/diesel product by oligomerization of light olefins, which was successfully demonstrated at one of Mobil's refineries [63].

As it can be inferred from the previous paragraphs, the general MTH process is a versatile technology in which the targeted products of the reaction can be tuned depending on the materials used as catalysts as well as on the operating conditions, giving rise to the different alternatives previously mentioned: MTG, MTO or MTP. A summary of the principles of each MTH-derived technology is given below:

- For the production of high quality gasoline, the preferred catalyst in the MTG or TIGAS process is H-ZSM-5, whose structure has been previously described (1.4.3). When this catalyst is used at temperatures between 350 and 410 °C and pressures around 20 bar, the primary product of the reaction is a hydrocarbon mixture stream rich in gasoline range compounds.

- A slight variation of the MTG is the Methanol-to-Propene (MTP). In this case, the catalyst used is also H-ZSM-5, but the operating conditions, higher temperatures and lower pressures than in the MTG, enhance significantly the selectivity towards propene, with some LPG and gasoline as by-products.

- In the conversion of Methanol-to-Olefins, the archetype catalyst used is H-SAPO-34. The structure of the catalyst is the main responsible for the production of ethene and propene as main products. The large cavities of the catalyst enable the formation of aromatics inside the cages; however, due to the presences of small and narrow pore openings, products larger than C_4 are not allowed to diffuse out from the crystal. Thus, aromatics further crack into smaller hydrocarbons, enhancing the selectivity to light olefins.

During the first years of the XXI century and owing to the incessant increase in the price of crude oil, different industrial commercialization processes derived from the general MTH technology were announced:

- In 2009, a semi-commercial demonstration UOP/Total MTO plant in Feluy, Belgium, able to process up to 10 tons/day of methanol was brought on-stream [50].
- In 2011, the construction of an MTO plant in Nanjing, China, processing $295 \cdot 10^3$ tons of methanol per year was announced.
- In 2010, a plant producing $600 \cdot 10^3$ tons per year of ethene and propene was started in Baotou, China.
- In 2014, Haldor Topsøe A/S was commissioned the construction of the largest synthetic gasoline plant ever built, in Turkmenistan, using the TIGAS technology with a daily production capacity of 15,500 bbl, expecting to be in operation in 2018.

Despite the intense commercialization efforts of the MTH technology [58], the sharp drop in crude oil prices from late 2014 until today may influence negatively the development of the mentioned projects owing to the high dependency of the MTH efficiency technology on the oil prices.

2.2 Mechanistic aspects in the MTH reaction

Intensive and detailed mechanistic studies of the conversion of methanol-to-hydrocarbons have been carried out and debated during the last four decades [27, 50, 64]. Owing to the complex reaction network and the autocatalytic nature of the MTH process, obtaining information about the elementary steps of the reaction is very challenging. Moreover, the fact that products of reaction are on the gas-phase whereas intermediates species are confined within the pores of the catalyst makes the elucidation of single reaction step more difficult. Finally, it is important to bear in mind that adsorption/desorption and diffusion phenomena are also involved in the reaction mechanism due to the porous nature of zeolite and zeotype materials, which induce another degree of complexity.

2.2.1 Initial Reaction Network

The first and very simplified reaction mechanism of the MTH process was proposed by Chang and Silvestri in 1977, where they looked into the influence of contact time on product distribution [49]. Resulting from this analysis, the overall MTH process was divided into three sub-sequent steps [27, 49, 65, 66]. During the first step, methanol is dehydrated to dimethyl ether and water until reaching the equilibrium concentration. Subsequently, olefins are formed from this mixture. Finally, olefins further react producing either higher olefins via methylation/oligomerization or naphthenes, aromatics and paraffins through cyclization and hydrogen transfer reactions as shown in Scheme 2.1. This first reaction pathway is represented below in Figure 2.2.

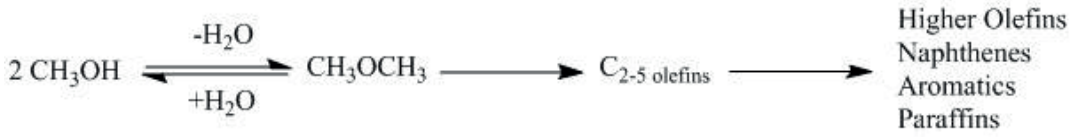

Scheme 2.1 Simplified MTH reaction pathway. Adapted from [49]

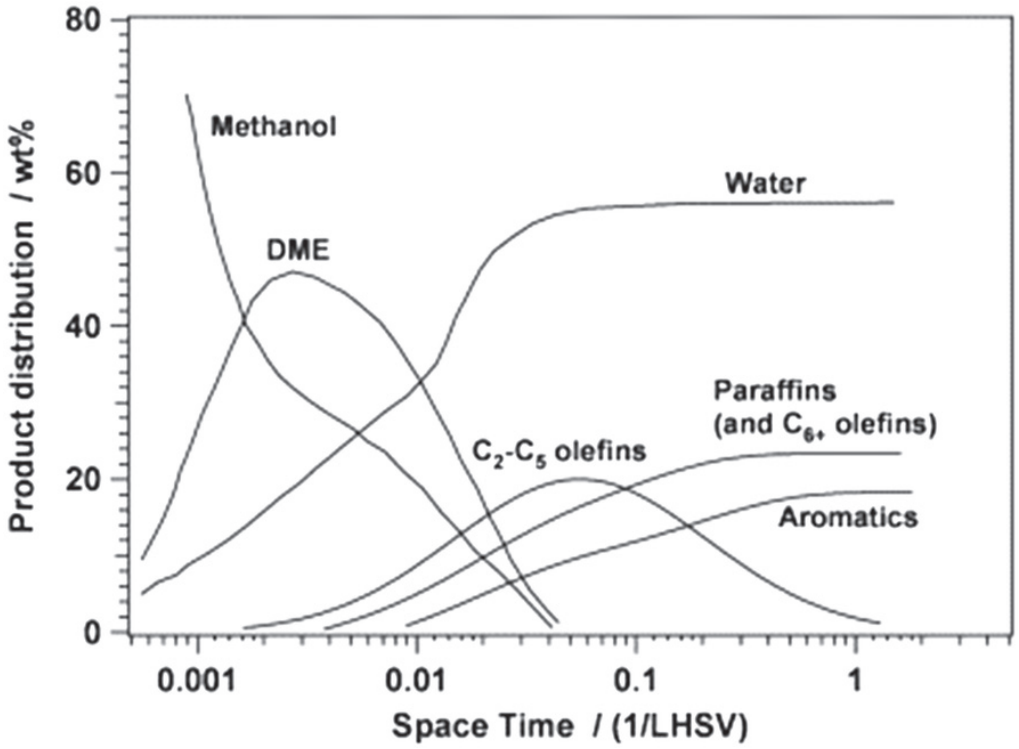

Figure 2.2 Reaction pathway of MTH process as originally proposed by Chang and Silvestri. Adapted from [49]

2.2.2 Formation of the first C-C bond

During the early years after the discovery of the MTH process, researchers tried to understand and elucidate the formation of the first C-C bond [67]. More than 20 different mechanisms for direct C-C coupling can be found in literature. Among them, oxomium ylides, carbocations, carbenes and free radicals have been proposed as plausible reaction intermediates [50]. Despite the relatively large number of proposed mechanisms for the first C-C bond formation, very little experimental evidence that supports any of these proposals has been published [50, 68].

In 1979, Chen and Reagan were the first to propose that the MTH reaction had an autocatalytic nature [69]. Twenty years later, Haw and collaborators performed the MTH reaction with highly purified reagents and they reported a decrease in several orders of magnitude in the initial rate of methanol conversion [70]. Authors further concluded that for a not highly purified feedstock, the rate at which the direct C-C coupling operates is probably irrelevant compared to the rate at which trace impurities initiate the reaction [50, 70]. The conclusion drawn by Song et al. was experimentally confirmed some years later [71]. Special

attention to the formation of the first C-C bond during the MTH reaction has been also paid by theoretical studies and the work of Lesthaeghe and collaborators is of particular interest [72]. They theoretically investigated a large set of proposed direct mechanisms for C-C bond formation determining rate coefficients and energy barriers. According to their findings, the direct C-C coupling is unlikely due to the high activation barriers as well as the unstable intermediates formed [72].

Since the direct mechanism of C-C bond formation is of little relevance when operating the MTH process under real industrial conditions [50], not further discussion will be established upon the first C-C bond coupling. However, it is worth highlighting that there are currently ongoing research activities still looking into the formation of the first C-C bond [73-76]. Lercher et al. have proposed a carbonylation-based mechanism via methyl acetates or acetic acid formation [74]. The use of UV/Vis diffuse reflectance spectroscopy and solid state NMR allowed Weckhuysen and co-workers to provide additional evidences of the formation of acetate and methyl acetate species [73].

Nowadays, the MTH reaction is accepted to proceed through a hybrid organic-inorganic route where hydrocarbon species act as reaction centers for the formation of products [50, 77-79]. The reaction centers can either be aromatic species [80-84] or alkenes [85, 86]. In the following section a chronological overview of the different contributions that have led towards the current mechanistic understanding of the MTH reaction is provided.

2.2.3 Evolution of the reaction mechanisms

As it has already been mentioned, Chen and Reagan were the first authors suggesting the autocatalytic nature of the MTH in 1979 [69]. During the early years of the 1980's additional mechanisms were reported. Dessau and co-workers from Mobil proposed that the autocatalytic effect during the conversion of methanol-to-hydrocarbons over H-ZSM-5 was driven by a continuous olefin methylation/cracking mechanism [85, 86] (Scheme 2.2). This mechanism suggests that initial alkenes are produced from reactions that involve C-C bond formation, but as soon as C_{2+} alkenes are present, the reaction leading to the C-C bond formation is irrelevant, in line with Chen and Reagan's autocatalytic reaction scheme [69]. This reaction mechanism considers ethene as a product formed by secondary re-equilibration of primary alkenes, instead of being a primary product obtained from methanol.

Moreover, aromatics and paraffins are presented as end products (i.e. coke precursors) resulting from aromatization and hydrogen transfer reactions.

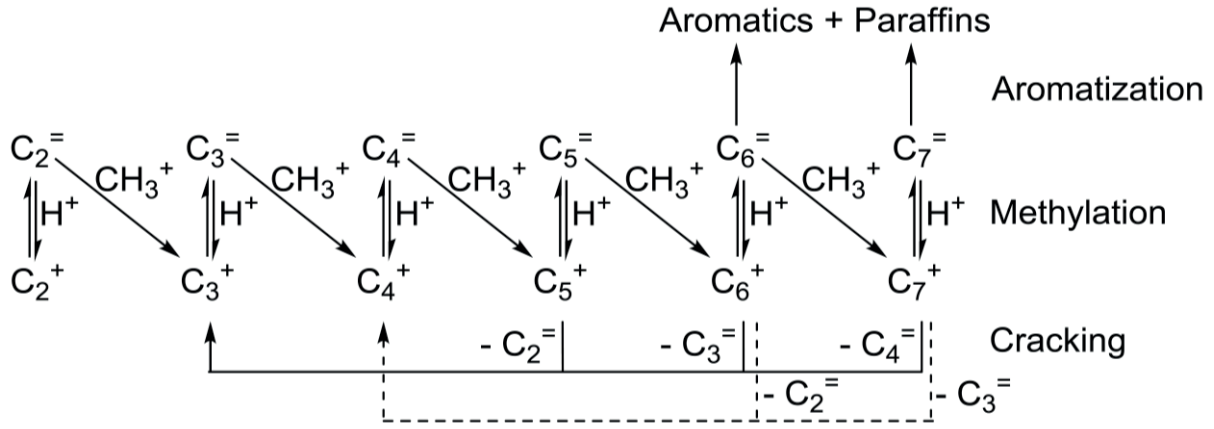

Scheme 2.2. Mechanism for methanol reaction over H-ZSM-5 proposed by Dessau. Adapted from [85]

Two independent studies presented approximately at the same time highlighted the importance of aromatic and unsaturated cyclic species as indirect propagators of the formation of alkenes during the MTH reaction. First, Langner investigated the effect of adding small amounts of higher alcohols to the methanol feed. It was found that by co-feeding methanol with 36 ppm of cyclohexanol, the induction period, i.e. time until launching the autocatalytic MTH reaction, was remarkably reduced when using NaH-Y zeolite[87]. Langner suggested a reaction mechanism where methylated cyclic intermediates could undergo a “paring reaction”, thereby producing light alkenes (Scheme 2.3) . Second, the work of Mole and co-workers [88, 89] led to a similar conclusion to that drawn by Langner based on the fact that when they added 1 wt% toluene or p-xylene to the methanol feed, a dramatic increase in the methanol conversion was detected. This effect was called co-catalysis [50]. However, according to the co-reactions with isotopically labeled aromatics using H-ZSM-5 catalysts, Mole proposed a mechanism for alkene formation where polymethylbenzenium ions are deprotonated forming ethylene in the so-called “side-chain” alkylation mechanism [88], exemplified in Scheme 2.3.

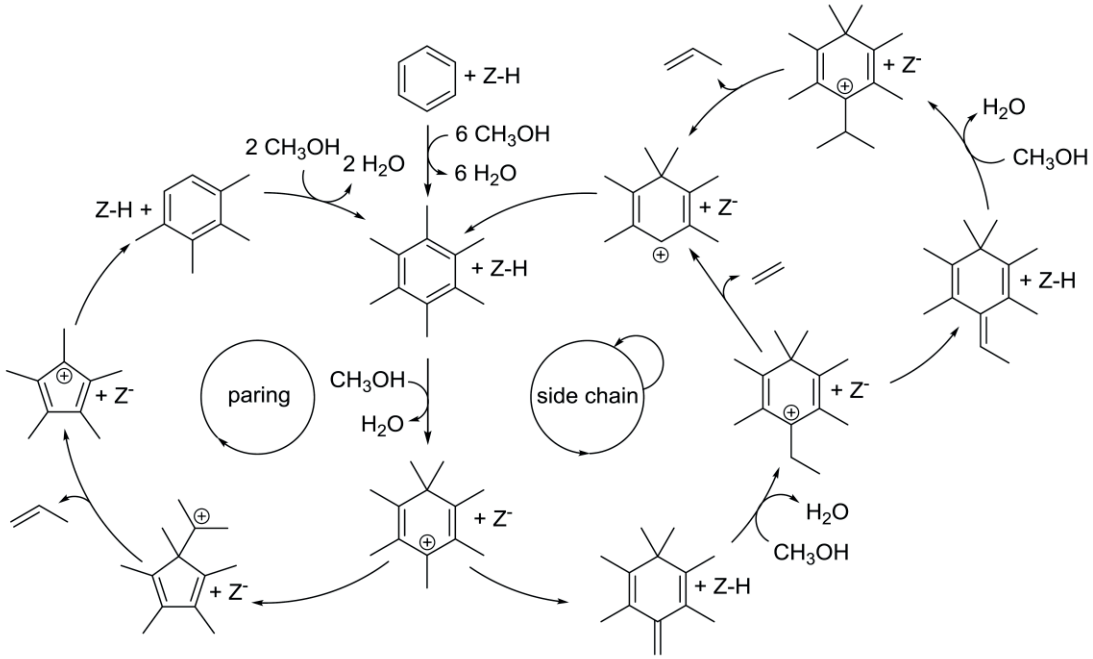

Scheme 2.3 Representation of the paring and side-chain reaction concepts in the MTH catalysis. Adapted from [90]

In the mid 1990's, Dahl and Kolboe used isotopic labeling experiments by co-feeding alkene precursors (ethanol and propanol) with ^{13}C-Methanol over H-SAPO-34. The analysis of the effluent led the authors to conclude that the lower alkenes, ethene and propene, had very little reactivity when co-reacted with methanol and that most of the products were formed exclusively from methanol under the reaction conditions investigated [77-79]. Consequently, a new mechanism called "hydrocarbon pool" was proposed. Even though the "hydrocarbon pool" has similarities with previous mechanistic studies, this schematic concept had a larger impact than the works published in previous years [91]. The "hydrocarbon pool" '(HCP) model, depicted in Scheme 2.4, assumes that methanol is being continuously added to a pool of adsorbed hydrocarbons that continuously eliminates light alkenes.

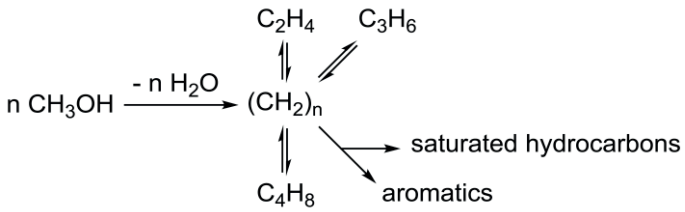

Scheme 2.4. The hydrocarbon pool mechanism proposed by Dahl and Kolboe Adapted from [78]

The hydrocarbon pool, with an initially specified overall stoichiometry $(CH_2)_n$, was proposed to represent an adsorbate which may have many characteristics in common with ordinary coke and might easily contain less hydrogen than specified [50]. However, the chemical structure of the pool was not further detailed [77-79]. Hence, the hydrocarbon pool mechanism can be seen as a generalization of all the indirect mechanisms proposed during the 1980´s.

During the decade of 1990's several groups further investigate the role of aromatics or cyclic intermediates in the conversion of methanol-to-hydrocarbons. The group of Haw used Magnetic Angle Spinning Nuclear Magnetic Resonance (MAS-NMR) for the identification of benzenium and cyclopentadienyl cations located inside the catalysts under working conditions [92-96]. Mikkelsen and co-workers co-reacted methanol and aromatics over large pore size zeolites and they found evidence that the hydrocarbon pool mechanism was also operative in this type of zeolites [83]. By using H-SAPO-34 (CHA structure), the groups of Haw and Kolboe simultaneously concluded that polymethylbenzene species (PMB) represented the main hydrocarbon pool species for H-SAPO-34 [81, 97, 98]. Hunger et al. provided experimental evidence of the hydrocarbon pool mechanism using catalysts such as H-ZSM-5 (MFI), H-SAPO-34 (CHA) and H-SAPO-18 (AEI) [99-101]. Additional studies of the MTH reaction performed over H-Beta (*BEA) confirmed the relevance of polymethylbenzene species in this particular topology [102, 103].

After a period of time when aromatic species were regarded as the intermediates of the MTH process, in 2006 and 2007 two related studies using steady-state isotope transient experiments over H-ZSM-5 proved that aromatic species were not the intermediate species for the entire range of alkenes formed in the reaction [80, 84]. Upon $^{12}C/^{13}C$-MeOH switching experiments, it was observed that ^{13}C-incorporation of ethene was in agreement with that of lower substituted methylbenzenes, suggesting that both species have a common reaction pathway.

Resulting from these findings, the "Dual Cycle Mechanism" was proposed. This mechanism, which is the currently accepted mechanism for the MTH reaction, states that the reaction proceeds simultaneously through two inter-connected cyclic reaction mechanisms, as exemplified in Scheme 2.5. The alkene cycle involves the methylation and cracking of alkenes

on a similar way to the previous propositions of Dessau [85, 86]. The main point of discrepancy between Dessau's model and the dual cycle mechanism is that the latter proposes that the formation of ethene resulting from the alkene cycle is negligible. The other cycle of the mechanism, the arene cycle, involves continuous methylation of aromatic species and their sub-sequent dealkylation. The link between the two individual cycles is set to be the cyclization and hydrogen transfer reactions between olefins, which result in the formation of aromatics and paraffins [50].

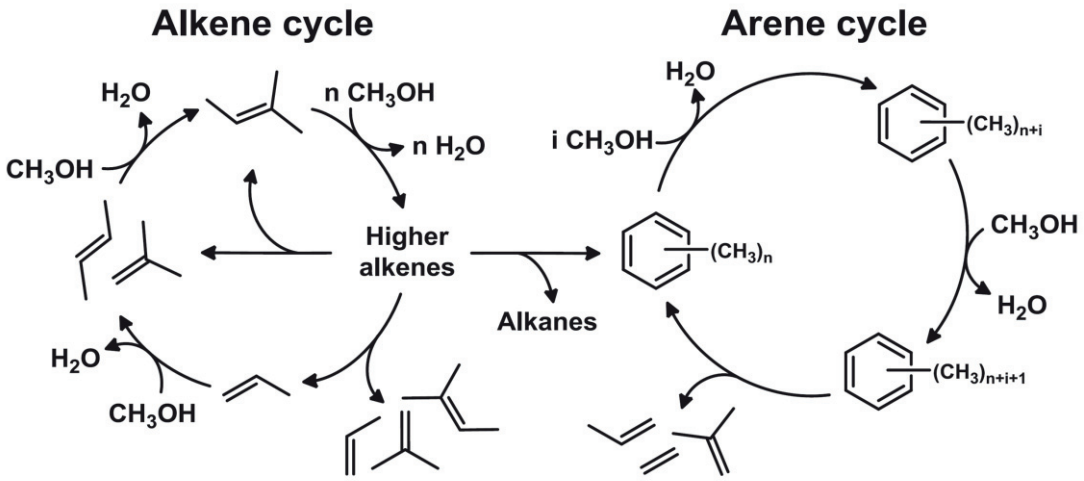

Scheme 2.5. General scheme of the dual cycle mechanism. The structure of the intermediates as well as the extension of each cycle is dependent on the catalyst used and the reaction conditions. Adapted from [50]

In a more recent contribution, Bhan and co-workers have proposed a descriptor that enables to assess the relative propagation of the alkene and the arene cycle over H-ZSM-5 catalysts [104]. Assuming that ethene is formed mainly from the arene cycle and that 2-methylbutane and 2,2-dimethylbutene are representative products of the alkene cycle, the authors proposed that the ratio between the yield of ethene divided by the yield of the two latter species describes the relative propagation of the arene or the alkene cycle. In additional contributions, Bhan and his group have evaluated the influence of temperature, particle size or co-feeding on the relative propagation of the two different cycles operating during the MTH reaction [105, 106].

Even though the dual cycle mechanism was proposed from experiments carried out on H-ZSM-5 catalysts, in the following years similar studies to those performed over H-ZSM-5 were conducted using other topologies with the aim of establishing structure-selectivity

relationships. Different reports have revealed that the pore size of the zeolite and the presence of cages in the structure are the most important parameters in determining the relative propagation of the alkene and aromatic cycle. Overall, it has been reported that in zeolites with large pore sizes, the aromatic cycle is more favored than when medium pore size materials are used [82, 107-110].

On the other hand, steady-state isotopic transient studies carried out over H-ZSM-22 (TON), a medium pore size zeolite with one-dimensional channels, demonstrated that such zeolitic catalyst favors strongly the propagation of the alkene cycle, with almost negligible contribution from the aromatic cycle. When using H-ZSM-22, or other zeolites with similar pore architecture such as H-ZSM-23 (MTT) in the conversion of methanol-to-hydrocarbons, the product spectrum is characterized for being rich in C_{3+} alkenes, with a large fraction of branched C_{5+} species and very low quantities of aromatics [111-114]. In this particular case, the zeolite structure was found to be the dominant parameter that forces the MTH reaction to proceed mainly through one of the two cycles of the dual cycle mechanism i.e. the alkene cycle.

Taking into consideration that the active sites in the MTH process are comprised by both an organic part (hydrocarbon species) and an inorganic contribution (Brønsted acid sites), the product distribution can be tuned not only by choosing appropriately zeolites with different pore size, but it can be also adjusted by altering the organic or inorganic contribution. The former has been shown to be achievable by techniques such as co-feeding [114-116], whereas the latter can be done during the synthesis process or by applying different post-synthetic ionic modifications [27, 117]. In this line, it has been reported that in catalysts with the same topology, those with lower acid strength favor the alkene cycle [118, 119].

3. Zeolite deactivation in the conversion of Methanol-to-Hydrocarbons

As stated in the introduction, despite the fact that zeolites are the preferred materials in industry to catalyze the conversion of methanol-to-hydrocarbons due to their properties i.e. Brønsted acidity, large surface area and shape selectivity, they also display some hurdles that prevent them from being ideal catalysts. The main drawback is that with increasing time-on-stream under reaction conditions the catalysts deactivate or, in other words, the activity of the zeolites drops gradually, converting less methanol molecules into valuable hydrocarbons.

Within zeolite deactivation, it is possible to distinguish two different types. On the one hand, the deactivation by deposition and accumulation of hydrocarbon residues (coke) on the zeolite that either poison the Brønsted active sites or block the zeolite channels is regarded as reversible deactivation process [68, 120, 121]. Hydrocarbon residues are considered as any carbon-containing compound, either of graphitic, aromatic or polymeric nature, which has too low vapor pressure, too high proton affinity or it is too spacious to leave the surface of the catalyst [68]. The coke accumulated on the zeolite resulting from the reversible type of deactivation is normally removed by oxidative regeneration at temperatures between 400 - 700 °C, leading to a recovery of the catalytic activity.

On the other hand, once the coke has been removed by oxidative regeneration a certain number of cycles, a permanent loss of zeolite activity is observed. Since during the removal of coke, both high temperatures and water are present in the reaction medium; such conditions favor the dealumination of the zeolite i.e. the removal of Al atoms from the zeolite framework, which turns into an irreversible loss of activity [122, 123].
In the course of this work, more efforts were devoted to investigate the reversible mode of deactivation, whereas the irreversible mode of deactivation has not been set as the focus of the work.
Zeolite deactivation in the MTH reaction has been a topic of interest since the discovery of the methanol-to-hydrocarbons process. A great effort has been made in recent years to gain knowledge about the deactivation phenomena in the MTH reaction [34, 68, 111, 120, 124-

130]. The majority of the studies in the last decades have been carried out *ex-situ*, by analyzing the *post-mortem* zeolite coke content accompanied by the loss of accessible surface area in the entire catalyst bed. However, when an autocatalytic reaction like MTH is carried out in a fixed bed plug flow reactor, an axial deactivation gradient is expected.

Under conditions where full initial conversion is achieved, the catalyst bed can be divided into three sequential reaction zones. The feed inlet segment is defined as the Initiation zone. In this first zone, partial conversion of methanol to dimethyl ether, as well as a slow formation and accumulation of autocatalytic species (alkenes and arenes) takes place. When sufficient autocatalytic species have been produced, the autocatalytic reaction dominates product formation, and this next zone is called the Autocatalytic zone. Finally, in the Product zone, located towards the bed outlet, oxygenates are fully consumed and only hydrocarbon inter-conversion reactions take place [68, 131].

A few studies have taken into account the axial mode of zeolite deactivation when the MTH reaction is performed in a fixed bed plug flow reactor. Haw and Marcus were the first who proposed a deactivation model, which was called “Burning Cigar Model”. This model described the deactivation and inhomogeneous aging of H-SAPO-34, in which a layer of active catalyst moves along the bed with increasing time-on-stream, leaving the deactivated catalyst in its wake [132]. This model was later confirmed by Wragg et al., who used operando time- and space-resolved X-Ray Diffraction to monitor the deactivation of H-SAPO-34 as MTH catalyst [133]. Moreover, Wragg et al. allocated the initial increase in methanol conversion with time-on-stream over this particular catalyst to the slow accumulation of autocatalytic species in the initiation zone, which is gradually transformed into an autocatalytic zone [133]. In a different contribution, Schulz studied the MTH reaction over H-ZSM-5 at 475 °C, also using a plug flow reactor, and visually observed that the spent catalyst was inhomogeneously deactivated [120]. The top black part, which was heavily deactivated due to coke located on the outer surface of the catalyst particles, was followed by a grey reaction zone, whereas a less deactivated zone with a light blue color was observed towards the end of the bed. This color was assigned by the authors to “coke seeds”, formed by secondary reactions of the MTH products [120].

In a very recent publication by Müller et al. [126], the deactivation rate of a H-ZSM-5 catalyst was evaluated in two different reactor setups: a plug-flow reactor (PFR) and a continuous stirred-tank reactor (CSTR). Results showed that meanwhile the catalyst tested in the PFR reactor was deactivated substantially fast and inhomogeneously along the reactor, due to the differences in methanol concentration in the bed (on a similar way to the previous studies presented above); the sample tested in the CSTR lost its activity at a much slower rate and it happened homogeneously in all catalyst particles due to the moderate methanol concentration in the whole bed achieved by the continuous movement of the catalyst particles. So, based on the type of reactor used, the deactivation phenomenon over H-ZSM-5 differs mainly due to the changes in methanol concentration. In this work, we have essentially used a PFR setup, which is the most common type of reactors in the laboratories, and it is also the type of reactor used for the MTH process at industrial scale. Thus, a deactivation gradient along the bed is expected during the deactivation process.

The formation of coke in zeolite catalysts is a very complex phenomenon and is dependent on different parameters such as zeolite topology [68, 110, 134], reaction temperature [120], acid strength and acid site density [121, 135, 136], nature of the reactants [137] and the physico-chemical properties of the catalysts [127, 128, 138, 139].

To exemplify the complexity of the deactivation process in the MTH process, depending on the topology of the zeolite, certain molecules are regarded as active species, whereas the same compounds are considered as deactivating molecules in other topologies [68]. This is the case of tri-methylbenzene and tetra-methyl benzenes, which are proven to be active species in H-ZSM-5 [80, 84], whereas the same molecules work as deactivating compounds in H-ZSM-22 [111].

In the case of large pore size zeolites, Bjørgen et al. carried out studies delving into the deactivation during the MTH reaction over H-Beta [140]. This zeolite has pores of dimensions such that they can accommodate species as large as bicyclic arenes [102]. Bjørgen and co-workers proposed that the reaction between methanol and hexamethylbenzene species over H-Beta zeolite led to the formation of hepta-methyl-benzenium cations which subsequently rearranged into a polycyclic coke precursor via methylation and hydride transfer reactions [140]. Later, researchers from the same group performed a comparative study over other large pore size catalyst such as Mordenite using

isotopic labeling experiments, which revealed that the same hydrocarbon species were built up and retained in the different zeolite structures. These results contributed to elucidate the dominant role of bicyclic species as coke precursors on large pore size zeolites [110].

Reaction temperature has been reported to play a crucial role in the methanol-to-hydrocarbons reaction by influencing both, product distribution and the deactivation process. Bhan and co-workers recently reported than an increase in the reaction temperature enhances the propagation of the olefin cycle (belonging to the dual cycle mechanism), boosting the selectivity towards C_4 hydrocarbons and decreasing the selectivity towards ethene [104]. Moreover, previous studies reported that when the MTH reaction is performed over H-ZSM-5 catalysts at mild temperatures (270-290 °C), alkyl substituted benzene molecules are responsible for the catalyst deactivation. However, at reaction temperatures above 350 °C, the alkylation-dealkylation equilibrium of benzene is shifted towards alkene formation, altering the mode of deactivation from pore filling to external coking, thereby extending the catalyst lifetime [68, 84, 120]. A similar effect of the reaction temperature on the catalyst lifetime, nature and amount of coke as that reported over H-ZSM-5, was observed in H-SAPO-34 and its zeolitic counterpart H-SSZ-13 [136].

The influence of acid site density and acid strength on product distribution as well as on zeolite deactivation in the MTH reaction has been also thoroughly studied. As a result of such investigations, it has been shown that the selectivity towards ethene increases monotonically with increasing aluminium content for H-ZSM-5 samples with similar crystallite sizes, as a result of the increase in the intracrystalline contact time between the reactants and the catalyst [141]. On the contrary, reducing the acid site density by decreasing the aluminium content on the zeolite favors the selectivity towards propylene [142].

Wan et al. reported that a decrease in the aluminium content on H-ZSM-5 catalysts resulted in both a slower catalyst deactivation due to coke formation and in a decline on the durene yield [143]. Similarly, Yarulina et al. found that a decrease in the acidity of zeolites with DDR topology led to a higher methanol conversion capacity (grams of methanol converted per gram of catalyst until complete deactivation) [139]. Reports from different research groups have shown that an increase in acid site density corresponds to a faster catalyst deactivation rate [27, 143-145].

In this line, Guisnet and co-workers reported that the higher the amount of acid sites in the zeolite, the faster the chemical steps and the larger the number of secondary reactions leading to the formation of coke precursors [121].

When looking into the role of acid strength into the reaction mechanism and deactivation, Westgård et al. used two isostructural catalysts having AFI topology (unidimensional, twelve membered ring channels), with similar acid site densities but different acid strength, i.e. zeolite H-SSZ-24 and zeotype H-SAPO-5. An increment in the selectivity towards aromatics, ethene and propene was observed when using the more acidic zeolite (H-SSZ-24) in comparison to the zeotype counterpart (H-SAPO-5) [118]. Other researchers have claimed that the formation of coke in catalysts with a high acid strength is due to the increase in the selectivity to hydride transfer reactions [146]. In a very recent contribution, the effect of the Brønsted and Lewis acid site density on the hydrogen transfer reactions and thus, on the deactivation, has been very elegantly presented [34]. Authors of this work have reported that on a purely Lewis acidic H-ZSM-5 catalyst, methanol and propene react over a Lewis site generating formaldehyde and propane. Furthermore, it was shown that over a H-ZSM-5 sample with both, Brønsted and Lewis sites, first formaldehyde is formed by transferring two H atoms from MeOH to an alkene on a Lewis site. Subsequently, another alkene reacts with several HCHO molecules on a Brønsted acid site generating dienes and aromatic species which have a high tendency to be adsorbed irreversibly, deactivating eventually the catalyst [34]. The role of HCHO as a faster deactivating agent suggested by Müller et al. is in line with the work carried out by Hutchings in the late 1980s' [147].

Very recently, researchers from our group have shown significant differences in the product distribution, conversion capacity and deactivation process when the MTH reaction was carried out using MeOH or DME as reactants. Authors observed that when using DME as feedstock, the catalytic activity and conversion capacity are higher than when feeding MeOH. In contrast, the use of MeOH resulted in a higher selectivity towards aromatics and ethylene, suggesting a larger contribution of the aromatic cycle. Authors hypothesized that MeOH favors the formation of formaldehyde, in agreement with the studies of Müller and Hutchings, which leads to a faster deactivation [137].

The influence of the physico-chemical properties of the zeolites in the deactivation has also been investigated during the conversion of methanol-to-hydrocarbons. The creation of a

secondary network of pores with mesopore dimensions within the existing micropore system in the zeolite framework has been a widely used technique to enhance the catalyst lifetime [127, 128, 148-153]. The improvement in catalyst lifetime is reported to be due to enhanced diffusivity of the intermediates and products of reaction through the crystal as well as the higher accessibility to the active sites. However, it is important to consider that the formation of a secondary network of pores in the structure also influences other properties such as acidity [31, 127], which can also modify the catalytic performance of the zeolites.

Subtle changes on the physical properties of zeolite structures, such as the size of the cavities formed by channel intersections on 3D 10-ring zeolites have been investigated during the conversion of methanol-to-hydrocarbons. It was reported that zeolites with larger cavities led to a significant increase in polyaromatic species trapped in the zeolite framework, which consequently shortened the catalyst lifetime [134].

In another study, the performance of a large set of H-ZSM-5 catalysts with different degrees of defects (measured by the ratio between internal and external silanol groups which corresponds to the bands in the infrared spectrum at 3726 and 3745 cm^{-1}, respectively) showed that the deactivation on H-ZSM-5 catalysts is governed by the internal defects. Authors pinpointed that materials with a low internal silanol density and/or large external surface area are expected to deactivate at a slower rate during the MTH process, and vice versa [154].

The same role of internal defects as that reported over H-ZSM-5 seems to be present in other zeolites with different topology, as it has been reported in materials with DDR structure. In this case, an analogous much faster deactivation was obtained on samples with large number of internal defects [139].

As it can be seen from the previous paragraphs, the formation and evolution of the species that lead to the deactivation of zeolite catalysts can be influenced by a large set of parameters. Therefore, various experimental techniques are required to provide insights into the properties of the coke formed.

Thermogravimetric analyses (TGA) are the classical tool for determining the amount and composition of deactivating species. They are carried out by monitoring the changes in weight and by obtaining the C/H/O ratio in the products detected by mass-spectrometry.

However, thermogravimetric techniques provide very limited information about the nature of the coke. This challenge was overcome in the late 1980s' by the introduction of the "Guisnet method" [155]. By this technique, the nature of coke species retained in the pores of the zeolite can be easily obtained. The addition of hydrofluoric acid to the zeolite results in the dissolution of the structure with the subsequent liberation of the retained hydrocarbon species, which are usually extracted by a solvent and further analyzed by GC-MS. In recent years, other *ex situ* and *operando* techniques, mainly spectroscopic, have been applied to monitor the formation and evolution of coke during the MTH reaction. Some of these studies have made used of FTIR techniques [156, 157], UV-vis [158-160], NMR [98, 161], Raman effect with UV light [162], EPR [126, 163], XRD [133], LDI-TOF-MS [164], TEOM [165], confocal fluorescence and UV-Vis micro-spectroscopy [158].

In addition to the large set of experimental techniques that provide meaningful information about the deactivation and the formation of coke, within the study of zeolite deactivation it is also of outmost importance the use of mathematical models that help us simulate and categorize the deactivation of zeolite catalysts in the methanol-to-hydrocarbons reaction. Among the different existing deactivation models [124, 125, 166, 167], those reported by Janssens` [124] and Janssens et al. [125] are of particular relevance for this PhD. Both models consider zeolite deactivation simply as a loss of effective contact time with time-on-stream. Janssens model [124] was initially developed for the commercially used H-ZSM-5 catalyst, and the approach resulted from the observation that the variation in product yield over H-ZSM-5, in particular an increase in ethene and propene yield before methanol break-through, was similar to the evolution of the products at increasing space velocity [65]. A pre-assumption of this model is that deactivation is non-selective, i.e. that the individual product yields obtained at a given conversion level are the same in a fresh catalyst as in a partially deactivated catalyst. This pre-assumption has been validated for H-ZSM-5 [168], H-ZSM-22, H-ZSM-23, H-EU-1 [113] and H-SAPO-5 catalysts [119]. A further assumption of Janssens' model is that the deactivation rate is first order in methanol and proportional to methanol conversion. These assumptions merely mean that coke formation from products alone is negligible (an assumption which was supported by experimental evidence on H-ZSM-5 [124]) and furthermore, that the selectivity to coke formation is constant from zero to full methanol conversion.

Janssens' model has been successfully applied to determine the deactivation rate of a large set of H-ZSM-5 catalysts [154]. However, a limitation of Janssens' first model lies in the fact that it does not take into account the autocatalytic nature of the MTH reaction. Therefore, the more complex correlation between the applied contact time and the methanol conversion capacity for catalysts with a non-negligible initiation zone was not accounted for. This limitation was addressed by the autocatalytic deactivation model, which was subsequently developed by Janssens et al. [125], based on the observation that the conversion capacity of H-ZSM-22 as MTH catalyst increases linearly with an increase in applied contact time, τ_0, i.e. with the ratio between catalyst weight and total gas flow (W/F). In this revised model of Janssens et al. the rate of methanol conversion is expressed as:

$$dM/_{d\tau} = -k_1 M - k_2 MP$$

Where: M is methanol concentration and P is product concentration. Such a simplified expression is warranted by the stable steady-state product distribution reported for many MTH catalysts in the 0 – 80 % conversion range [169]. Mathematical manipulation led to the following simplified correlation between the catalyst lifetime to 50 % methanol conversion, $t_{1/2}$, and the deactivation coefficient (a):

$$t_{1/2} = (\tau_0 - \tau_{crit})/_a$$

Where: τ_0 is the applied contact time (W/F) and τ_{crit} is the critical contact time, i.e. the contact time needed to build up sufficient autocatalytic pool species to launch the autocatalytic reaction. Using this autocatalytic deactivation model the deactivation over H-ZSM-22 catalyst was successfully modeled [125].

Since the usefulness of mathematical models in the description of zeolite deactivation is obvious, Janssens' and Janssens et al. models have been extensively used as a tool for analyzing the results obtained during the PhD as it is shown in Section 5: Summary of the results.

With these paragraphs, the third chapter of the Thesis concludes after having reviewed the main drawbacks that zeolite display as solid catalysts and the different ways of studying and categorizing the deactivation of zeolites in the MTH.

In the subsequent chapters, an overview of the experimental techniques used throughout this work is provided and finally, a summary with the most important findings resulting from the last three years of research is shown .

4. Experimental

This section provides a general description of the various characterization techniques used during this work.

4.1 Catalyst preparation

The primary focus of this Thesis is to investigate the long-term catalytic performance of various zeolite catalysts during the conversion of Methanol-to-Hydrocarbons. For practical reasons, no particular emphasis was given to the synthesis of the catalysts. The majority of the zeolites employed were commercially available. It is important to remember that commercial catalysts are not model materials. Specific properties such as particle size or acid site density were not decided beforehand in most of the materials used in this work. The main point of using commercial catalysts, which are more difficult to work with than model materials, is that the relevance and application of the studies performed are inherently of a higher degree of interest.

However, some zeolites were synthesized by other members of the Catalysis Group of the University of Oslo. A description of the most relevant samples, with their Si/Al ratio provided by the supplier is given below. For additional information about the entire set of catalysts used throughout the Thesis, see Table A-1 in Appendix A.1. Additional results.

- ZSM-5
    - MFI-27 (Si/Al = 15): Süd-Chemie.
    - Pentasil (Si/Al = 45) : Süd-Chemie.
    - PZ-2-25H (Si/Al = 12): Zeochem International.
    - PZ-2-100H (Si/Al = 50): Zeochem International.
- Mordenite
    - Mordenite 14-386 (Si/Al = 11): Ventron.
    - CBV-21A (Si/Al = 11): Zeolyst International.
- ZSM-22
    - ZSM-22 (Si/Al = 45) Zeolyst International.

- Beta
    - Beta-CP806 (Si/Al = 17): Zeolyst International.
    - Beta-CP7119 (Si/Al =13) : Zeolyst International.
    - Beta-CP814E (Si/Al = 14): Zeolyst International.

Calcination and ion exchange.

Regardless of the origin (industrially available or in-house synthesized) of the materials, zeolites were firstly calcined using a pure flow of oxygen in a tubular oven at 550 °C for 12 h to ensure the complete removal of the organic template used during synthesis.

After calcination, zeolites were ion exchanged three times with a 1M NH_4NO_3 solution in a plastic flask at 70 °C during two hours each exchange. The protonated zeolite with Brønsted acidity was obtained after calcination of the materials in static air at 550 °C for 10 h.

4.2 Catalyst characterization

Physico-chemical properties of the fresh, partially or completely deactivated zeolite catalysts were obtained using diverse characterization techniques. An overview of each of them is outlined below.

Powder X-Ray Diffraction (XRD)

Diffraction is defined as the phenomenon that occurs when an incident radiation, whose wavelength is in the same order of magnitude as the distance between the crystal planes of the sample, *d*, interacts with an ordered solid structure; in this case zeolites. In this work, zeolites are analyzed in powder form, and the resulting X-Ray diffractogram can be used as a unique “fingerprint” to a particular crystalline phase.

X-Ray Diffraction is a suitable tool not only for identifying the zeolite structure, but also for investigating the purity phase of the materials. Besides, more complex applications such as deriving models of unknown zeolite structures from X-Ray diffraction patterns can also be done [170]. Owing to its broad applicability, XRD represents a key analytical tool in the zeolite science.

Most of the powder X-Ray diffractograms were collected between 2-θ=5-50 ° using a Bruker D8 Discover instrument with CuKα radiation (λ = 1.5406 Å).

Elemental analysis

Provided that zeolites displayed their corresponding crystalline phase, the amount of Si and Al was quantified by elemental analysis.

Chemical compositions on fresh zeolites were performed using a Microwave Plasma Atomic Emission Spectrometer (MP-AES 4100) from Agilent Technologies. Approximately 50 mg of zeolite was dissolved in 1 mL 15 wt% HF for 30 minutes in a home-made Teflon vial. The dissolved zeolite was transferred to a 50 mL polypropylene volumetric flask containing 0.15 g of boric acid to neutralize the remaining hydrofluoric acid. The flask was subsequently filled with deionized water.

Scanning Electron Microscopy

Scanning Electron Microscopy (SEM) was performed to evaluate the particle size as well as the morphology of the zeolite catalysts. Zeolite samples were dispersed over a carbon tape attached to a copper grid, which was mounted inside the instrument. The excess of sample was removed by blowing pressurized air onto the tape. Micrographs were recorded under high vacuum conditions using a Hitachi SU 8230 FE-SEM working at 5-10 kV, with beam acceleration mode at working distances of around 10 mm. In addition, the instrument provided the possibility of determining the composition by Energy Dispersive Spectroscopy (EDS).

Physisorption measurements

N_2 adsorption isotherms were performed to assess the textural properties, i.e. surface area and pore volume of the zeolites studied.

Measurements were carried out at 77 K on a Bel Belsorp-mini II apparatus. The surface area was obtained using the Brunauer–Emmett–Teller (BET) model [171, 172] in the range of validity for microporous materials [173], the external surface area were evaluated using the *t-plot* method [174, 175], and the micropore volume was evaluated using two approaches. First, the standard *t-plot* approach was used, which is suitable for materials displaying

isotherms types I and IV [176]. Second, the micropore volume was estimated from the N_2 uptake at a relative pressure p/p_0 = 0.2, converting the gas uptake to the equivalent liquid volume. This second approach is introduced primarily due to difficulties in applying the *t-plot* method to partially deactivated catalysts with low pore volumes.

When textural properties were evaluated on fresh zeolites, samples were outgassed in vacuum for 4 hours. First, 1 h at 80 °C followed by 3 h at 300 °C. However, when the surface area and pore volumes were determined in totally or partially deactivated samples, materials were pretreated for 1 h at 80 °C and 3 h at 200 °C in order to remove exclusively the water content, avoiding the removal of deactivating species.

Infrared Spectroscopy (IR)

The accessibility, strength and concentration of the acid sites on the protonated zeolites, and in some partially deactivated catalysts, were investigated using Fourier Transformed Infrared (FTIR) spectroscopy. CO and pyridine were chosen as probe molecules to evaluate the strength and concentration of active sites, respectively.

FTIR spectra were collected on a Bruker Vertex 80 instrument with a Mercury Cadmium Telluride (MCT) detector using a resolution of 2 cm^{-1}. An in-house designed transmission cell with KBr windows was used for the experiments.

Catalysts were prepared as thin wafers and supported in a gold envelope. Fresh zeolites were pre-treated in vacuum (<10^{-5} mbar) for 3 hours: 1 h at 150 °C followed by 1 h at 300 °C and finally 1 h at 450 °C. Partially deactivated samples were pretreated at 80 °C for 1 h and for 3 h at 200 °C. After activation, the spectrum of the fresh zeolites was recorded, ensuring that materials were completely dehydrated, which is confirmed by the observation of a flat line in the frequency range 3300-2500 cm^{-1} in the sample spectrum.

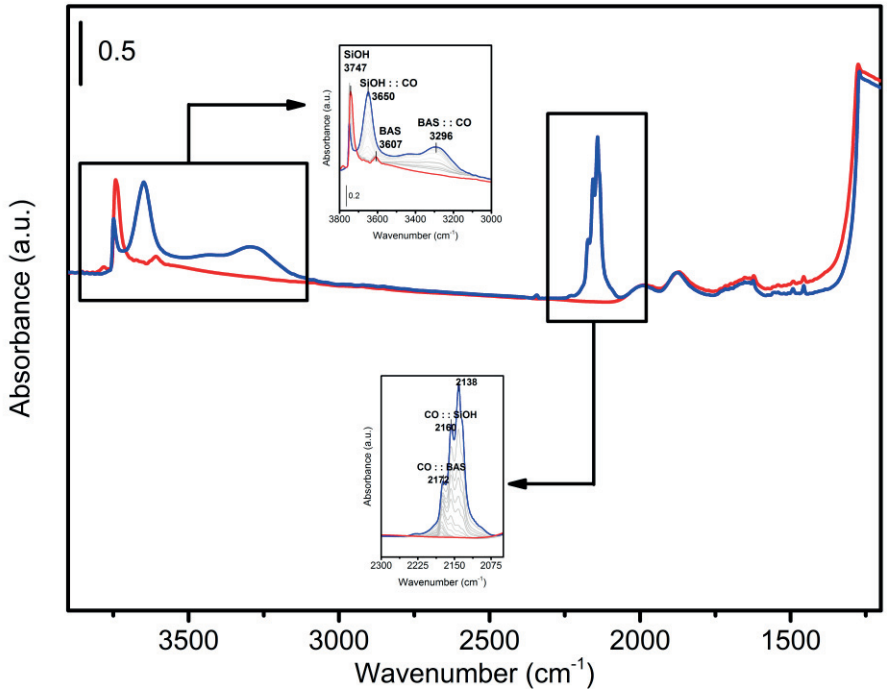

Figure 4.1. FTIR spectra of a H-Beta zeolite interacting with CO. Red spectrum was collected at room temperature after the zeolite activation. Blue spectrum was collected at 77 K and corresponds to the maximum dosage of CO. The top inset shows the FTIR spectra on the hydroxyl region whereas the bottom inset displays the stretching modes in the CO region. Grey spectra were collected while CO desorption.

On an activated zeolite, two well-distinct features are distinguishable in the –OH stretching region, ranging from 3750 cm^{-1} to 3610 cm^{-1}. The band detected at 3750 - 3745 cm^{-1} is assigned to isolated silanol groups on the external surfaces, whereas the band in the observed at 3610 cm^{-1} corresponds to the stretching mode of bridging hydroxyl groups (BAS) (-Al(OH)Si-)[9, 29] (Figure 4.1 top inset)

When CO was used as probe molecule, it was dosed into the cell before zeolites were cooled down to liquid N_2 temperature (77 K). Then, spectra were recorded while CO was desorbed by evacuation at regular intervals. Carbon monoxide acts as a weak base when it interacts with the hydroxyl groups of the zeolites. As a result, a red shift (shift towards shorter wavenumbers) is observed in the bridging hydroxyl bands. As an example, the intensity of the bridging Brønsted acid sites (BAS) (3610 cm^{-1}) decreases, whereas a broad band at around 3280-3295 cm^{-1} concomitantly appears. The degree of this red shift can be considered as an estimation of the zeolite acid strength. Similarly, upon increasing CO coverage, the band associated with external SiOH groups (3750 cm^{-1}) shifts towards lower wavenumbers (Figure 4.1 top inset). On the other hand, upon adsorption of CO, different bands appear on the CO stretching region (Figure 4.1 bottom inset). The sharp band at 2138

cm^{-1} is assigned to liquid-like CO physically adsorbed on zeolites[29]. Besides, the bands at 2172 and 2160 cm^{-1} correspond to the interaction between CO with the Brønsted acid sites and with silanol groups, respectively.

While the information that can be obtained about acid strength when CO is used as probe molecule is mainly qualitative, the use of pyridine as probe molecule allows us to get quantitative information about the concentration of Brønsted and Lewis acid sites (BAS, LAS, respectively) on fresh and on partially deactivated zeolites. Upon Py dosage, complete consumption of the band assigned to Brønsted acid sites (3610 cm^{-1}) is observed. In addition, bands appear centered at 1544 and 1455 cm^{-1}, which are assigned to pyridine adsorbed on Brønsted and Lewis acid sites, respectively [177] (Figure 4.2). The adsorption of pyridine was done by exposing the pellets to the vapor pressure of pyridine at room temperature. Spectra were recorded while excess pyridine was desorbed. The samples were considered to be saturated when no differences between two consecutive spectra were observed. Then, catalysts were evacuated at 200 °C for 2 hours in order to remove the physisorbed species. Afterwards, the final spectrum used for quantitative measurement was recorded. The concentration of Brønsted and Lewis acid sites was calculated using the equations shown below, by integrating the bands at 1544 and 1455 cm^{-1} and using Integrated Molar Extinction Coefficient (IMEC), which are reported elsewhere [177], for the BAS and LAS, respectively.

$$[\text{Brønsted Acid Sites}]\left(\frac{\text{mmol}}{\text{g}}\right) = \frac{\text{IA}_{1544} \cdot \text{Area}_{\text{wafer}}\,(\text{cm}^2)}{\varepsilon_{\text{BAS}}(0.73) \cdot \text{Mass}_{\text{wafer}}(\text{mg})}$$

$$[\text{Lewis Acid Sites}]\left(\frac{\text{mmol}}{\text{g}}\right) = \frac{\text{IA}_{1454} \cdot \text{Area}_{\text{wafer}}\,(\text{cm}^2)}{\varepsilon_{\text{LAS}}(0.64) \cdot \text{Mass}_{\text{wafer}}(\text{mg})}$$

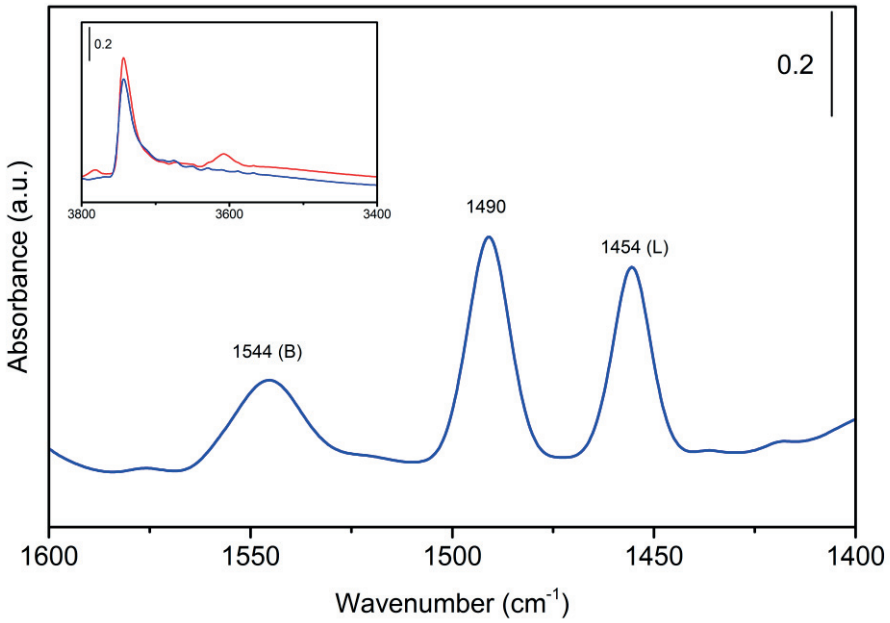

Figure 4.2. FTIR spectra of H-Beta zeolite interacting with pyridine. The inset shows the hydroxyl region where the red spectrum corresponds to the activated zeolite and the blue is the spectrum at the maximum coverage of pyridine.

UV - Raman Spectroscopy

Raman Spectroscopy is a vibrational technique that originates from the inelastic scattering of the electromagnetic radiation i.e. the kinetic energy of an incident radiation is not conserved. The inelastic scattering of the light is defined as the process by which a wave, or particle, is deflected from its original trajectory as a consequence of the interaction with another particle or wave. This spectroscopic technique has been used in this work to investigate both *ex-situ* and under *operando* conditions the nature of the active and deactivating species on the MTH reaction using different zeolite topologies.

In order to minimize the presence of fluorescent species formed upon the interactions of methanol with zeolites, instead of exploiting the Raman effect using visible light, we investigate the Raman effect using UV light. By using this technique most of the targeted molecules are not emissive in this region of the spectrum.

The UV-Raman experiments were performed at the Department of Chemistry-University of Turin, an associated partner in the ZeoMorph Project. Measurements were carried out in collaboration with Dr. M. Signorile under the supervision of Dr. F. Bonino and Prof. S.

Bordiga. UV-Raman spectra were collected on a Renishaw inVia Raman Microscope spectrometer, equipped with a 3600 lines/mm grating to disperse the scattered light on a UV enhanced, Peltier cooled Charge-coupled device (CCD) detector. The excitation beam was focused on the sample through a 15× long working distance objective. The Rayleigh peak was removed by a dielectric edge filter. A Coherent MotoFred 300C frequency doubled Ar^+ laser, emitting at 244 nm, was used as excitation source. In order to exploit the full power of the laser on the samples (about 5 mW) without beam induced damage, the measurements were performed with continuous movement of the samples, using two different setups. On the one hand, the sample prepared as a thin pellet, was in continuous movement exploiting the features of an in-house designed cell [178, 179]. On the other hand, a commercial Linkam CCR1000 reactor cell was used. Catalysts on the latter cell were continuously fluidized using a device that generates pulses with regular frequency, as reported in literature [162].

Thermogravimetric Analysis (TGA)

Thermo-gravimetry has been a technique of particular use in this work because it allows us to determine quantitatively the amount of deactivating species formed in the zeolite catalysts. Experiments were performed on a Rheometric Scientific STA 1500 instrument. Typically, 15 mg of catalyst was heated to 700 °C with a flow of 25 mL min^{-1} of synthetic air using a heating rate of 5 °C min^{-1} and a hold time of 40 min. Total coke is obtained in wt% relative to the regenerated catalyst (final mass in the TGA profiles).

Analysis of the retained coke species.

The identification, distribution and quantification of deactivating species retained in the zeolite structure was performed following the Guisnet method [155]. This method is based on the dissolution of the zeolite structure using HF, thus liberating all the compounds trapped in the pores. Then, soluble coke species, which are extracted using a solvent, are analyzed by Gas Chromatography-Mass Spectrometry (GC-MS).

Experimentally, 15 mg of completely or partially deactivated sample was dissolved in small Teflon vials using 1 mL 15% HF during 60 min. The addition of 1 mL of CH_2Cl_2 with ortho-chloro-toluene as internal standard, allowed the extraction of the soluble fraction of coke,

which was subsequently analyzed and quantified by GC-MS using an Agilent 7890 GC with a HP5-MS column (60 m, 0.25 mm i.d, stationary phase thickness 0.25 µm) connected to an Agilent 5975 mass spectrometer. The oven temperature was increased from 50 °C to 300 °C with a heating rate of 10°C min^{-1} (hold time 3 minutes at 50 °C and 15 minutes at 300 °C). For compound identification, the NIST98 database was used.

4.3 Catalytic testing

The core of this PhD Thesis is focused on the investigation of the long term catalytic performance of various zeolites. Hence, special efforts were made in evaluating the activity and lifetime of different zeolite catalysts. This was carried out at two different places during the PhD: at the Chemistry Department of the University of Oslo and at Haldor Topsøe A/S facilities.

Catalytic testing at the University of Oslo

Catalytic testing experiments were performed in a Plug Flow Reactor using both, U-shaped and straight quartz reactors with inner diameters of 9 or 6 mm. In addition, a 2 mm thermocouple well was inserted in the reactor and placed in contact with the catalyst to monitor the temperature of the reaction. Catalyst particles were pressed, gently crushed and sieved to sizes between 250-420 µm, to avoid pressure build-up. As a general rule, catalytic tests were performed at atmospheric pressure and 400 °C. In addition, Weight Hourly Space Velocity (WHSV) of 2 $g_{MeOH}\ g_{cat}^{-1}\ h^{-1}$ was normally used in the experiments. Should different WHSV values were desired for a particular reaction, either the mass of catalysts or the reactant flows were modified accordingly. Prior to reaction, catalysts were pretreated at 550 °C under He flow. At this temperature, catalysts were calcined in situ for 1 hour using a flow of pure O_2. Then, the temperature was lowered to the actual reaction temperature (400 °C) and He, used as a carrier gas, was bubbled through a methanol saturator. MeOH (supplied by BDH Laboratory > 99.8% purity) was kept at 20 °C, giving rise to a methanol partial pressure of 130 mbar.

Products of reaction were analyzed on-line using an Aglient 6890 A GC with a Flame Ionization Detector (FID). The equipment has a Supelco SPB-5 capillary column with dimensions of 60 m × 0.53 mm × 3 µm.

A basic Process Flow Diagram (PFD) of the setup used in the catalytic experiments is provided in Figure 4.3.

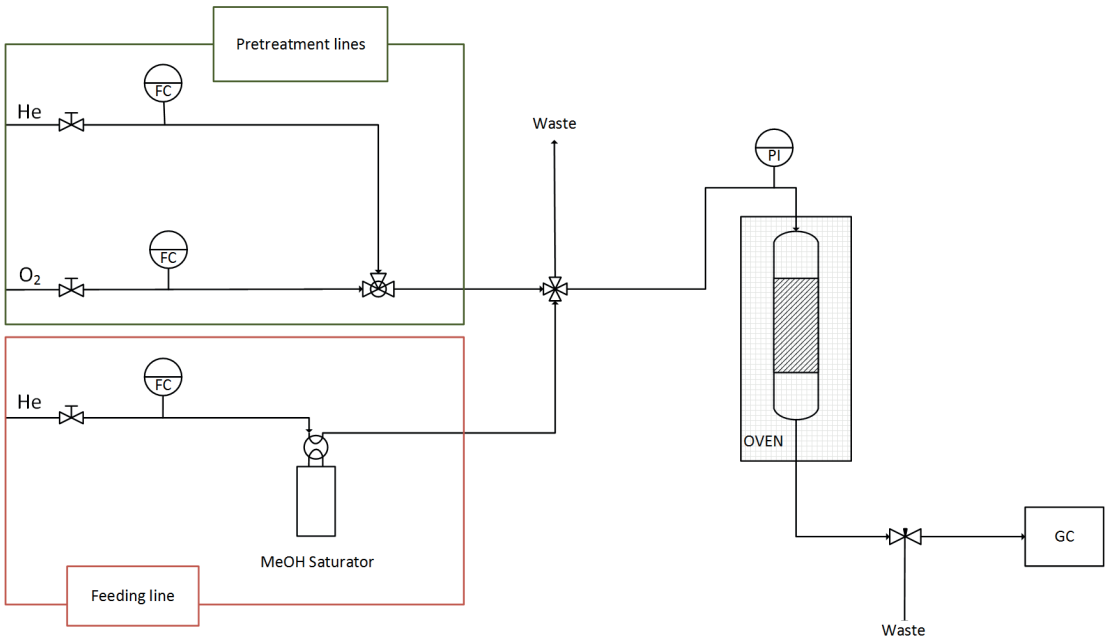

Figure 4.3. Schematic Process Flow Diagram (PFD) of the setup used for the catalytic tests performed at the laboratories of the University of Oslo.

Catalytic tests at Haldor Topsøe

During the period spent at Haldor Topsøe A/S, MTH reactions at industrial relevant conditions using H-ZSM-5 catalysts were performed. The capabilities of the industrial partner of the project allowed us to evaluate the catalytic performance at elevated pressures, thereby simulating the experimental conditions of MTH processes available in the market such as TIGAS (Topsøe Integrated Gasoline Synthesis). The application of reaction conditions similar to the ones in the industrial processes and the use of commercial H-ZSM-5 catalysts, provides an additional relevance to this work.

Catalytic results shown in **Paper III,** in addition to some of the results presented in **Paper IV** were obtained in a Micro-Reactor unit available at Haldor Topsøe A/S.

The catalytic behavior of various H-ZSM-5 catalysts was evaluated at 643 K and 20 bar_g in a 2 mm I.D. down-flow fixed-bed stainless steel U-shaped reactor using 150 mg (sieved fraction 150-300 µm). Prior to the reaction, catalysts were activated for 2 hours at 773 K using a

stream of N_2 with 2 % of O_2. Then, the temperature was lowered to the reaction temperature (643 K) and methanol was pumped into an evaporator at the rate of 0.025 ml min^{-1}. The gaseous methanol was mixed with N_2, resulting in a WHSV of 8 g_{MeOH} $g_{catalyst}^{-1}$ h^{-1} and the mixture was subsequently fed to the reactor. Reactor effluent was analyzed by online gas chromatography using an Agilent 7890A, with flame ionization detector, equipped with a Restek Rtx®-DHA-150 column (150 m, 0.25 i.d., stationary phase thickness 1 µm).

A flow diagram of the reactor setup used at Haldor Topsøe is shown in Figure 4.4.

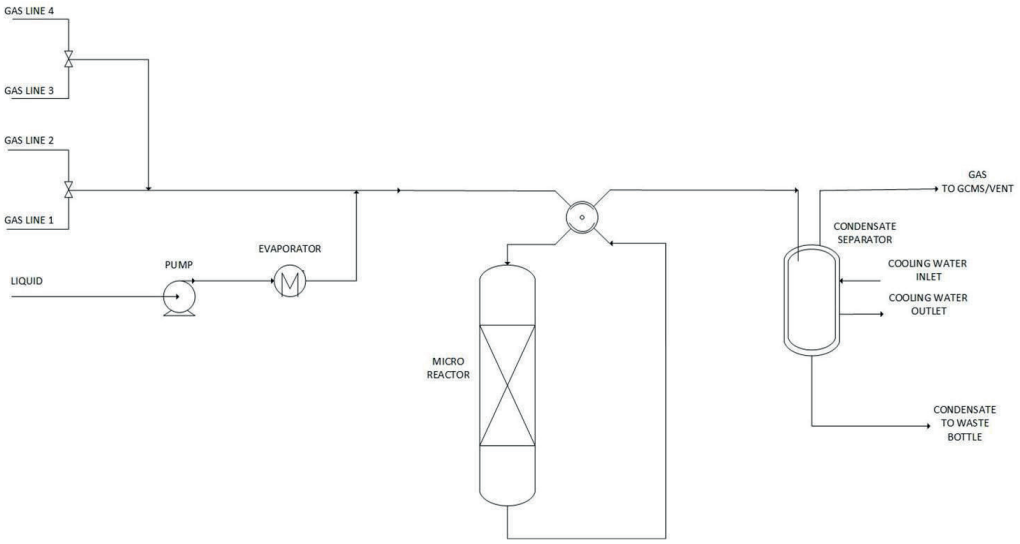

Figure 4.4. Process Flow Diagram (PFD) of the catalytic testing setup used at Haldor Topsøe.

Regardless of the setup used for the catalytic testing experiments (at the University of Oslo or at Haldor Topsøe A/S), the resulting areas from the GC-FID chromatogram were used to evaluate parameters such as: the conversion of methanol (X), product selectivity (S_i) and product yield (Y_i), using the equations reported below. It is important to note that both, methanol and DME were considered as reactants. Besides, adequate response factors were used for these oxygenates whereas no additional correction was used for the integrated peaks corresponding to the products of reaction.

$$X(\%) = \frac{Total\ area - area\ of\ MeOH\ - area\ of\ DME}{Total\ area} \times 100$$

$$S_i(\%) = \frac{Area\ of\ Product_i}{Total\ area\ of\ Products} \times 100$$

$$Y_i(\%) = \frac{Area\ of\ Component_i}{Total\ area} \times 100$$

4.4 Operando High Energy XRD

Time- and space- resolved High Energy X-Ray Diffraction (HXRD) studies of the MTH reaction were performed under *operando* conditions on the Swiss-Norwegian Beamline (BM01) at the European Synchrotron Radiation Facility (ESRF), in Grenoble (France).

The MTH reaction at the ESRF was carried out using capillary reactors with 0.5 mm O.D. and 0.49 mm I.D. Approximately 1 mg of catalyst (212-250 µm size) was placed between two thin layers of quartz wool. The reactor was mounted horizontally on a Huber station enabling the translation of the reactor in the axial direction, so that XRD measurements were collected on different sections of the catalyst bed. Even though it is known that horizontal reactors may increase the risk of uneven flow, the design of the setup at ESRF allowed us only to work using the horizontal reactor configuration. Nevertheless, in order to ensure a homogeneous flow, the capillary reactor was rotated 30° clock- and counterclockwise in each individual areas of the bed during the data collection. In addtion, relatively high space velocities were used.

The reactor was connected on one side, to the gas system used as inlet and to the Huber goniometer used for alignment (Figure 4.5). On the other side of the capillary (outlet), products of reaction were analyzed on-line by a Pfeiffer Omnistrar Mass Spectrometer. The reactor was heated with an Osram Sylvania heat blower which provided an isothermal zone with temperature gradients of less than 5 °C along the reactor, as it was measured by placing a thermocouple inside of an empty capillary reactor.

In order to maximize the number of experiments performed during the allocated synchrotron time, the MTH reaction was carried out at higher space velocities than the ones used at the home laboratories, achieving faster deactivation, yet, with initial full conversion of methanol. In these experiments, H-ZSM-5 zeolites with different properties (composition and crystal size) were used as acid catalysts. First, catalysts were heated up with inert gases up to temperatures between 450 – 500 °C (depending on the experiment). The activation of the catalysts was carried out for 1 h using a flow of synthetic air. Subsequently, the temperature was lowered to the desired reaction temperature (400 or 450 °C depending on the samples). 2.2 mL min^{-1} of Ar, used as carrier gas, was bubbled through a methanol saturator kept at room temperature, resulting in a WHSV of 20 $g_{MeOH}\ g_{catalyst}^{-1}\ h^{-1}$.

Powder X-Ray Diffraction Data was measured using a wavelength of 0.7743 Å and acquired on a Pilatus 2M detector. Data was subsequently integrated into a 1D powder diffraction pattern. During the data collection, the capillary reactor was moved horizontally along the beam, so that diffraction patterns were collected on 10-14 different positions of the reactor, using a time resolution of approximately 180 seconds to perform a complete scan of the entire reactor. A graphical description of the setup used during this experiment is shown in Figure 4.5.

Results from each fraction of the catalyst bed were refined in sequential mode, putting special interest to the evolution of the unit cell parameters at increasing degree of deactivation on the different sections of the bed.

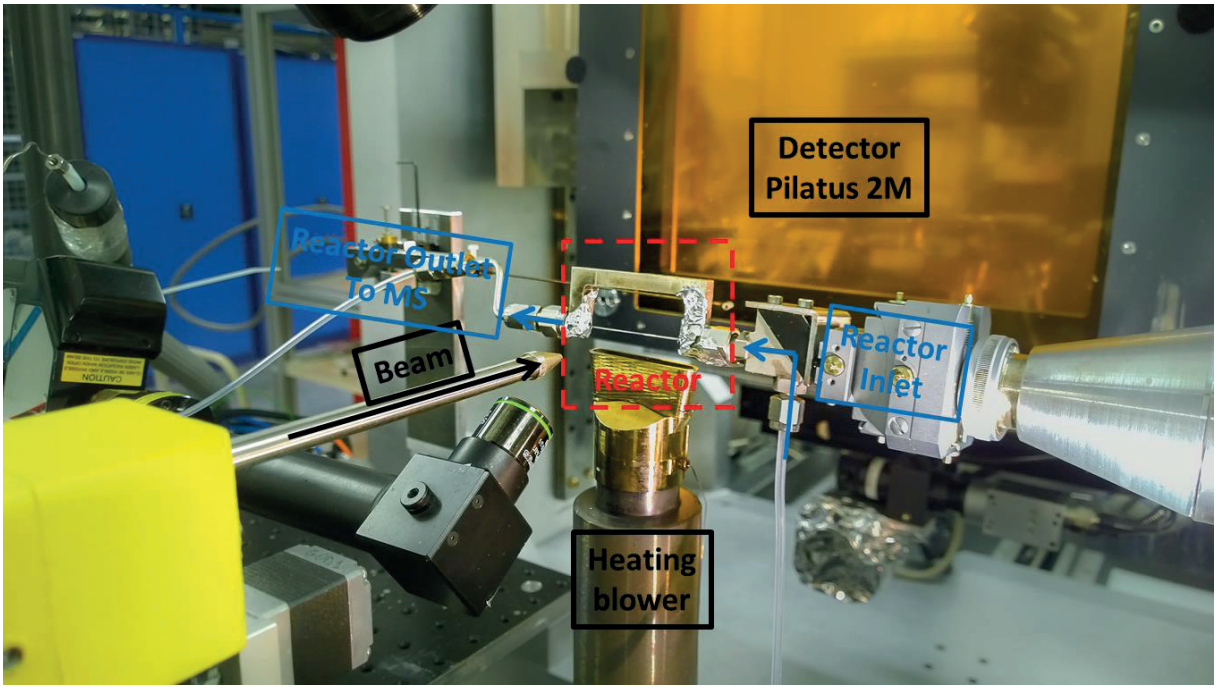

Figure 4.5 Overview of the setup used during the acquisition of *operando* high energy XRD at ESRF

5. Summary of the results

This chapter provides a summary of the most relevant results obtained during the PhD. It is divided in three sections; each of them is focused on the most important topics of the investigation. Presenting the results in this way creates a more coherent overview and it enables the reader to follow the work more straightforwardly than what it would be possible by presenting the papers in chronological order. Extended discussions of the results as well as additional figures and graphs can be found in the manuscripts attached as appendices to this Thesis.

Section 5.1 focuses on the influence of zeolite topology on the catalyst deactivation by hydrocarbon deposition. More specifically, the nature of coke, its content, and the axial deactivation profiles during the conversion of methanol-to-hydrocarbons were investigated, being the zeolite topology the main parameter varied on the studies. Resulting from this investigation, 2 manuscripts are published.

In section 5.2, the role of particle morphology on the catalyst performance and deactivation during the MTH process is looked into. In this work, the topology of the catalyst was maintained. H-ZSM-5 with MFI topology was selected because of the importance of this catalyst in the MTH process at industrial scale. Three samples with different particle shapes and sizes were tested as acid catalysts under industrial relevant conditions. Resulting from this investigation, one manuscript is being prepared.

Finally, the last section of this chapter, 5.3, provides an overview of the results obtained when the deactivation over H-ZSM-5 catalysts is investigated, using the changes that take place in the zeolite framework as parameter of study. This section arises as a consequence of the findings presented in 5.2. However, owing to the novelty of the results obtained, a dedicated passage is included.

5.1 Influence of the zeolite topology on the deactivation by coke during the conversion of Methanol-to-Hydrocarbons

Role of zeolite topology in the nature and content of the deactivating species in the MTH reaction

The first objective of the PhD was to evaluate the influence of the zeolite topology on the deactivation during the MTH process. Particularly, special efforts were devoted to the quantitative assessments of the coke content, and also to the determination of the coke nature for the different catalysts used. In order to achieve this goal, the evolution of deactivating species was studied in 5 different catalysts, 4 aluminosilicates zeolites (H-Mordenite, H-ZSM-22, H-ZSM-5 and H-Beta) and one silicoaluminophosphate zeotype (H-SAPO-34), as function of the MTH reaction time. Rather than relying on model materials, all the catalysts investigated were supplied by commercial zeolite manufacturers (except the H-SAPO-34, which was synthesized according to the patent literature [180]). This approach was chosen to make probable that the materials studied reflect the behavior of actual, commercial catalysts. The topologies of the catalysts used in this work are described in the Supplementary Material of **Paper I**.

For each topology, a series of catalysts with increasing degree of deactivation were obtained by performing the methanol-to-hydrocarbons reaction at increasing times-on-stream using a fix-bed reactor. The conditions for the experiments were 400 °C, P_{atm} and a Weight Hourly Space Velocity (WHSV) of 2 $g_{MeOH}\ g_{cat}^{-1}\ h^{-1}$ for all the materials. Subsequently, the partially deactivated catalysts were characterized using N_2 adsorption to determine the textural properties at increasing degree of deactivation and thermogravimetric analyses to obtain the total amount of coke. Furthermore, the nature of the deactivating species was studied by the dissolution-extraction protocol. Finally, UV-Raman spectroscopy was applied to shed further light on the chemical nature of the deactivating species.

Basic characterization results of the five different catalysts used in this study is provided on the main text as well as on the Supplementary Material of **Paper I**.

First, an experiment until total deactivation was performed with each catalyst to evaluate the overall lifetime. Subsequently, suitable reaction times were specifically chosen to follow the deactivation for each catalyst topology. Figure 5.1 shows the lifetime for the five catalysts used. In agreement with previously reported results [50], the topology of the materials plays an important role on the catalyst lifetime. In general, zeolites with unidimensional pores and channels, i.e. H-Mordenite and H-ZSM-22, lose their activity rapidly and therefore deactivate faster than zeolites whose channels are distributed in the three dimensions, as it is the case in H-ZSM-5, H-Beta and H-SAPO-34. It is also well established that the product distribution in the MTH process is directly correlated with the zeolite topology [50]. The 8-rings of the H-SAPO-34 limits the production to linear alkenes, whereas 10-ring structures, depending on the exact channel diameters and interconnectivity, allow branched olefins and small methylated benzene species to diffuse out the crystal. Finally, large pore size zeolites let the formation and diffusion of aromatic species as big as hexamethylbenzene out of the zeolite channels. The product yields and selectivities for the five catalyst used in this work, which are shown in **Paper I**, support the idea that an increase in pore size leads to an increase in the size of the molecules that can diffuse from the zeolite structure.

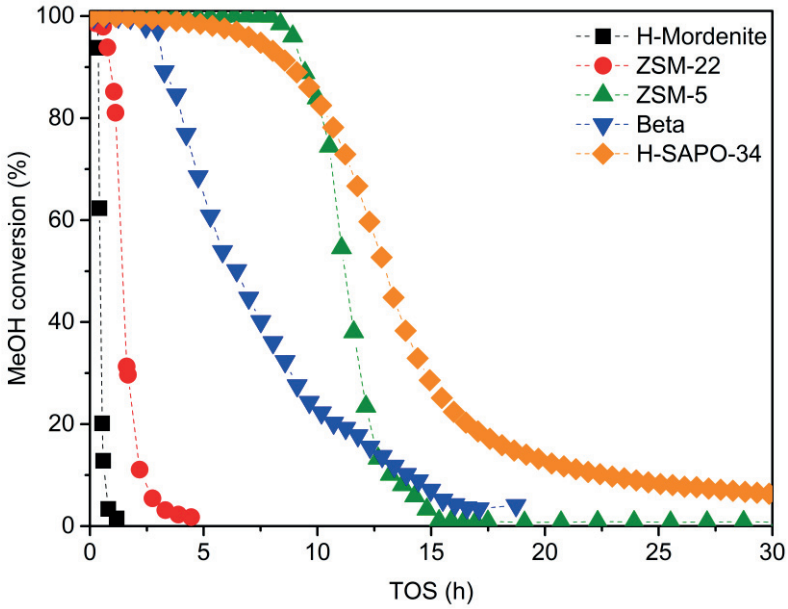

Figure 5.1 Catalyst lifetime for the five zeolite-based catalysts investigated. Experiments were performed at 400 °C, Patm and with a WHSV of 2 $g_{MeOH}\ g_{cat}^{-1}\ h^{-1}$

The conversion of methanol (Figure 5.1) and product selectivity were proven to be influenced by the zeolite topology, however, the main objective was to assess quantitative- and qualitatively the coke content and its evolution as well as the nature of the deactivating species on the five catalysts studied. The times-on-stream when each reaction was quenched, the textural properties, coke content and conversion obtained at increasing degrees of deactivation for the five different microporous catalysts are shown on Table 2-Table 6 in the main text of **Paper I**. In addition, the chromatograms obtained upon the dissolution-extraction protocol are shown in the Supplementary Material of **Paper I**.

At this point, it should be emphasized that it was the whole catalyst bed which was analyzed. This means that the data shown correspond to an average, disregarding the axial distribution of coke along the bed. It is important to keep this in mind because in subsequent parts of this section, additional studies showing the spatial and time evolution of coke content along the bed will be presented.

The first approach carried out in this work was to analyze the conversion curves using the deactivation model proposed by Janssens [124] in order to obtain the deactivation coefficient (a), the rate constant (k), and the total conversion capacity (R_0). The deactivation coefficient, (a) corresponds to the amount of catalyst (or number of active sites) lost when a mol of reactant is transformed into hydrocarbons, i.e. how rapidly the catalyst is deactivated. The rate constant, (k) gives the activity of the catalyst in millimoles of methanol converted per acid site per hour, and the conversion capacity provides the total amount of methanol converted to hydrocarbon per acid site until complete deactivation. This value can also be obtained by integrating the area under the conversion curves (Figure 5.1). The data obtained is presented in Table 5-1.

Table 5-1 Experimental times to reach 50% and 80% MeOH conversion ($t_{0.5}$) ($t_{0.8}$), rate constants (k), deactivation coefficients (a), conversion capacities (R_0), and overall selectivities to coke for the five catalysts.

Sample	$t_{0.5}$ (h)	$t_{0.8}$ (h)	k (mmol $mol_{acid\ site}^{-1}$ h^{-1})	a (g_{cat} mol_{MeOH}^{-1})	a ($mol_{acid\ site}^{-1}$ mol_{MeOH} $*10^{-3}$	R_0 (mol_{MeOH} $mol_{acidity}^{-1}$) [a]	R_0 (mol_{MeOH} $mol_{acidity}^{-1}$) [b]	Coke selectivity (C%)
H-Mordenite	0.5	0.4	3.7	4.0	3.1	64	72	9.8
H-ZSM-22	1.4	1.1	1.1	1.3	0.5	491	514	1.0
H-ZSM-5	11	10	9.1	0.2	0.2	1415	1405	0.4
H-Beta	6.5	3.4	2.2	0.3	0.3	898	1055	1.2
H-SAPO-34	13.3	10	5.5 [c]	0.1	0.1	1136	1163	0.7

a. Conversion capacity derived from Janssens´ model.
b. Conversion capacity obtained by integration of the conversion curves.
c. For SAPO-34, no experimental measure of the density of Brønsted acid sites could be obtained, and the acid site density is estimated from the composition.

When comparing the activity of the catalysts according to the rate constant, *k*, H-ZSM-5 clearly surpasses the rest of catalysts. For a series of H-ZSM-5 catalysts, it has been shown that the rate constant, when expressed in units per mass of catalyst, is linearly dependent on the density of acid sites [154]. This in turn means that a fixed rate constant would be observed when expressed in units per acid site. When comparing the rate constants in Table 5-1, it becomes evident that such a correlation does not exist when comparing different topologies. The most active catalyst (H-ZSM-5) is able to convert very nearly 10 times as much methanol into hydrocarbons per hour as the least active catalyst (H-ZSM-22). Such topology dependent variations in activity, even when normalized to acidity, have also been observed previously [82]. However, in this contribution, we are able to express the topology dependency of the rate constant (expressed per acid site) in a strictly quantitative manner, which constitutes a significant improvement over previous works.

H-Mordenite displays the highest deactivation coefficient value followed by H-ZSM-22. As shown earlier, the lifetime of these two catalysts is much shorter than in H-ZSM-5, H-Beta and H-SAPO-34. For H-ZSM-5, it has been shown that the deactivation coefficient depends on the intensity ratio of the bands at 3726 and 3745 cm^{-1} in the FT-IR spectrum of the dehydrated catalysts [154], as described in section 3. We attempted to carry out the same analysis for the five catalysts of different topology studied here (FT-IR spectra are shown in Figures S.5-S.9 and the ratio is shown in Figure S.23 in the Supplementary material of **Paper**

I), but no correlation could be found. This demonstrates that the link between silanol defects and deactivation coefficient previously found for H-ZSM-5 catalysts cannot be extended across different catalyst topologies.

For the rapidly deactivating Mordenite catalyst, the large deactivation coefficient is coupled with a remarkably high selectivity towards coke. However, for the other four materials, there is no correlation between the deactivation coefficient and the selectivity towards total coke. Clearly, the catalysts respond very differently when a certain amount of coke is deposited, again emphasizing the importance of topology on the deactivation during the MTH process.

The second approach carried out was to analyze and compare the results from the coke content. Results revealed that the total amount of coke for the fully deactivated catalysts varies greatly among the topologies, (for example in H-ZSM-22 the coke content for the completely deactivated sample was 3.0 %wt, whereas in H-SAPO-34, the amount of coke was 21.2 %wt). Additionally, it was decided to perform structure-deactivation relationships to obtain additional insights into the mode of deactivation and evolution of coke.

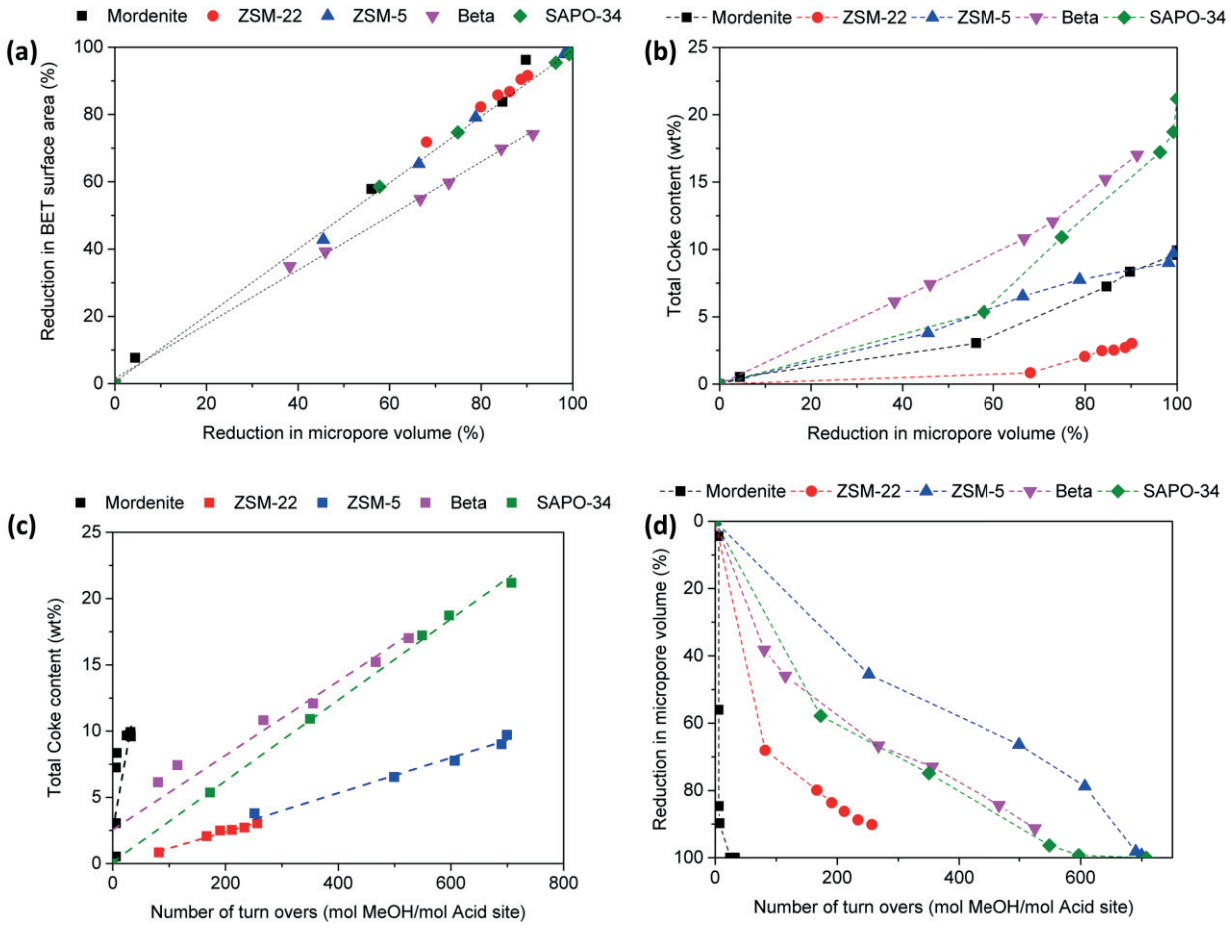

Figure 5.2 Structure-deactivation relationships for the five catalysts: (a) Reduction of BET surface area versus the reduction in micropore volume; (b) Total coke content from TGA versus reduction in micropore volume; (c) Total coke content from TGA versus number of turnovers of methanol; (d) Reduction in micropore volume versus number of turnovers. In panel a), the lines are obtained by regression with one separate regression analysis for H-Beta; the data for the other zeolites are fitted together. In panels (b) – (d), the data points are connected by straight lines.

Panel (a) of Figure 5.2 shows the reduction of the BET surface area against the reduction in micropore volume. It may be noted that for H-ZSM-22 and H-Beta, the reduction of the micropore volume was not complete, even for the fully deactivated catalysts. Interestingly, for H-Mordenite, H-ZSM-22, H-ZSM-5, and H-SAPO-34, these values are very strongly correlated, and an excellent linear fit is achieved even when all four datasets are analyzed jointly. For zeolite Beta, the data follow a different line and parity. This is presumably a consequence of the significant contribution of the external surface area to the total BET area of this sample. According to these results, it is safe to conclude that for all catalysts, the micropore volume and the BET surface area are reduced faster than the deposition of coke. Panel (a) shows that the BET surface area and micropore volume are strictly linearly dependent. Therefore, further analysis may be carried out according to either value without arising different conclusions.

Panel (b) of Figure 5.2 displays the evolution of the total coke content from TGA against the reduction in the micropore volume. For all topologies, an upwards curvature is seen, meaning that the total coke content increases more slowly than the micropore volume/BET surface area is reduced with reaction time.

The panel (c) displays the accumulation of coke as a function of the amount of methanol converted into hydrocarbons per acid site. The shapes of these curves warrant further discussion, keeping Haw's "burning cigar" model in mind [132]. A strictly linear relationship between coke content and the number of turnovers suggests that coking occurs only in the zone of the catalyst bed where methanol is being converted, that the selectivity to coke is constant, and that the actual rate of coke formation therefore depends on the degree of methanol conversion, in accordance to one of the assumptions made by Janssens [124]. A downwards curvature would suggest that coke may be formed also from the products in the length of the reactor bed after the methanol conversion zone. The idea is that as the active zone moves from inlet to outlet, the bed length available for coke formation from the products becomes smaller, and the overall coke formation is reduced. An upwards curvature would imply an increase in coke formation as the catalyst bed progressively becomes deactivated, which is hard to imagine. Results obtained enable to distinguish two different scenarios. For H-Mordenite and for the H-Beta, linear regression does not reasonably yield an intercept through the origin. Rather, a positive intercept is found, and the data appear to level off with increasing number of turnovers. For H-ZSM-22, H-ZSM-5 and H-SAPO-34, on the other hand, a linear fit through the origin does appear reasonable. Thus, the data indicate that coke formation from the products is relevant for H-Mordenite and H-Beta or perhaps for 12-membered ring catalysts in general. Whether the deactivating compounds are formed solely from methanol, as advocated by Schulz [120], or from a combination of methanol and products, or even by product-product condensation [68], constitutes a profound difference in the deactivation mechanism, which we identify as a key topic of study in **Paper II**. On the other hand, the data show that Janssens' model might be somewhat less suited for some topologies, which is not unreasonable, bearing in mind that it was developed originally for H-ZSM-5.

The panel (d) of Figure 5.2 shows the reduction of micropore volume against the number of turnovers. This chart shows two differentiated regimes; the most pronounced decrease in

micropore volume is seen initially, whereas at longer reaction times the reduction occurs more slowly. This is essentially the same behavior as discussed for panel (b).

Turning now to the evaluation of the chemical nature of coke, UV-Raman spectroscopy was applied on the completely deactivated samples. UV-Raman has been proved to be a powerful tool in the qualitative analysis of carbonaceous species formed during the MTH process [162, 181, 182], and it allows to discriminate among the several allotropic forms of carbon [183-185].

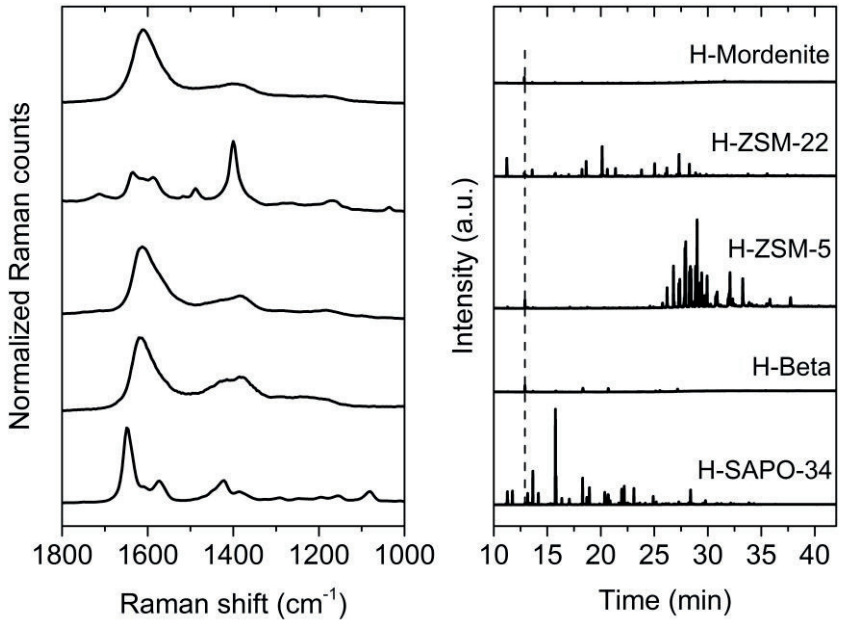

Figure 5.3 (Left) UV-Raman (λ = 244 nm) spectra of completely deactivated samples. (Right) Chromatograms from the dissolution-extraction experiments for completely deactivated samples. All the peaks are normalized relative to the standard peak ortho-chloro-toluene indicated by the dashed line in the chromatograms.

From the UV-Raman experiments (Figure 5.3-left), we classify the materials into two main classes. The zeolites with 3D medium and large pores (H-Mordenite, H-Beta and H-ZSM-5) show relatively simple UV-Raman spectra dominated by the two major bands associated with extended carbon, whereas the spectra obtained for the samples with more constrained 1D medium and small pores (H-ZSM-22 and H-SAPO-34) display much more fine structure, indicative of molecular species.

Even though the UV Raman spectra of the completely deactivated samples of H-Mordenite, H-Beta and H-ZSM-5 show generally broad and overlapping bands, they can be assigned to extended carbonaceous species for all catalysts [186]. However, it is difficult to unequivocally attribute the bands to a single kind of carbon. The most probable phase,

according to the positions of D and G bands and their intensity ratio is an amorphous carbon (low sp^3 content, disordered graphitic domains), but also some H containing species can contribute. On H-ZSM-5, better defined peaks are superimposed on the carbon signals discussed so far. These are related to more well-defined, molecular coke species. For example, on H-ZSM-5, it is possible to identify biphenyl (shoulder at 1585 cm^{-1} and small peaks at 1290 cm^{-1} and 1185 cm^{-1}) and naphthalene and/or anthracene (possibly both contributing to the peak at 1390 cm^{-1}).

The situation is quite different for H-SAPO-34 and H-ZSM-22, which have small pore apertures and medium sized pores, respectively, and restricted transport properties. Sharp, molecule-like spectral features are observed in Figure 5.3, and the complexity of the spectra points to the coexistence of several species, as also observed in the extracts (Figure 5.3-right). A more detailed assignment of the peaks in the chromatograms of the soluble coke extracts is provided in the Supplementary Material of **Paper I**.

In the case of H-ZSM-22, the deactivation is related to polyaromatic species. The main signals are in agreement with the reference spectra of anthracene (main signal at 1400 cm^{-1}, peak at 1630 cm^{-1}), biphenyl (peaks at 1585 cm^{-1} and 1610 cm^{-1}), fluorene (peaks at 1485 cm^{-1} and 1610 cm^{-1}, the latter overlapping with one of biphenyl peak), and naphthalene (1630 cm^{-1}, this peak is too intense to be related only to anthracene, and shoulder at 1380 cm^{-1}). The most distinct feature observed for H-SAPO-34 is the intense peak with maximum at 1650 cm^{-1}. The high frequency of this signal is probably related to the presence of heavy olefins.

So, taking into account all the findings made in this work, several conclusions can be drawn when the deactivation is compared for different zeolite topologies. Regarding the methodology applied, we have attempted to bring the commonly qualitatively used dissolution-extraction protocol on a quantitative foundation. It was found that dissolution of spent catalysts followed by extraction and GC-MS analysis affords detection of only a fraction of the total coke content (as determined by TGA). Moreover, the magnitude of this fraction varies strongly among the topologies. The maximum value of this fraction is about 5 % for zeolite H-Beta and 52 % for H-SAPO-34 (Results shown in the Appendix **Paper I**). We have

successfully demonstrated that UV-Raman spectroscopy provides a non-destructive method to attain the fingerprint of all the hydrocarbon compounds deposited on the spent catalysts.

In terms of the deactivation behavior, it has been observed that the final, total amount of coke as detected by TGA for the completely deactivated catalysts varies strongly among the topologies. H-SAPO-34 requires 7 times more coke that H-ZSM-22 to be fully deactivated. Furthermore, the total coke content is well correlated to the BET area and to the micropore volume. This indicates that for the totally deactivated samples, both the internal volume and the external surface are occupied by coke.

Concerning both the fraction of coke compounds detected by the dissolution-extraction method relative to the total coke from TGA and the absolute amount of soluble compounds, it appears that for H-Mordenite and H-Beta, a small maximum is seen at short reaction times, before the amount of soluble compounds essentially goes to zero. For H-ZSM-22, H-ZSM-5, and H-SAPO-34, the fraction of soluble compounds remains appreciable with reaction time (See Supplementary Material Appendix **Paper I**). Consequently, there is an accumulation of soluble compounds as the total coke content increases. There is a clear link between the detection of soluble compounds and the UV-Raman spectra: For fully deactivated H-Mordenite and H-Beta, virtually no soluble compounds are detected, and the UV-Raman spectra are basically the signature of extended carbonaceous (graphitic) species. For H-ZSM-22 and H-SAPO-34, on the other hand, a large fraction of soluble compounds is found, and the UV-Raman spectra correspondingly show distinct molecular features of relatively high intensity. For the particular H-ZSM-5 sample employed here, an intermediate behavior is seen. By evaluating the product selectivities, it appears that for the catalysts with limited mass transport properties (H-ZSM-22 and H-SAPO-34); even the smallest aromatic compounds remain trapped within the pore systems, giving rise to a significant fraction of molecular coke.

Summing up, it is clear that the soluble coke detected in the extracts and seen using UV-Raman for H-SAPO-34 and H-ZSM-22 can be considered to be largely internal coke, as the molecular structures of the trapped coke compounds reflect the pore systems of the materials. This is also in agreement with previous studies relying on XRD and theoretical simulations [133, 187]. For H-Mordenite and zeolite H-Beta and to some extent H-ZSM-5, the

formation of coke compounds which are too large to reasonably be characterized as molecules or internal coke species, appears to dominate. These materials show relatively simple UV-Raman spectra dominated by the two major bands associated with extended carbon phases or external coke.

Operando UV-Raman studies as a tool for investigating the influence of zeolite topology on the deactivation

After having shown a summary of the role of zeolite topology on the coke nature and content, a natural extension of the work was to perform the MTH reaction using the same catalysts and conditions as the ones previously used (400 °C, P_{atm} and WHSV = 2 g_{MeOH} g_{cat}^{-1} h^{-1}) under operando conditions exploiting the Raman effect with UV light. In previous paragraphs it has been reported that UV-Raman measurements are advantageous in the sense that they probe the entire range of coke compounds, from molecular to graphitic species. Moreover, this technique has scarcely been used as analytical tool in the conversion of methanol-to-hydrocarbons [181, 188].

Therefore, after having characterized ex-situ the deactivated catalysts, we decided to apply operando conditions, which inherently provide deeper insights into the deactivation by combining spectroscopic and catalytic measurements [189].

As mentioned in section 4.2, to avoid material damaging from the UV-laser, catalysts need to be in continuous movement. Thus, it was decided to perform the MTH reaction using two different reactor-cells. First, we used a flow cell setup developed by Dr. Matteo Signorile and co-workers which has been used in previous studies [190]. In this cell the sample is in pellet form, supported on a gold envelop, and has a magnetic element attached underneath that allows the sample to be in continuous movement. Herein, this reactor will be referred as spinning-pellet cell. The second setup was a fluidized-bed reactor based on the commercial Linkam CCR1000 cell, which has also been used in previous investigations [162]. Regardless of the type of reactor used, a mass spectrometer (MS) connected to the cell analyzed online the products of the reaction. For the acquisition of the UV-Raman spectra, two approaches were followed. During the first 5 minutes of reaction, spectra were collected continuously

every 30 seconds. This relatively short time resolution was chosen to obtain as much information as possible about the early stages of the reaction. From the first 5 minutes of reaction onwards, the acquisition time was increased to 5 minutes per spectrum (to enhance the signal-to-noise ratio). Spectra were collected until the desired time-on-stream in each experiment was reached.

It is worth highlighting that individual peak assignments are hampered by the lack of a comprehensive database of reference compounds. In this work, the assignments are based on the few studies available in literature [181, 188, 191-193].

An overview of the results obtained for the H-ZSM-5 sample using the two different setups is presented in Figure 5.4.

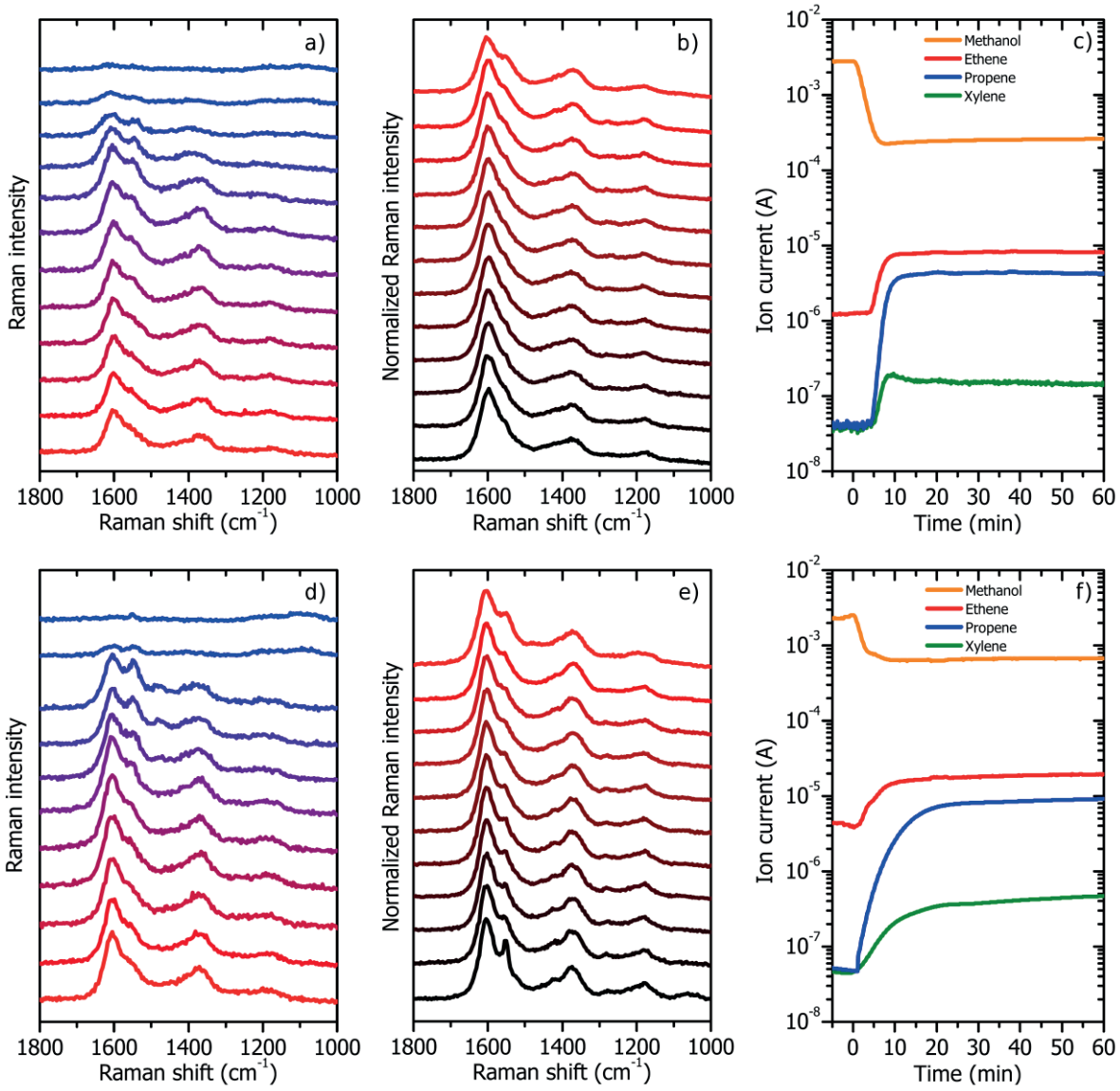

Figure 5.4 UV-Raman spectra of H-ZSM-5 catalyst when reacting with MeOH at 400 °C under operando conditions. Top: results from the spinning-pellet cell. a) from the beginning of the reaction to 5 minutes on stream (time evolution from blue to red, 30 s accumulation of each spectrum); b) during the 5-60 minutes on stream (time evolution from red to black, 5 min of acquisition for each spectrum); c) Ion currents measured for representative reactants and products. Bottom: results obtained in the Linkam CCR1000. d) 0-5 minutes on stream (time evolution from blue to red, 30 s of acquisition per spectrum); e) 5-60 minutes time on stream (time evolution from red to black, 5 minutes of acquisition per spectrum); f) ion currents of representative reactants and products of the reaction.

During the first 4-6 Raman spectra (from top-blue to bottom-red) in Figure 5.4 (a, d) a sudden growth of the features at 1600 cm^{-1} and 1400 cm^{-1} is observed. This initial stage can be preliminary ascribed to the formation of the hydrocarbon pool species (induction period), and until a sufficient amount of autocatalytic species are not formed, the MTH reaction does not proceed. When comparing the spectra of initial stages of the reaction for the two reactors used, the features detected are very similar, suggesting that the initial reaction mechanism on H-ZSM-5 is independent of the type of reactor employed. However, in the

fluidized bed reactor (Linkam CCR1000), a minor difference is observed by the presence of a feature with its maximum around 1450 cm^{-1} at the beginning of the reaction (Figure 5.4 d), ascribable to methanol on the catalyst surface. This peak might be detected as a result of the better contact between the reactants and the catalysts established when using the fluidized bed reactor. However, as soon as the induction period is completed, the signal is no longer detected and thus, all the methanol molecules fed in the reactor participate in the reaction.

Regarding the spectra acquired at later stages of the reaction, as observed in the panels b) and e) of Figure 5.4, the features detected over H-ZSM-5 on the two different setups are very similar and relatively stable with time. This is in agreement with the plateaus observed in the MS signals, suggesting that catalysts are working on steady state conditions, and little changes in the relative intensities of the hydrocarbon species are expected, as it is corroborated by the UV-Raman spectra.

The same type of experiments as those performed with H-ZSM-5 were carried out using the other 4 catalysts presented in the previous section: H-Mordenite, H-ZSM-22, H-Beta and H-SAPO-34. An overview of the results obtained after 1 h on stream is provided in Figure 5.5.

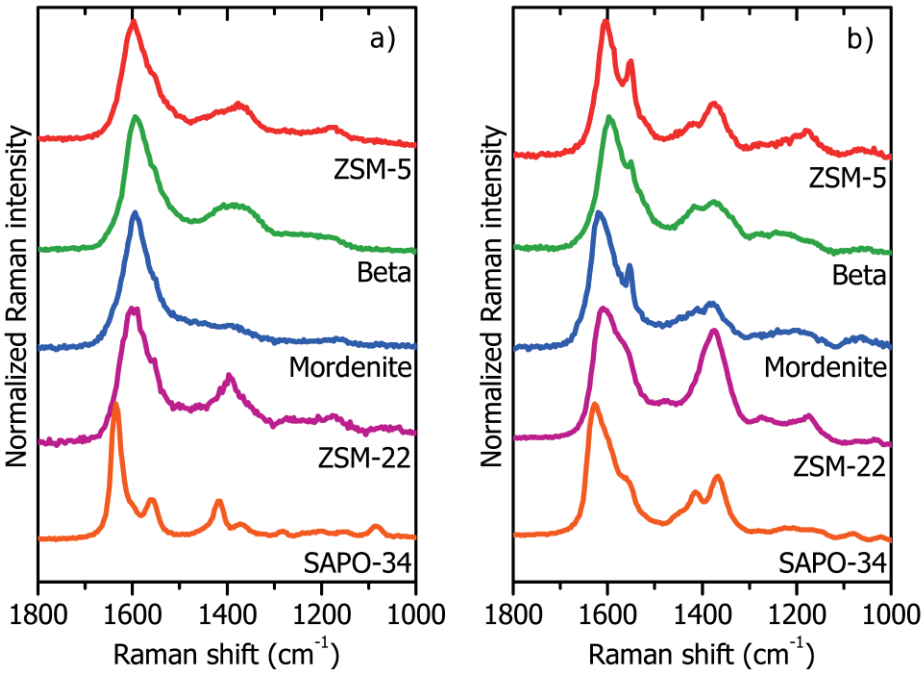

Figure 5.5 Comparison of the UV-Raman spectra of the five different zeolite topologies collected after 1 h under reaction conditions on a) the spinning-pellet cell and b) the fluidized bed reactor (Linkam CCR1000)

The first aspect to comment about is that the unequivocal assignment of the spectral features is not straightforward. Moreover, some fingerprints of the most important compounds in the MTH reaction somewhat overlap, which make the peak assignment less evident [193].

Owing to the preliminary status of the results presented here, a detailed analysis of the spectral components is not provided. However, it is worth highlighting that most of the features observed during the operando experiments are coincident with those resulting from the ex-situ analysis, which have been shown earlier. As explained, results allow us to differentiate the catalysts in two families. On the one hand, materials with limited diffusion properties, as it is the case on H-ZSM-22 and H-SAPO-34, display relative sharp features in the spectra which are associated to soluble coke species retained in the zeolite structure. On the other hand, over H-Mordenite, H-Beta and partially over H-ZSM-5, extended bulk carbon phases are detected, most likely located on the external surface of the catalysts. However, in the case of H-ZSM-5, an intermediate behavior with contributions from both, molecular species and extended carbon phases is seen.

Influence of zeolite topology on axial deactivation patterns

The third study presented in this Thesis, also deals with the role of zeolite topology in the deactivation. Whereas on the first part of section 5.1 we disregarded the evolution of coke along the bed; in this study we investigate influence of the zeolite topology on the axial deactivation patterns along the catalyst bed during the MTH reaction. An extension of the summary presented here can be found in Appendix **Paper II**.

In the first part of the study, 7 different zeolite topologies comprising 1D 10-ring structures (H-ZSM-22 and H-ZSM-23), 3D 10-ring structures (H-ZSM-5, H-IM-5, H-ITQ-13), a 1D 12-ring zeolite (H-Mordenite) and a 3D 12-ring material (H-Beta) were tested at 400 °C, P_{atm} and P_{MeOH} 130 mbar on a fix bed reactor at three different contact times, all of them yielding 100 % initial methanol conversion, in order to calculate the deactivation rates and critical contact times (i.e. contact time needed to launch the autocatalytic MTH reaction) for each zeolite catalyst using the model developed by Janssens et al. [125]. It is worth noting that the application of the autocatalytic deactivation model requires the use of at least 3 different contact times between the reactant of the catalyst in order to determine the deactivation

coefficient (a). Further details of the autocatalytic deactivation model are provided in chapter 3. The first approach of the study was performed with the aim of unraveling the influence of zeolite topology, i.e pore size, on the critical contact time and on the evolution of conversion capacity.

During the second part of the study, a selection of the catalysts used on the first part of the work were subjected to life-time performance studies by carrying out the MTH reaction at 4 times-on-stream with increasing degree of deactivation. After quenching the reaction, the catalyst bed was divided from top to bottom i.e. inlet to outlet, in 4 layers which were individually characterized to elucidate the role of zeolite topology on the axial deactivation patterns and to determine the origin of coke formation.

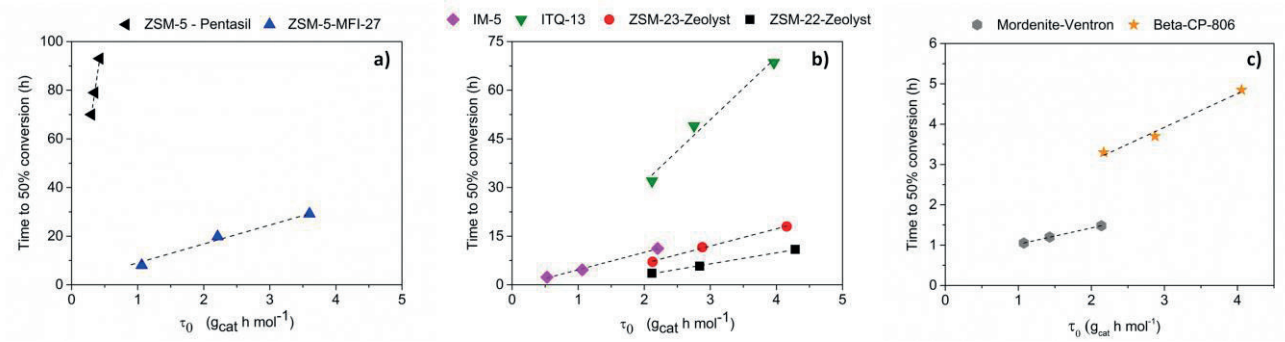

Figure 5.6 Catalyst lifetime to 50% MeOH conversion ($t_{1/2}$) as a function of the applied contact time, τ_0 (weight to flow ratio W/F) on (a) ZSM-5-pentasil and ZSM-5-MFI-27, (b) IM-5, ITQ-13, ZSM-22-Zeolyst and ZSM-23-Zeolyst and (c) Mordenite-Ventron and Beta CP-806. The dotted lines are added as a visual guide.

Figure 5.6 shows the catalyst lifetime to 50% MeOH conversion ($t_{1/2}$) versus the applied contact time (τ_0) for each catalyst. Results show that $t_{1/2}$ depends linearly on the applied contact time, as predicted by the autocatalytic deactivation model [125]. Using such model and the data presented in Figure 5.6, the deactivation constant (a) and the critical contact time (τ_{crit}) were calculated and are presented in Table 5-2.

Table 5-2 Calculated values of critical contact time and deactivation coefficients using the autocatalytic deactivation model

Sample	τ_{crit} (gh mol^{-1})	a (g mol^{-1})
H-ZSM-5-Pentasil	0	0.004
H-ZSM-5-MFI-27	0	0.128
H-IM-5	0.136	0.186
H-ITQ-13	0.363	0.052
H-ZSM-22-Zeolyst	1.107	0.292
H-ZSM-23-Zeolyst	0.759	0.242
H-Mordenite-Ventron	-1.534	2.478
H-Beta-CP806	-1.688	1.194

Furthermore, the change in methanol conversion capacity (g_{MeOH} converted per $g_{catalyst}$) at increasing contact times, shown in Figure 5.7, was evaluated for each catalyst. The conversion capacities at each contact time were obtained by integrating the area under the conversion versus time on stream curves until complete deactivation.

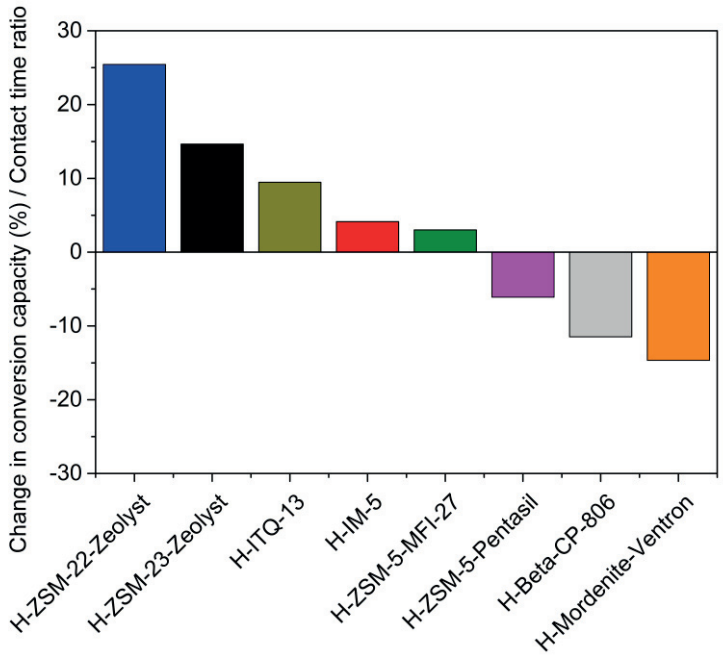

Figure 5.7 Normalized variation of the methanol conversion capacity with respect to the increase in contact time on the different zeolite catalysts investigated.

According to the results presented above, an interesting observation is the increase in critical contact time (the time needed to start the autocatalytic reaction) with decreasing pore size for the 10-ring zeolites (the pore size, measured as the largest sphere that can fit in the zeolite structure, is found in Figure 11 in Appendix **Paper II**). A physical interpretation of the critical contact time would be associated with the zone of the catalyst bed which instead of converting methanol into hydrocarbons, is used for the buildup of the autocatalytic species that initiate the MTH reaction. Consequently, the longer the critical contact time, the less catalyst bed is used in the formation of hydrocarbons. τ_{crit} is particularly long for 1D-10 ring materials, H-ZSM-22 and H-ZSM-23, shorter for H-IM-5 and H-ITQ-13, and zero for H-ZSM-5 (Table 5-2). A similar τ_{crit} value for H-ZSM-5 as the one obtained in this study has been previously reported [125]. Such result suggests that the autocatalytic reaction dominates throughout the whole H-ZSM-5 catalyst bed.

Furthermore, we observe an increase in the total amount of methanol converted per gram of catalyst when longer contact times between methanol and the catalyst were applied. This increase in methanol throughput is particularly evident for H-ZSM-22, H-ZSM-23 and H-ITQ-13, which correspond to the catalyst with the highest τ_{crit} i.e. the least active catalysts. Minor changes in the conversion capacity were seen for H-IM-5, and for H-ZSM-5. Previous results on H-ZSM-5 showed that the conversion capacity is independent of the contact time applied [168], and minor differences in the conversion capacity for H-ZSM-5 were found in this work.

In the case of 12-ring zeolites, in spite of the linear dependency of $t_{1/2}$ on τ_0 (panel c) in Figure 5.6), results of the deactivation constant (a) and critical contact time (τ_{crit}) are markedly different from those obtained over medium pore size zeolites. Curiously, a negative value for the τ_{crit} is obtained for the two 12-ring zeolites: H-Beta-CP806 and H-Mordenite-Ventron (Table 5-2). This result lacks of physical meaning, because according the deactivation model it would mean that even without feeding methanol the autocatalytic reaction would dominate. This result evidences the shortcoming of the autocatalytic deactivation model for large pore size zeolites. At the same time, an increase in the contact time for H-Beta-CP806 and H-Mordenite-Ventron, results in a substantial reduction in the conversion capacity. This observation might be explained by an increase of the secondary reactions between the hydrocarbon products in the large pore size catalysts, ultimately leading to the experimentally observed faster deactivation.

With the aim of getting a further insight into the distribution of coke along the bed with the goal of evaluating the role of methanol and hydrocarbon products as deactivating agents, the deactivation in H-ZSM-5, H-ZSM-22, H-ZSM-23, H-Beta and H-Mordenite was investigated spatially and temporally. An overview of the results is presented here, but the complete dataset is provided in Appendix **Paper II**.

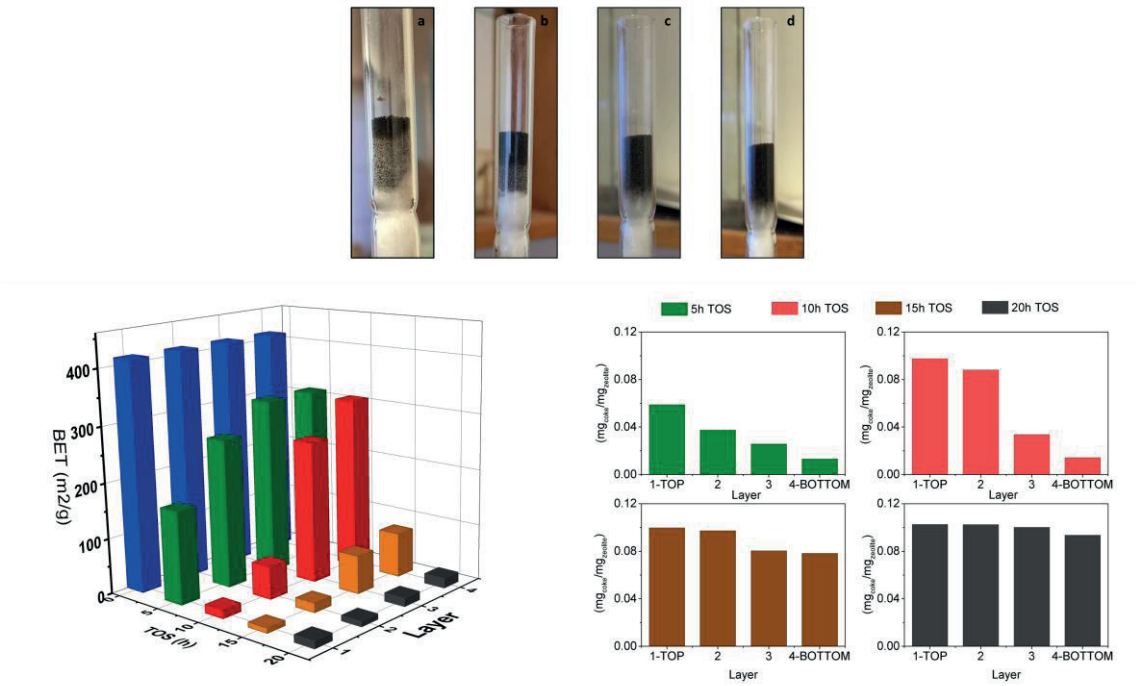

Figure 5.8 Top: H-ZSM-5-MFI-27 deactivated at t = 5, 10, 15 and 20 hours (a, b, c and d, respectively) at 400 °C, τ_0 = 2 g_{cat} h mol_{MeOH}^{-1}. Bottom-left: BET area on fresh and partially deactivated catalysts layers of H-ZSM-5-MFI-27 at increasing reaction times. Bottom-right: Normalized amounts of total coke content in the different fractions of the bed at increasing times-on-stream.

Figure 5.8 shows the results of the spatial and temporal deactivation analysis performed over one of the H-ZSM-5 previously used: H-ZSM-5-MFI-27. The photographs of the catalyst bed after each test shown in the top part of Figure 5.8 display a color gradient along the catalyst bed, which is particularly clear after 5 and 10 hours on stream i.e. before the methanol breakthrough took place. The dark first layers of the catalyst bed evidence a more deactivated region, whereas the light grey color of the lower part of the bed suggests that this region is deactivated to a lesser extent. This visual evidence of different degrees of deactivation along the bed is experimentally confirmed by the results of BET area and the total amount of coke evaluated in each layer, shown in the bottom part of Figure 5.8. Concerning the spatial distribution of coke, after the 5 and 10 h experiments, thermogravimetric analysis unequivocally shows that there is a substantial decrease in the total amount of oxidizable coke when moving from the entrance towards the outlet of the catalyst bed. Besides, the BET area is strongly reduced in the top (entrance) layer owing to the amount of coke deposited in this fraction, while it is gradually less reduced in the subsequent layers of the bed. The large gradient in coke content observed during the first 10 hours of reaction was reduced for the 15 h experiment, where still a minor difference

between the top and bottom layers is observed due to the residual activity of the bottom-most catalyst layer. However, in the completely deactivated sample (20 h on stream), the differences in coke amount and BET area along the catalyst bed are negligible. These data are in line with previous studies of H-ZSM-5 catalysts [120, 126, 127, 131]. In addition, dissolution-extraction experiments (Fig. S.8. in the Appendix **Paper II**) confirm that the deactivation front is moving downwards along the bed, and it is only the fractions of the bed where methanol is present that contain soluble coke species.

When the axial deactivation patterns were evaluated over H-ZSM-22 and H-ZSM-23, the results obtained are comparable to those observed over H-ZSM-5. During the early stages of the reaction, the catalyst layer closest to the reactor entrance suffers from a higher degree of deactivation i.e. larger reduction in BET area and higher accumulation of coke, compared to the subsequent catalyst layers. At longer reaction times, particularly after the methanol breakthrough, the differences in terms of coke content and BET surface area are minimized among the layers of H-ZSM-22 and H-ZSM-23, suggesting that the catalyst bed is deactivated to a similar extent.

Together, current and previous contributions from our group [114, 124, 194] suggest than methanol is a main source of coke formation for these medium pore size topologies, with lower contribution of coke from product-product reactions.

In contrast to the results obtained over medium pore size catalysts, very distinct deactivation patterns were observed when large pore size zeolites were subjected to spatio-temporal studies.

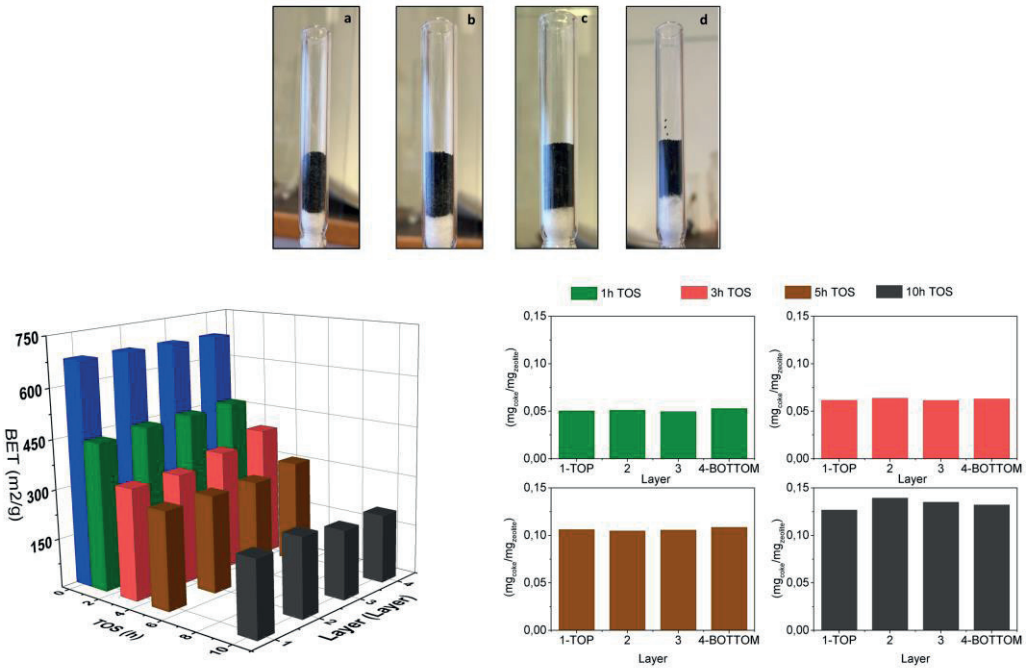

Figure 5.9 Top: Photos of the H-Beta-CP-806 zeolite after quenching the reaction at 1, 3, 5 and 10 h on stream (a, b, c and d, respectively). Bottom: Evolution of BET area (left) and normalized total coke content (right) in the different layers at increasing reaction time.

Figure 5.9 shows the total coke content and the BET surface area of the partially deactivated layers of H-Beta-CP-806. The first remarkable difference with respect the 10-ring zeolites is the visual aspect of the catalyst bed. Even for the shortest reaction time (1 hour on stream and full methanol conversion. See Fig. 1 in Appendix **Paper II**), the catalyst bed is completely black without any axial gradient in color along the bed. Moreover, no significant differences in the reduction of BET area compared to the fresh sample were observed between the catalyst layers, again suggesting that they are deactivated to the same extent (Figure 5.9, blue bars). With increasing time on stream the degree of reduction of BET area compared to the parent material increases; and again, the deactivation is homogeneous along the bed. Thermogravimetric analyses also show that coke is evenly distributed throughout the segments of the catalysts, in contrast to the clear gradients observed in H-ZSM-5, H-ZSM-22 and H-ZSM-23. Moreover, the chromatograms of the soluble coke species extracted in H-Beta-CP-806 (Figure S.9 in **Paper II**) show that soluble deactivating species are homogeneously distributed along the catalyst layers, even before the breakthrough of methanol.

Additional spatiotemporal studies were performed using two other H-Beta zeolites to investigate whether the observed deactivation pattern is a general feature of the BEA topology. Both, in the two extra H-Beta samples analyzed and on the H-Mordenite zeolite, results show a very similar axial deactivation pattern to that observed in H-Beta-CP-806: a uniform decrease in the BET surface area accompanied by an even accumulation of coke for the different segments of the catalyst bed quenched at the same time-on-stream.

Considering the origin of coke formation in medium and large pore size zeolites, i.e. methanol versus hydrocarbon products, the impact of hydrocarbons alone as coke precursors can quite straightforwardly be assessed from the spatio-temporal studies. In particular, the coke amounts formed in the product zone compared to that formed in the initiation and autocatalytic zones. As such, a clear correlation is observed between zeolite topology and the axial deactivation pattern: the larger the pore size, the more important the influence of coke formed from conversion of hydrocarbon products. Conversely, the smaller the pore size, the more important is the coke formation from methanol. The distinction between 10-ring and 12-ring topologies with respect to coke formation from hydrocarbon products alone is likely related to the facile diffusion of products on large-pore size zeolites.

Finally, to shed more light on the influence of catalyst topology on the origin and impact of coke formation, a simple model recently proposed by Olsbye et al. [68], which distinguishes between coke formation from reactants and products, was applied. For additional details about this model, see Appendix **Paper II**.

Results from the model (Table 3 Appendix **Paper II**) reveal that over the three medium-pore size zeolites, the rate constant corresponding to the formation of coke from the reactants (k_2) is larger than the one assigned to the formation of coke from products of reaction (k_3). In particular, for H-ZSM-22 and H-ZSM-23, where the flattening of the conversion versus time on stream is less pronounced than for H-ZSM-5, the model provides a value equal to 0 for k_3. This can be interpreted as if coke originates exclusively from reactions involving methanol in these narrow-pore 10-ring zeolites. In H-ZSM-5, the value of k_2 is more than two-fold to that of k_3, suggesting that methanol is a main source of coke formation also in this case, however, results show a significant contribution of coke formed from hydrocarbon products.

Conversely, results from the three Beta zeolites reveal that the value of k_3 is at least two-fold that of k_2, suggesting that coke is formed to a larger extent from the products of reaction. Finally, the calculated rate constants of Mordenite indicate that the formation of coke is due to both reactants and products, but the latter contribute somewhat more to the formation of coke.

As a summary, this work has contributed to the understanding of zeolite deactivation in the MTH process. On the one hand, we have shown that the autocatalytic deactivation model was successfully applied over medium pore size zeolites and it was found that the critical contact time increases with a decrease in pore size for this type of materials. Besides, the methanol conversion capacity of H-ZSM-5 was found to be independent of contact time. However, the conversion capacity of 12-ring zeolites, H-Mordenite and H-Beta, decreases with an increase in contact time, in contrast to the 10-ring zeolites with pore sizes smaller than H-ZSM-5, for which the conversion capacity concomitantly increases with contact time. On the other hand, the spatiotemporal deactivation studies revealed that zeolite topology affects not only catalyst lifetime and product distribution, but also influences the axial mode of catalyst deactivation. Whereas the deactivation over medium pore size zeolites occurs gradually from the entrance towards the outlet of the catalyst bed, with gradients in the total coke content and evolution of the BET area, in the case of large pore size zeolites, the accumulation of coke and reduction of the BET area does not substantially vary along the different sections of the reactor, resulting in uniform catalyst deactivation throughout the catalyst bed.

With these paragraphs, the first section of the summary of the results concludes, after having shown an overview of the most interesting findings obtained when the catalyst deactivation in the MTH reaction was investigated as a function of the zeolite structure.

5.2 Effect of crystal morphology on the catalytic performance and deactivation of H-ZSM-5 catalysts during the conversion of Methanol-to-Hydrocarbons at industrial relevant conditions

The second axis used for conducting research in this Thesis dealt with the role of zeolite morphology during the deactivation by coke in the conversion of methanol-to-hydrocarbons. The influence of particle size on the catalytic activity has been studied for many decades. Resulting from this thorough research, for example, important parameters such as the degree of utilization for catalysts with different size and morphology is straightforwardly described by the effectiveness factor, derived from the Thiele modulus [195].

In this work, it was decided to use a single zeolite topology, MFI. Since the main objective of the work was to assess the influence of particle morphology on the catalytic performance and deactivation, three H-ZSM-5 samples with similar composition and acid strength, but varying morphology were used as acid catalysts. The election of the MFI topology relies on its importance for being the catalyst used in the industrial MTH process. Moreover, the catalytic tests were carried out at Haldor Topsøe A/S, using similar reaction conditions as those employed in the industrial TIGAS process.

Two of the three H-ZSM-5 samples were commercially available; PZ-2-100H purchased to ZeoChem had a crystal size in the range of microns; Pentasil was obtained from Süd-Chemie and the zeolite crystal size was in the range of nanometers. The third sample, synthesized at the home laboratories at the University of Oslo, has been previously used in other studies from the group [196] and it displays nano-sheet morphology. The diffusion properties of this sample are significantly enhanced because its morphology is such that the crystallites have a thickness of approximately two unit cells [196]. Samples are denoted as ZSM-5-m, ZSM-5-n and ZSM-5-s, corresponding to the samples with micron-, nanometer- size and with nanosheet morphology, respectively.

Catalysts were characterized by XRD, ICP, N_2 adsorption, TPD and SEM to evaluate their properties. The SEM images of the 3 different samples are provided in Figure 5.10. A summary with additional characterization results is reported in Appendix **Paper III**.

The characterization of the materials revealed that, as desired, the Si/Al ratio and the acid site density measured by means of ICP and TPD were very similar in the 3 samples. This indicates that the influence of other properties than the morphology is minimized when the activity and deactivation of the catalysts are studied.

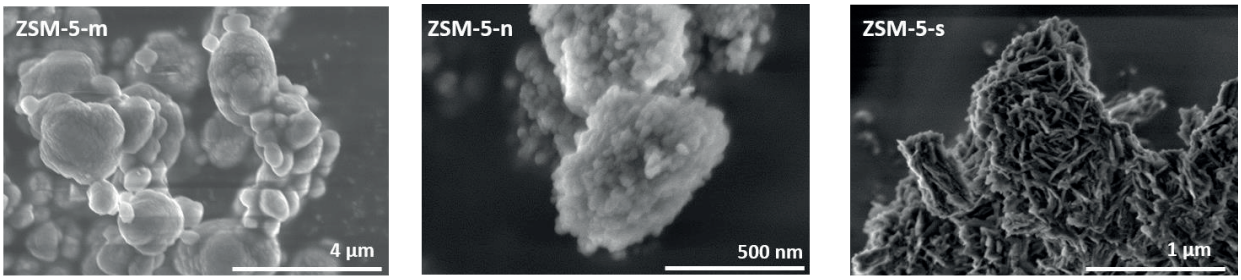

Figure 5.10 Scanning Electron Micrographs of the three ZSM-5 samples used.

The catalytic activity was evaluated using 2 different reactions. On the one hand, we used the catalytic cracking of n-hexane to determine the so-called α-value. This parameter is defined as the ratio between the experimental and the theoretical rate constant at a temperature of 811 K, which corresponds to the temperature at which the maximum n-hexane conversion is achieved. The former is experimentally obtained assuming a first-order reaction, whereas the latter is calculated using the reported apparent activation energy (Ea = 125 kJ mol^{-1}) for the conversion of n-hexane over ZSM-5 [197].

Results from the α-test, which are reported in Appendix **Paper III**, show that ZSM-5-n has the largest α-value, suggesting that it is the catalyst with the highest catalytic activity. Despite the improvement in diffusion properties of ZSM-5-s compared to the other 2 counterparts, results from the α-test reveal that ZSM-5-s is the least active catalysts for hexane cracking.

In order to further assess the catalytic performance of the three H-ZSM-5 catalysts, the methanol-to-hydrocarbons reaction was carried out. Experiments were conducted at 20 bar_g, 370 °C and WHSV = 8 $g_{MeOH}\ g_{cat}^{-1}\ h^{-1}$.

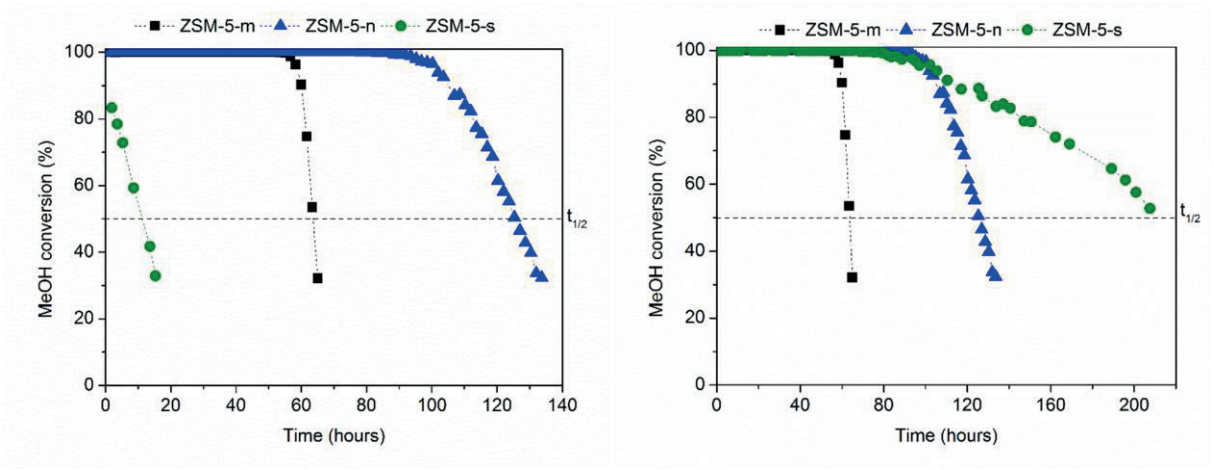

Figure 5.11 Methanol conversion versus time on stream at 20 bar_g, 370 °C over ZSM-5-m, ZSM-5-n and ZSM-5-s. Left) WHSV = 8 g_{MeOH} g_{cat}^{-1} h^{-1} for the three catalysts. Right) WHSV = 8 g_{MeOH} g_{cat}^{-1} h^{-1} for ZSM-5-m and ZSM-5-n, and WHSV = 3 g_{MeOH} g_{cat}^{-1} h^{-1} for ZSM-5-s

The left graph of Figure 5.11 shows the conversion of methanol for the three H-ZSM-5 catalysts measured at WHSV = 8 g_{MeOH} g_{cat}^{-1} h^{-1}. In line with the results obtained in the cracking of n-hexane previously shown, ZSM-5-s displays a significantly lower catalytic activity than that observed for the two commercially available samples. As depicted in the left graph of Figure 5.11, whereas full initial conversion is achieved for ZSM-5-m and ZSM-5-n, a modest 85% of initial conversion is attained with ZSM-5-s, followed by a sharp decline in conversion, reaching 30% conversion after 20 hours on-stream. To establish comparisons about the stability of samples, the Janssens model [124], used in section 5.1, was applied. However, the applicability of such model requires initial full conversion. Thus, an additional reaction with ZSM-5-s was carried out at higher contact time i.e. WHSV = 3 g_{MeOH} g_{cat}^{-1} h^{-1}. The conversion of methanol obtained in the second experiment over ZSM-5-s is shown in the right panel of Figure 5.11. With these conditions, full conversion on ZSM-5-s was obtained. In agreement with pervious reported results using H-ZSM-5 catalyst with nanosheet morphology in the conversion of methanol-to-hydrocarbons [196], longer contact time between methanol and the catalyst i.e. smaller space velocity, had to be applied to obtain the same conversion as on commercial H-ZSM-5 catalysts.

Because of the flow conditions are different over the three catalysts, instead of considering the catalyst lifetime the parameter for evaluate the zeolite stability; the methanol conversion capacity was considered a more accurate parameter to study.

Table 5-3 Parameters derived from Janssen´s model for the three ZSM-5 catalysts.

Sample	$t_{1/2}$ h	$a = (\tau_0 / t_{1/2})$ $g_{cat}\ mol^{-1}$	k mol $g_{cat}^{-1}\ h^{-1}$	exp ($k\tau_0$)	Conversion Capacity $g_{MeOH}\ g_{cat}^{-1}$
ZSM-5-m	65	0.008	84	1.5E+19	522
ZSM-5-n	125	0.004	26	1.1E+06	1002
ZSM-5-s	237	0.006	3	3.5E+01	711

The physical meaning of parameters *a* and *k* derived from Janssens' model has been provided in section 5.1. Results show that the ZSM-5-n shows the best catalytic performance, owing to the low deactivation constant (a=0.004 $g_{cat}\ mol^{-1}$) coupled with a remarkable conversion capacity of more than 1 kg of MeOH converted per gram of catalyst. In contrast, for ZSM-5-m, an increase in particle size to the micrometer range has associated a two-fold increase in the deactivation constant and a decrease in the methanol conversion capacity by almost the half in comparison to results obtained for ZSM-5-n. In the case of ZSM-5-s, provided that sufficient contact time was used, an intermediate conversion capacity between ZSM-5-n and ZSM-5-m was achieved. However, and opposite to what could be expected, the remarkable improvement in diffusion properties on ZSM-5-s does not result in a great enhancement in the methanol throughput.

Nevertheless, the improved diffusivity on ZSM-5-s does significantly influence the product selectivity. As it can be seen in the PIONA (Paraffins, iso-Paraffins, Olefins, Naphthenes and Aromatics) distribution reported in the Supplementary material of Appendix **Paper III**, the selectivity to aromatics was higher in ZSM-5-s compared to ZSM-5-m and ZSM-5-n at all methanol conversion levels owing to the facile diffusion of the products from the zeolite crystal. Moreover, when evaluating the selectivity to tetra-methylbenzenes, the selectivity to this species on ZSM-5-s is more than two- and three-times larger than that measured over ZSM-5-n and ZSM-5-m, respectively. Since TetraMB and ethene are mechanistically related [80, 84], as it could be expected, ZSM-5-s displays the lowest selectivity towards ethene. Over ZSM-5-m, the sample with the largest crystal size, the selectivity to ethene is more than 3 times that obtained in ZSM-5-s at high methanol conversion levels (Figure 10 Appendix **Paper III**). The monotonic increase in ethene selectivity with increasing crystallite size on ZSM-5 catalysts has been previously reported by Bhan and co-workers [105] on the basis of the intracrystalline residence time. The increase in crystal size results in an increase in the intra-crystalline residence time of methylbenzenes due to the increased transport

restrictions, which allows methylbenzene species to undergo dealkylation reactions , leading to ethene formation, prior to exiting the crystal [105].

The second interest of this work was to assess the differences in the deactivation pattern throughout the catalyst bed on the three ZSM-5 samples with different morphology. To accomplish that, we performed a second MTH reaction with the same conditions as those previously used (20 bar_g, 370 °C, WHSV = 8 for ZSM-5-m and ZSM-5 and WHSV = 3 for ZSM-5-s) but, in this second experiment, the reaction was quenched on purpose after 30 h, 60h and 50h over ZSM-5-m, ZSM-5-n and ZSM-5-s, respectively. By quenching the reaction after the mentioned times-on-stream and also taking into account the catalyst lifetimes obtained in previous experiments (right panel of Figure 5.11), we assure that full conversion of methanol was achieved, but at the same time a deactivation gradient along the catalyst bed was expected, based on previous investigations (See section Influence of zeolite topology on axial deactivation patterns). As it can be seen, the approach used in this work is similar to the one presented in Appendix **Paper II**. After quenching the MTH reaction, the catalyst bed was divided in 3 layers from inlet to outlet. The top layer was the catalyst bed zone closest to the methanol feed. The bottom layer corresponded to the part of the bed next to the reactor outlet, and the middle layer, was to the zone of the bed in between the previous ones.

The three catalyst layers were subsequently subjected to Temperature-Program-Oxidation (TPO) experiments to determine the amount of coke formed on the different areas of the reactor.

Table 5-4 Coke content determined by TPO on the different zones of the reactor for the three ZSM-5 samples used.

Sample	Position	Coke content (% wt)
ZSM-5-m	Top	12.4
	Middle	13.2
	Bottom	3.4
ZSM-5-n	Top	12.4
	Middle	12.4
	Bottom	2.5
ZSM-5-s	Top	2.3
	Middle	4.4
	Bottom	9.7

The results obtained in the TPO experiments are shown in Table 5-4. Additional details about the loss of weight on the different layers of the bed are reported in the Supplementary

Material of Appendix **Paper III**. From the results presented in Table 5-4, two different deactivation patterns can be detected. On the one hand, ZSM-5-m and ZSM-5-n contain a higher amount of coke on the top and middle layers than on the bottom one. On ZSM-5-n the top and middle layers display the same amount of coke, suggesting that they are similarly deactivated. However, the bottom layer has a significant lower content of deactivating species, indicating that the reaction front moves from top to bottom, and that there is catalyst still active on the area close to the reactor outlet.

On ZSM-5-m, a similar figure as the obtained over ZSM-5-n can be drawn when comparing the upper and lower areas of the reactor. Results show that the reaction front moves downwards in the bed, and that the reaction could have proceeded further because some catalyst particles were not fully coked. The fact that on ZSM-5-m the top layer has a lower amount of coke than the middle one can be explained taking into consideration the catalytic activity of the catalyst as well as the space velocities used in the experiment.
First, the α-test revealed that the catalytic activity of ZSM-5-m was lower than that of ZSM-5-n (Figure 4 Appendix **Paper III**). Second, when using relatively high space velocities and reactors with small diameters (as it is the case in this work: WHSV = 8 $g_{MeOH}\ g_{cat}^{-1}\ h^{-1}$ and I.D. 2 mm), even on ZSM-5 catalysts which are known to be very active in catalyzing the MTH reaction, an initiation zone on the top part of the catalyst bed can be expected. Studies which tested H-ZSM-5 catalysts under very short contact times i.e. high space velocities [168], have reported the existence of a thin initiation zone on the top of the catalyst bed.
Thus, on ZSM-5-m the initiation zone induced a minor accumulation of coke on the top layer, however, a clear top-to-bottom reaction pattern is observed from the results.

In contrast, a substantial different pattern in terms of coke content is detected on the three layers of ZSM-5-s. Results show that the top and middle areas of the bed contain approximately 4 and 2 times less amount of coke than the bottom layer, respectively. Moreover, bearing in mind that the contact time used in this experiment was more than twice as long as the one used over ZSM-5-m and ZSM-5-n, and that the cumulative conversion capacity on ZSM-5-s was substantially lower than that for ZSM-5-n, it becomes evident that the ZSM-5-s is a substantial less active catalyst than the two other counterparts.

Results suggest that ZSM-5-s has a very large initiation zone, or in other words, that a large area of the catalyst bed instead of catalyzing the conversion of methanol-to-hydrocarbons is used for the formation of the autocatalytic species.

In summary, in this work we have investigated the role of ZSM-5 crystal morphology during the conversion of methanol-to-hydrocarbons, evaluated at industrial relevant conditions. Results have shown that when the morphology is the main parameter assessed, the best catalytic performance, measured by means of activity and conversion capacity, is obtained for catalysts with small crystal size and with spherical shape. In addition, it has been observed that when a model ZSM-5 material with almost no diffusion limitations is tested under industrial conditions, the catalytic performance is not as outstanding as it may be expected. The improvement in diffusion properties also induces side effects such as a lower catalytic activity, which ultimately leads to a lower methanol throughput and to a minor utilization of the catalyst bed, resulting in a worse performance.

With these paragraphs, which have aimed at providing an overview of the influence of catalyst morphology on the catalytic performance and deactivation during the MTH process, the second section of the Summary of the results concludes. For additional results and discussions, readers are encouraged to go through Appendix **Paper III**, where a preliminary version of the manuscript, which is in preparation, is provided.

5.3 Structure-deactivation relationships on H-ZSM-5 catalysts during the Methanol-to-Hydrocarbons reaction.

In the last section of this chapter, the deactivation of H-ZSM-5 catalysts in the MTH process is investigated from a different angle. A novel methodology for assessing accurately and straightforwardly the extent of deactivation is presented. The approach reported herein is based on the changes observed on the unit cell parameters of H-ZSM-5 catalyst with increasing degree of deactivation.

The outset of this study is linked with the results presented in section 5.2, where the catalyst bed of H-ZSM-5 was axially analyzed to elucidate the differences in deactivation pattern. In addition to the TPO analyses, XRD measurements on the different catalyst layers were performed, and a very interesting feature was noticed. Upon deactivation, the doublets of the fresh MFI topology appearing in the diffractogram at 23.08 ° and 23.32 °, and at 45.05° and 45.53 ° disappeared and a single peak emerged instead. It was observed that the higher the degree of the deactivation, the sharper the shape of the single peak. However, when the extent of deactivation was minor, the doublet present in the fresh zeolite was still observed. So, we found that with increasing deactivation, a gradual change in the zeolite structure took place.

Figure 5.12 shows the range of interest of the diffractograms for the fresh ZSM-5-m (sample used in section 5.2) and for the top, middle and bottom layers. The doublets detected in the fresh sample around 23 ° and 45 ° are transformed into a single peak in the top and medium layers, which correspond to the most deactivated areas of the bed, whereas in the bottom layer, since the deactivation was not particularly high, the doublets were still detected.

It is important to highlight that the change in the diffractogram was reversible, and that upon the removal of coke, the doublets were again observed on the different areas of the bed. So, the distortion in the diffractogram is believed to be related to the formation and buildup of hydrocarbon residues in the zeolite structure.

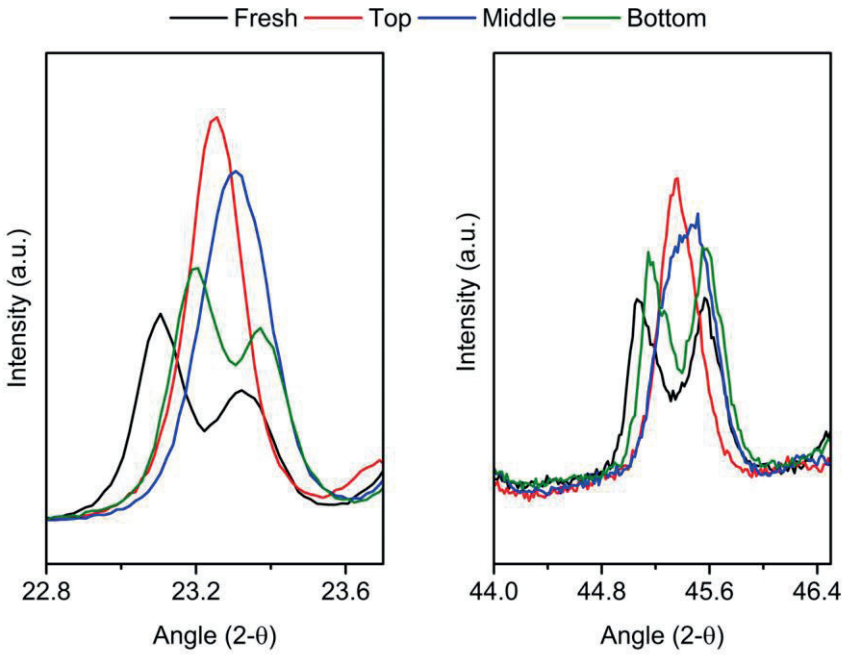

Figure 5.12 Zoom in the XRD diffractograms of the fresh and partially deactivated layers of ZSM-5-m sample used in section 5.2

The main objective of this work was to conduct a detailed investigation of the reversible changes observed in the diffractogram upon deactivation using a set of six H-ZSM-5 catalysts with different physico-chemical properties. Six samples were selected to show that the change is solely related to the build-up of coke species in the framework, and not a particular feature of a single H-ZSM-5 sample.

In this work we combined both experimental and theoretical approaches. On the one hand, the dissolution and extraction experiments on deactivated H-ZSM-5 catalysts were performed to identify the soluble coke species retained in the structure; XRD measurements were applied to determine the unit cell parameters as well as the occupancies of selected coke molecules; Py-FTIR experiments were performed to evaluate the Brønsted acidity on partially deactivated layers of catalyst; TPO analysis allowed us to evaluate the coke content on H-ZSM-5 catalysts with different degree of deactivation, and N_2 adsorption experiments enabled the evaluation of the surface area. On the other hand, DFT calculations were performed to model the forces that the species exert on the zeolite framework.

Since I have been strongly involved in the experimental part of this work, more emphasis will be given to the analysis of the experimental results. The theoretical contribution to the work was carried out by Malte Nielsen (PhD candidate working on the ZeoMoroph project).

In order to make the conclusions of the work as extensive as possible for the MFI structure, six ZSM-5 samples with different composition and properties were used. Five of the samples were commercially available and the other material was synthesized in the laboratory. A summary with the basic characterization results is provided in Appendix **Paper IV**.

We performed the experiments using two different reaction conditions. When evaluating the performance of ZSM-5-MFI-27 and ZSM-5-hm the reaction conditions were P_{atm}, 400 °C and WHSV =2 $g_{MeOH}\ g_{cat}^{-1}\ h^{-1}$. However, the reaction over ZSM-5-PZ-2-100-H, ZSM-5-Pentasil, ZSM-CBV-8014 and ZSM-5-S-CBV-8014 was carried out at 20 bar_g, 370 °C and WHSV = 8 $g_{MeOH}\ g_{cat}^{-1}\ h^{-1}$. Similar to the experimental approach presented in section 5.2, two MTH reactions were performed. First, an experiment was conducted to evaluate the catalyst lifetime of the different zeolites. Second, the reaction was quenched before complete deactivation, making sure that full conversion was achieved, but at the same time, enabling an axial deactivation gradient in the catalyst bed.

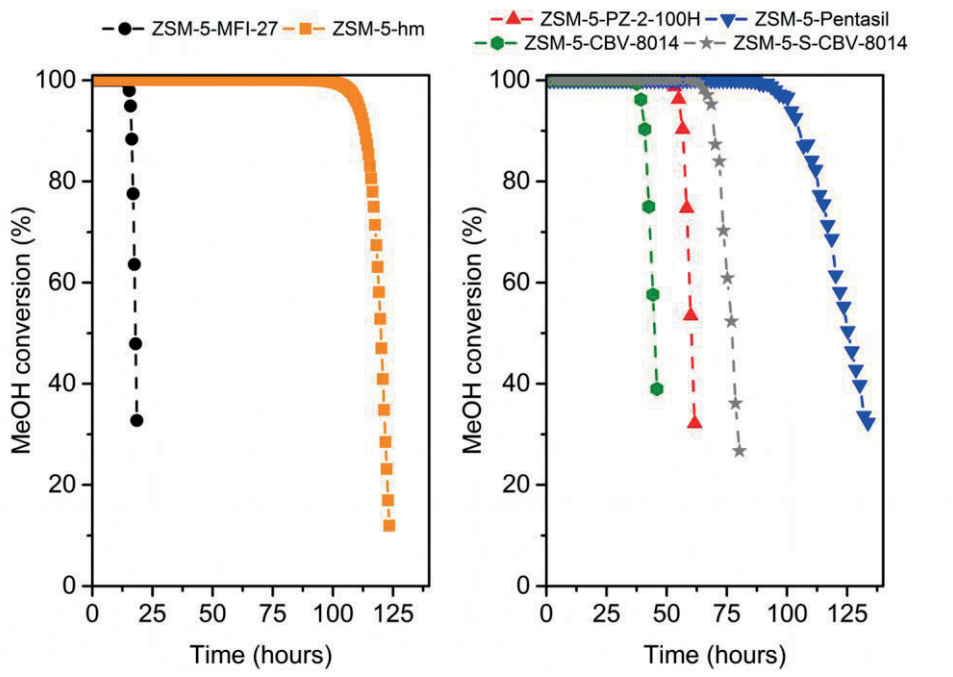

Figure 5.13. Methanol conversion at increasing time-on-stream for the six H-ZSM-5 catalysts used. The left graph corresponds to the catalysts tested at 400 °C, P_{atm} and WHSV = 2 $g_{MeOH}\ g_{cat}^{-1}\ h^{-1}$. The right graph shows the conversion of H-ZSM-5 catalysts tested at 370 °C, 20 bar_g and WHSV = 8 $g_{MeOH}\ g_{cat}^{-1}\ h^{-1}$.

Figure 5.13 shows the lifetime obtained on the first MTH experiment that allowed us to have an overview of the differences in lifetime for the six ZSM-5 samples.

On the second MTH experiment, the reaction over ZSM-5-MFI-27 was quenched after 7 hours on stream; over ZSM-5-hm after 48 h; over ZSM-5-PZ-2-100H after 30 h and over ZSM-5-pentasil after 60 h. In the case of ZSM-5-CBV-8014 and ZSM-5-S-CBV-8014 the MTH reaction was quenched after 24 and 36 hours on-stream, respectively. Subsequent to the quenching of the reaction, the catalyst bed was divided in three sections from the inlet to the outlet of the reactor (top, medium and bottom). In Figure A-1, (Appendix A.1. Additional results) a photograph of the catalyst bed corresponding to ZSM-5-MFI-27 sample after 7 hours on stream is provided.

All the catalyst layers were subjected to N_2 adsorption measurements and to XRD analysis to evaluate the unit cell parameters. Partially deactivated layers of ZSM-5-MFI-27 and ZSM-5-hm were also characterized by Py-FTIR experiments to determine the remaining Brønsted acidity and TPO analysis to evaluate the coke content.

Interestingly, the same changes in the diffractogram as those reported in Figure 5.12 were observed for the six ZSM-5 samples. Figure 3 in Appendix **Paper IV** shows the results for the different catalyst layers. Additionally, the unit cell parameters of the fresh and partially deactivated ZSM-5 samples are reported in Table 3 in Appendix **Paper IV**. A remarkable finding in this study is that the difference between the a- and b- axes of the unit cell parameters provides a reliable indication of the degree of deactivation on ZSM-5 catalysts. The more deactivated the sample is, the smaller the (a-b) parameter becomes. In a fresh H-ZSM-5 catalyst, the difference between a- and b- is between 0.2 and 0.3 Å for different samples. Upon deactivation, it is observed that the b- axis of the unit cell expands and therefore the (a-b) parameter decreases.

Furthermore, it was found that the three main parameters that determine the extent of the deactivation on an acidic zeolitic catalyst: Brønsted acidity, coke content and remaining BET surface area are linearly correlated with the expansion on the unit cell measured by the difference between a- and b-.

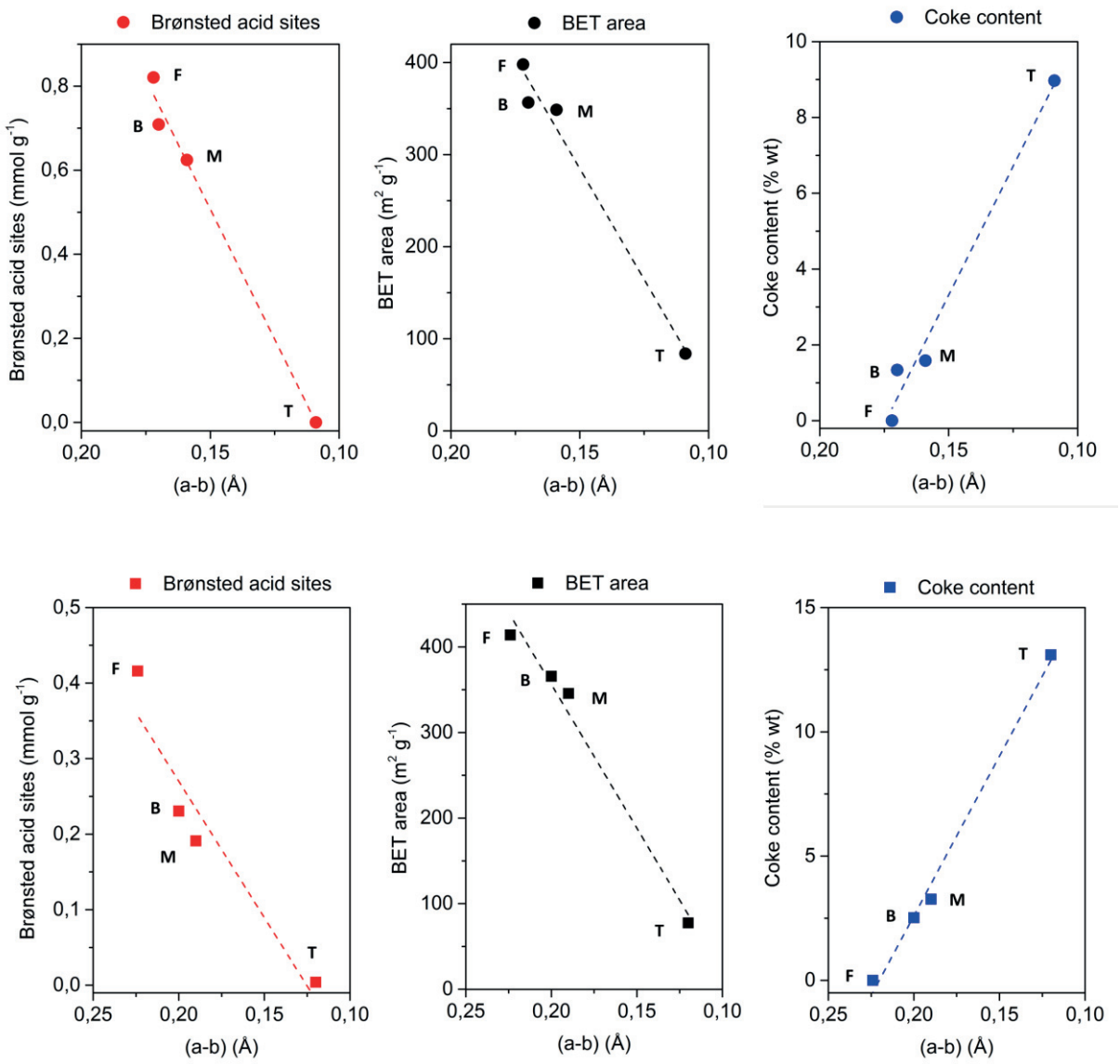

Figure 5.14 Relationships between Brønsted acidity, BET surface area and total coke content on: (TOP) ZSM-5-MFI-27 and (BOTTOM) ZSM-5-hm with respect to the absolute change in the (a-b) parameter. F, T, M and B stand for the Fresh catalysts, Top, Medium and Bottom layers of the partially deactivated catalysts, respectively.

As observed in the graphs of Figure 5.14, the top layer (T) of the catalyst bed displays a total consumption of the Brønsted acid sites and the largest accumulation of coke species. In the subsequent layers, the difference between a- and b- increases, suggesting a minor expansion of the b- axis and therefore, a lesser extent of the deactivation. At the same time, the concentration of Brønsted acid sites, the BET area and the coke content vary linearly on the middle and bottom layers.

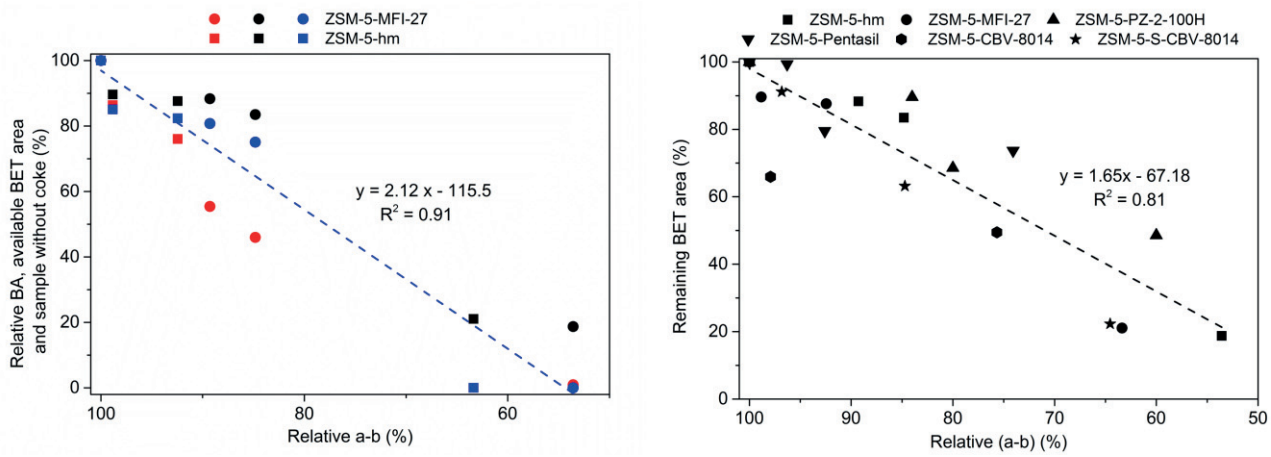

Figure 5.15 Left) Correlation between the normalized values of Brønsted acidity (red), BET surface area (black) and (100 – coke content) (blue) with the (a-b) parameter on ZSM-5-MFI (circles) and ZSM-5-hm (squares). Right) Correlation between the normalized BET area values versus the normalized (a-b) parameter for all the different catalyst layers obtained using the six ZSM-5 samples

Interestingly, it was observed that when the Brønsted acidity, the BET area and the coke content, (properly speaking is (100 – coke content) in order to have the lines with decreasing slopes) are normalized to 100 %, the results obtained for the layers of ZSM-5-MFI-27 and ZSM-5-hm are fairly-well linearly correlated (R^2 = 0.91) with respect the normalized (a-b) descriptor, as shown in the left graph of Figure 5.15.

Furthermore, we assessed the relationship between the normalized (a-b) parameter and the normalized BET area of the partially deactivated layers corresponding to the six H-ZSM-5 catalysts. Results (Right graph Figure 5.15) revealed that the linear relationship between these two values was somehow maintained. Despite the modest R^2 obtained in the fitting (0.81) and taking into consideration the differences among the samples in terms of composition and reaction conditions, the result shows the potentialities of using the (a-b) parameter as a descriptor to study the deactivation for H-ZSM-5 catalysts.

Additional investigations such as dissolution-extraction experiments and DFT calculations were performed to evaluate the link between retained molecules and the expansion of the unit cell determined by XRD.

The dissolution-extraction experiments (Figure 4 Appendix **Paper IV**) performed on the completely deactivated samples obtained during the first MTH experiment reveled that in most of the ZSM-5 samples polymethylated benzene species are the most abundant compounds retained in the structure, in line with results previously reported [84, 107, 127,

134]. Among the polymethylated benzene species, trimethylbenzene and tetramethylbenzene, which are the active species for the formation of ethene during the MTH reaction over H-ZSM-5 [80, 84], seem to be the main compounds retained in the zeolite structure.

When applying DFT calculations, different coke molecules were inserted in the structure of H-ZSM-5 and subsequently the unit cell was relaxed. Based on the results from the dissolution experiments, the following molecules were chosen as representative coke species: naphthalene, anthracene, hexamethylbenzene, 1,2,3,4-tetramethylbenzene, 1,2,3-trimethylbenzene, 1,3,5-trimethylbenzene and m-xylene. As a summary, DFT calculations revealed that the expansion of the unit cell in the b- direction happened to a larger extent due to the methylated benzene species than due to the polyaromatic species, thus confirming the findings of the dissolution-extraction experiments. Moreover, the intersection between the straight and sinusoidal channels of ZSM-5 was the more probable location in the structure where coke molecules, leading to the expansion of the unit cell, would be located.

In addition, the occupancies of different coke molecules were calculated using both DFT and Rietveld refinement and, as shown in Figure 5 and Table 4 in Appendix **Paper IV**, the theoretical and experimental approaches provided similar results.

To conclude the first part of section 5.3, it is important to highlight that experimental and theoretical methods were used to investigate how hydrocarbon molecules trapped in the framework of H-ZSM-5 influence the unit cell with the aim of establishing structure-deactivation relationships. Experiments show that six H-ZSM-5 catalysts with different catalytic properties all exhibit the same behavior: the difference between the a- and b-dimensions of the unit cell decreases with increasing deactivation, mainly due to the expansion of the b- axis.

It was found that polymethylated benzene species, in particular tetramethylbenzenes, are responsible for the expansion of the unit cell, which induces the changes in the diffractogram. In addition, the most interesting finding of this work was that we were able to correlate the changes in the unit cell parameters to a number of catalyst properties that characterize the extent of deactivation such as Brønsted acidity, total coke content and BET

surface area. To the best of our knowledge, this work is the first that shows a direct link between the deactivation of H-ZSM-5 catalysts in the MTH conversion and the species formed inside the framework.

After having observed that the (a-b) parameter is a suitable descriptor to assess the degree of deactivation, a step further was taken by performing the MTH reaction under *operando* conditions using High Energy X-Ray Diffraction at the European Synchrotron Radiation Facility (ESRF). The principal advantage of conducting the experiments at ESRF is that the time resolution of the measurements is significantly improved compared to that achieved in the home facilities.

Experiments were carried at the Swiss-Norwegian Beamline (BM-01). H-ZSM-5-MFI-27 was used as acid catalyst and reactions conditions were optimized to enable a relatively fast catalyst deactivation, but giving full MeOH conversion at the beginning of the reaction, in order to maximize the number of experiments performed during the allocated beam-time. The reaction conditions were P_{atm}, WHSV = 20 $g_{MeOH}\, g_{cat}^{-1}\, h^{-1}$ and 400 °C. The results depicted in Figure 5.14 show that Brønsted acidity, BET area and coke content are linearly related to the expansion of the unit cell (a-b descriptor) over H-ZSM-MFI-27.

A capillary reactor of 0.5 mm O.D. and 0.49 mm I.D. was loaded with approximately 1 mg of catalyst (212-250 µm size). The reactor was mounted horizontally on a Huber station enabling the horizontal translation of the reactor in the axial direction, so that XRD measurements were collected on 10different sections of the catalyst bed and products of reaction were analyzed on-line by Mass Spectrometry. A complete scan of the entire reactor lasted for approximately 180 seconds. A graphical description of the setup used during this experiment is shown in Figure 4.5.

Powder X-Ray Diffraction data was measured using a wavelength of 0.7743 Å and acquired on a Pilatus 2M detector. Subsequently, data was integrated into a 1D powder diffraction pattern and the unit cell parameters were evaluated for each area of the catalyst bed at increasing reaction times, thereby monitoring precisely and with high time and spatial resolution the evolution of the unit cell parameters along the reactor.

The evolution of the (a-b) parameter on the different fractions of the bed at increasing reaction times when H-ZSM-5-MFI-27 was used as catalyst in the MTH reaction is shown in

Figure 5.17. Very interesting features about the evolution of the reaction can be extracted from this graph. First, it is observed that in slices number 0 and 1, corresponding to the area of the reactor closest to the methanol feed, the (a-b) parameter does not decrease as much as on the rest of the catalyst bed, suggesting a lower degree of deactivation than in subsequent layers. It is believed that the minor decrease in the (a-b) on the first layers is likely due to the short contact time between the methanol and the catalyst applied in the reaction. As a result, the initial layers of the catalyst bed represent the initiation zone. This observation confirms the idea that the contact time applied in the reaction plays an important role on the extension of the initiation zone because on previous experiments performed over H-ZSM-5-MFI-27 with significantly higher contact time (results presented in section 5.1), no initiation zone was detected. Moreover, the fact that the first area of the bed did not turn black with increasing TOS or even in the completely deactivated stage supports the idea that the first layer was used for MeOH dehydration and the formation of autocatalytic species rather than for catalyzing the MTH reaction (Figure 5.16).

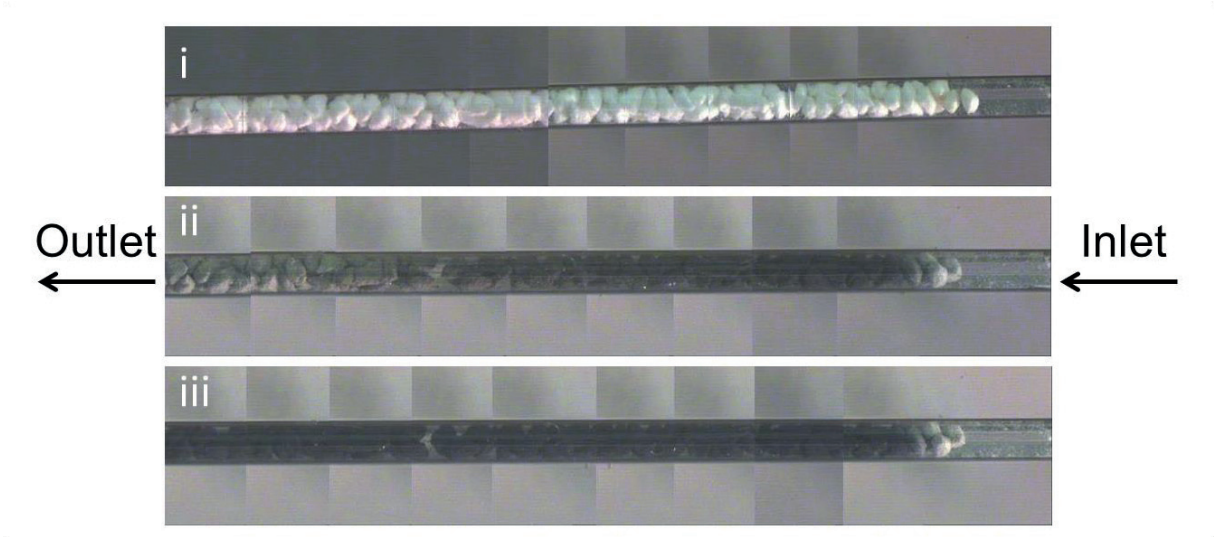

Figure 5.16. Photographs of the capillary reactor of H-ZSM-5-MFI-27 during the experiments at ESRF. i) Fresh activated catalyst, ii) appearance of the catalyst after 75' TOS, iii) completely deactivated catalyst.

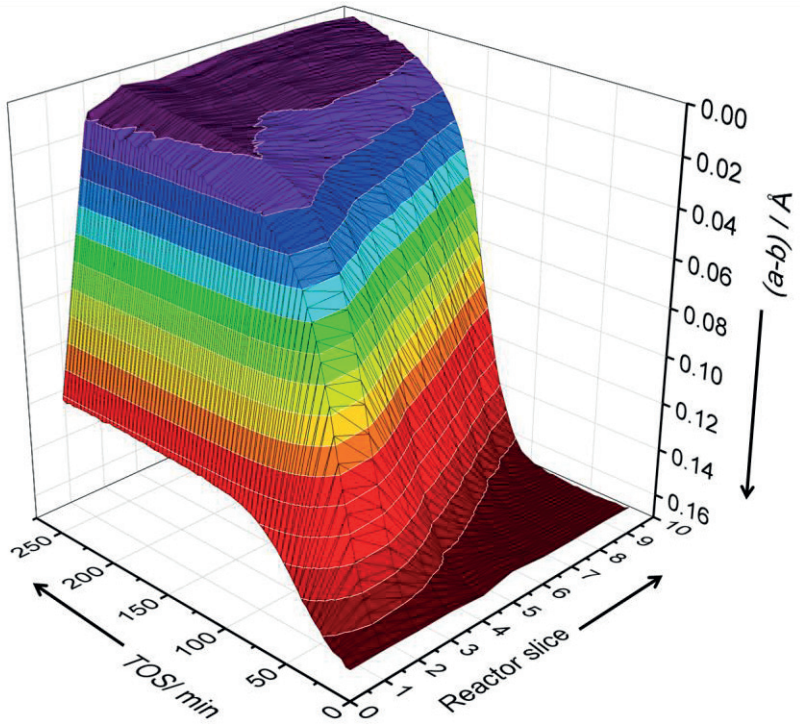

Figure 5.17 3D surface graph showing the evolution of the (a-b) parameter on the Z-axis for the different layers of the catalyst at increasing reaction times. Reaction performed at 400 °C, P_{atm} and WHSV = 20 g_{MeOH} g_{cat}^{-1} h^{-1}. Note that the Z-axis decreases upwards

Second, it is also evident from the results presented in Figure 5.17 that the reaction front moves downwards through the bed. On slice numbers 2 and 3, the decrease in the (a-b) parameter was observed from the beginning of the reaction. However, on layers of catalyst located downwards in the bed, the (a-b) parameter remains stable at the beginning of the reaction and only after a certain time-on-stream, when the methanol is being converted into hydrocarbons in that specific part of the bed, the expansion of the b- axis of the unit cell is experimentally observed. The closer the location of the layer to the outlet, the longer it took until the expansion of the cell was observed, unequivocally showing that the reaction front is going from the inlet to the outlet (in agreement with the results reported in the section 5.1)

Third, results show that the (a-b) parameter decreases until reaching a plateau with increasing times on stream, which would represent a complete deactivation of the layer. Taking this observation into consideration, we decided to normalize the (a-b) between 0-100 %, and assuming that the (a-b) parameter could be interchanged by conversion; the surface plot shown in Figure 5.17 was transformed in a 2 dimensional plot as shown in Figure 5.18.

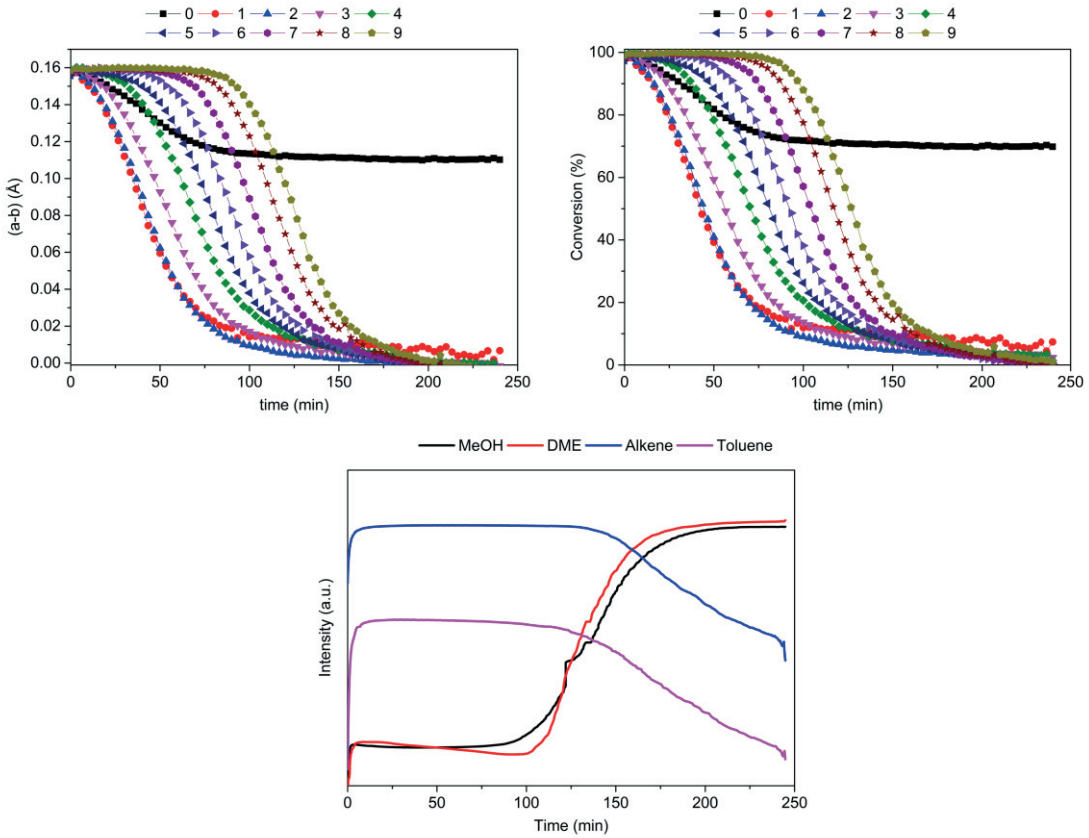

Figure 5.18 Top-left) Evolution of the (a-b) parameter on the 10 reactor slices of H-ZSM-5-MFI-27 at increasing time on stream. Top-right) Evolution of the conversion on the 10 reactor slices assuming that the (a-b) parameter can be interchanged by MeOH conversion. Bottom) MS signals of representative ions for the MTH reaction.

The top graphs of Figure 5.18 show the absolute (a-b) parameter (left), and the corresponding methanol conversion resulting from the normalization of the (a-b) (right). The assessment of the MS data, shown at the bottom of Figure 5.18, indicates that the assumption made during the analysis of the data (normalized (a-b) is equivalent to MeOH conversion) is acceptable to a certain extent because, when evaluating at the MS data, the breakthrough of MeOH and DME takes place approximately around 100 minutes, which is when the breakthrough is detected on the final layer of the reactor (top-right graph of Figure 5.18). So, this fact evidences the potentialities of the (a-b) parameter to be used as a direct measurement of the conversion of methanol.

Summing up, in the last section of this chapter we have shown a novel methodology for evaluating the deactivation on H-ZSM-5 zeolite catalysts. The method relies on the changes of the unit cell parameter, experimentally observed by XRD, which take place when the catalyst becomes inactive in the conversion of methanol-to-hydrocarbons. It has been observed that the differences between the a- and b- axes of the unit cell parameters are

linearly correlated with the remaining Brønsted acidity, the BET surface area and the total coke content. With this methodology we have set the ground for future investigations, because according to our results and provided that a suitable calibration line is obtained for a given H-ZSM-5 catalyst, it will be possible to evaluate the extent of deactivation by a fast and a routinely XRD measurement.

Moreover, High Energy X-Ray measurements have shown that the (a-b) parameter can be used for evaluating precisely the level of methanol conversion on the different areas of the catalyst bed.

6. Main conclusions

As anticipated in previous sections, the investigation of the zeolite deactivation during the conversion of methanol-to-hydrocarbons is a complex phenomenon influenced by different factors such as zeolite framework, composition or acid site denstity, reaction temperature and pressure or contact time.

In this Thesis, the deactivation of zeolite catalysts in the MTH reaction has been investigated from three different perspectives. First, research was conducted looking into the influence of zeolite topology on the nature, content and evolution of coke with increasing time-on-stream. Moreover, the axial deactivation pattern was assessed as function of zeolite structure.

Second, the effect of H-ZSM-5 particle morphology on the deactivation during the MTH process evaluated at industrial conditions (temperature, pressure and contact time) has been investigated.

Third, the deactivation of H-ZSM-5 catalysts has been studied following the changes on the unit cell parameter as a consequence of the buildup of hydrocarbon residues inside the structure.

Resulting from these years of work, the following conclusions can be drawn.

Zeolite topology has been proven to be a parameter that not only plays a role on the catalyst lifetime and product distribution, but also the nature of the deactivating species, its amount and the mode of deactivation along the catalyst bed are parameteres heavily dependent on the structure of the catalyst employed.

It has been shown that for zeolite catalysts with unidimenstional channels such as ZSM-22 or with restricted pore connectivity such as SAPO-34, the loss of activity is to a large extent due to species which are soluble in dichloromethane and give rise to distinct features in the Raman spectra. In contrast, for materials with bigger pore sizes or better channel connectivity i.e. H-Mordenite, H-Beta the accumulation of more coke species, which are insoluble in dichloromethane, is observed presumably on the external surface of the zeolite

crystals. This is linked to the appearance of more pronounced D and G bands in the Raman spectra, indicative of extended carbon species.

In the case of H-ZSM-5, an intermediate situation regarding the location of coke species is observed. On the one hand, XRD experiments show that the unit cell parameters change upon deactivation, suggesting that the coke species located inside the material exert some forces, thereby distorting the zeolite structure. On the other hand, UV-Raman spectra display features that can be assigned to both extended carbon phases (similar to H-Beta and H-Mordenite) and some molecular species which were also observed in H-SAPO-34 and H-ZSM-22.

This work has enabled us to verify that the autocatalytic deactivation model, originally proposed for H-ZSM-5 catalysts, can also be successfully applied to other medium pore size zeolites, providing accurate critical contact times and deactivation parameteres. However, over large pore size zeolites, such as H-Mordenite or H-Beta, the autocatalytic deactivation model fails to provide reasonable critical contact times and deactivation rate constants.

In addition, we have shown that over large pore size zeolites, the deactivation of the catalyst occurs homogeneously throughout the bed and that the conversion capacity decreases with increasing contact times. In contrast, over the medium pore size zeolites tested in this work, the deactivation occurs gradually from the entrance towards the outlet of the reactor and the conversion capacity increases with longer contact times, with the exception of H-ZSM-5 whose conversion capacity remains virtually independent of the contact time applied.

Turning now to the influence of H-ZSM-5 particle morphology on the deactivation, we have shown that when the reaction is conducted at industrial conditions the best catalytic performance is attained with sphreical shaped catalysts whose size is in the range of nanometers. Surpringsily, and in contrast to what it could be anticipated, the activity of the catalyst with nanosheet morphology is remarkably worse than the obtained for the other commercial samples. ZSM-5 nanosheets require a contact time, at least, as double as the one used for the commecial counterparts to achieve full conversion of methanol.

This observation may suggest that even though the diffusion is significantly improved on ZSM-5 nanosheets, as it can be observed in the product distribution and the larger amount

of aromatic species detected on this particular sample, its use as a commercial catalysts might not very promising.

Finally, this work has revealed that the structure of the zeolite and its changes upon deactivation can be of special interest to assess the degree of deactivation. Particularly, we have shown that the unit cell parametres of a large set of H-ZSM-5 catalysts with different properties are distorted due to the hydrocarbon species located inside the zeolite framework. With increasing degree of deactivation the difference between the a- and b-dimension decreases, mainly due to the expansion of the b- axis. In addition, we have been able to establish linear relationships between the difference in the unit cell axes and the parameters governing the deactivation i.e. Brønsted acidity, coke content and BET surface area on H-ZSM-5 catalysts. This shows that the degree of catalyst deactivation can be directly assessed by a single XRD measurement. It also demonstrates a direct link between the deactivation on H-ZSM-5 and the species formed inside the zeolite framework.

The use of High Energy X-Ray Diffraction confirmed that the expansion of the unit cell on H-ZSM-5 catalysts, measured as the difference between the a- and b- axes (a-b), is a novel and reliable parameter for studying both the conversion of methanol into hydrocarbons and the zeolite deactivation. Finally, it has been shown that this approach for evaluating the loss of activity can also be applied under operando conditions.

7. Suggestions for further work

Even though the work carried out in this Thesis has contributed to gain a better insight into the deactivation of zeolites during the conversion of Methanol-to-Hydrocarbons, many questions about zeolite deactivation are yet to be unraveled. Therefore, some suggestions for future work that may contribute to understand the deactivation of zeolites are the following:

- UV-Raman spectroscopy has been found to be a non-destructive technique that provides information about the nature of coke formed on the zeolite. Using this spectroscopic method, it is possible to distinguish between molecular and graphitic coke compounds, but also between single species or single functional groups. However, the main drawback of this technique is the limited availability of spectra to use as reference for the analysis of the results. Therefore, in order to exploit the UV-Raman spectroscopy in the MTH process, it would be very beneficial to generate a library with a relatively large amount of reference compounds that could help elucidate the formation, transformation and accumulation of different active and deactivating species.

- In addition to the ex-situ experiments performed on this study using partially or completely deactivated samples, the influence of zeolite topology on the deactivation can be further investigated by performing operando MTH studies coupled with the techniques presented here. Besides, for a thorough analysis of the coke content in zeolites, it would be beneficial to develop a methodology that could selectively extract, first, the coke deposited on the surface of the catalyst, and subsequently apply the Guisnet method to evaluate the coke located inside the framework. This may provide a better understanding of the mechanism of the formation and evolution of coke.

- If additional quantitative analyses of zeolite deactivation are to be carried out, it would be worth doing some statistical and thorough reproducibility analysis of the experiments performed. It would be recommended at least to repeat five times the same experiment to obtain standard deviation parameters.

- The role of zeolite morphology on the catalytic performance and deactivation during the MTH reaction would require an expansion of the work presented here, by introducing additional H-ZSM-5 catalysts with different particle sizes and morphology before drawing any definitive conclusion. It would be also interesting to compare the catalytic performance when the conditions are different from the industrial ones, to elucidate whether the sample with nanosheet morphology shows a substantial improvement in the methanol throughput.

- It has been shown that the degree of deactivation on H-ZSM-5 catalysts can be determined by powder XRD measurements. In order to assess the applicability of this methodology, it would be advantageous to obtain an even larger set of catalyst layers with different degrees of deactivation to evaluate whether the correlation reported in this Thesis is maintained. Besides, and provided that the relationship between deactivation parameters and unit cell expansion is kept, this new method would be very useful for industrial players of the MTH, where in most of the cases, a single type of H-ZSM-5 catalyst is used. The application of this method would require the generation of a calibration line, which afterwards can provide the coke content, BET area and Brønsted acidity using the unit cell parameters obtained from XRD measurements.

- Finally, it could also be very useful to perform analysis with X-Ray Diffraction-Computed-Tomography (XRD-CT) over H-ZSM-5 catalysts. This technique, which enables the reconstruction of 3-dimensional models, can be used to monitor axially and radially of deactivation along and across the catalyst bed, which in turn, it may provide valuable information about the process of coke formation in zeolites during the methanol-to-hydrocarbons reaction.

References

[1] I. Chorkendorff, J.W. Niemantsverdriet, Introduction to Catalysis, in: Concepts of Modern Catalysis and Kinetics, Wiley-VCH Verlag GmbH & Co. KGaA, 2005, pp. 1-21.

[2] A. Zecchina, S. Califano, The Development of Catalysis: A History of Key Processes and Personas in Catalytic Science and Technology, John Wiley & Sons, 2017.

[3] A. Dyer, An Introduction to Zeolite Molecular Sieves. Chichester., 14 (1988).

[4] B. Smit, T.L.M. Maesen, Towards a molecular understanding of shape selectivity, Nature, 451 (2008) 671-678.

[5] IUPAC, Compendium of Chemical Terminology. Version 2.3.3.

[6] H. Robson, Verified synthesis of zeolitic materials, Gulf Professional Publishing, 2001.

[7] E.M. Flanigen, Molecular sieve zeolite technology-the first twenty-five years, Pure and Applied Chemistry, 52 (1980) 2191-2211.

[8] A.F. Cronstedt, J.L. Schlenker, G. Kuhl, Observation and description on an unknown mineral-species called zeolites, Svenska Ventenskaps Akademiens Handlingar Stockholm, 18 (1756) 120-123.

[9] J. Cejka, H. Van Bekkum, A. Corma, F. Schueth, Introduction to Zeolite Molecular Sieves, Elsevier, 2007.

[10] A.F. Masters, T. Maschmeyer, Zeolites–From curiosity to cornerstone, Microporous and Mesoporous Materials, 142 (2011) 423-438.

[11] J. Weitkamp, Solid state ionics, Zeolites and catalysis, 131 (2000) 175-188.

[12] C.S. Cundy, P.A. Cox, The hydrothermal synthesis of zeolites: Precursors, intermediates and reaction mechanism, Microporous and Mesoporous Materials, 82 (2005) 1-78.

[13] C.S. Cundy, P.A. Cox, The hydrothermal synthesis of zeolites: history and development from the earliest days to the present time, Chemical Reviews, 103 (2003) 663-702.

[14] L.B. Sand, F.A. Mumpton, Natural zeolites: occurrence, properties, and use, in, Pergamon Press, Inc., Elmsford, NY, 1978.

[15] S. Kulprathipanja, Zeolites in industrial separation and catalysis, John Wiley & Sons, 2010.

[16] J.A. Rabo, M.W. Schoonover, Early discoveries in zeolite chemistry and catalysis at Union Carbide, and follow-up in industrial catalysis, Applied Catalysis A: General, 222 (2001) 261-275.

[17] C. Baerlocher, L.B. McCusker, D.H. Olson, Database of Zeolite Structures, in, http://europe.iza-structure.org/.

[18] J. Jiang, J. Yu, A. Corma, Extra-Large-Pore Zeolites: Bridging the Gap between Micro and Mesoporous Structures, Angewandte Chemie International Edition, 49 (2010) 3120-3145.

[19] M.E. Davis, Ordered porous materials for emerging applications, Nature, 417 (2002) 813-821.

[20] M.E. Davis, C. Saldarriaga, C. Montes, J. Garces, C. Crowder, VPI-5: The first molecular sieve with pores larger than 10 Ångstroms, Zeolites, 8 (1988) 362-366.
[21] B.M. Lok, C.A. Messina, R.L. Patton, R.T. Gajek, T.R. Cannan, E.M. Flanigen, Silicoaluminophosphate molecular sieves: another new class of microporous crystalline inorganic solids, Journal of the American Chemical Society, 106 (1984) 6092-6093.
[22] J.M. Thomas, R. Raja, G. Sankar, R.G. Bell, Molecular-sieve catalysts for the selective oxidation of linear alkanes by molecular oxygen, Nature, 398 (1999) 227-230.
[23] W. Meier, Zeolites and zeolite-like materials, Pure and Applied Chemistry, 58 (1986) 1323-1328.
[24] J. Smith, Definition of a zeolite, Zeolites, 4 (1984) 309-310.
[25] A. Corma, State of the art and future challenges of zeolites as catalysts, Journal of Catalysis, 216 (2003) 298-312.
[26] S.M. Auerbach, K.A. Carrado, P.K. Dutta, Handbook of zeolite science and technology, CRC press, 2003.
[27] M. Stöcker, Methanol-to-hydrocarbons: catalytic materials and their behavior, Microporous and Mesoporous Materials, 29 (1999) 3-48.
[28] A. Corma, Acids, Inorganic Solid. Their Use in Acid-Catalyzed Hydrocarbon Reactions. , Chemical Reviews, 95 (1995) 559-614.
[29] S. Bordiga, C. Lamberti, F. Bonino, A. Travert, F. Thibault-Starzyk, Probing zeolites by vibrational spectroscopies, Chemical Society Reviews, 44 (2015) 7262-7341.
[30] M.-C. Silaghi, C. Chizallet, P. Raybaud, Challenges on molecular aspects of dealumination and desilication of zeolites, Microporous and Mesoporous Materials, 191 (2014) 82-96.
[31] M.S. Holm, S. Svelle, F. Joensen, P. Beato, C.H. Christensen, S. Bordiga, M. Bjørgen, Assessing the acid properties of desilicated ZSM-5 by FTIR using CO and 2,4,6-trimethylpyridine (collidine) as molecular probes, Applied Catalysis A: General, 356 (2009) 23-30.
[32] W. Lutz, C. Rüscher, D. Heidemann, Determination of the framework and non-framework [SiO 2] and [AlO 2] species of steamed and leached faujasite type zeolites: calibration of IR, NMR, and XRD data by chemical methods, Microporous and Mesoporous Materials, 55 (2002) 193-202.
[33] R. Shannon, K. Gardner, R. Staley, G. Bergeret, P. Gallezot, A. Auroux, The nature of the nonframework aluminum species formed during the dehydroxylation of HY, The Journal of Physical Chemistry, 89 (1985) 4778-4788.
[34] S. Müller, Y. Liu, F.M. Kirchberger, M. Tonigold, M. Sanchez-Sanchez, J.A. Lercher, Hydrogen Transfer Pathways during Zeolite Catalyzed Methanol Conversion to Hydrocarbons, Journal of the American Chemical Society, 138 (2016) 15994-16003.

[35] C.J. Mota, D.L. Bhering, N. Rosenbach, A DFT study of the acidity of ultrastable Y zeolite: Where is the brønsted/lewis acid synergism?, Angewandte Chemie International Edition, 43 (2004) 3050-3053.

[36] P. Weisz, V. Frilette, Intracrystalline and molecular-shape-selective catalysis by zeolite salts, The Journal of Physical Chemistry, 64 (1960) 382-382.

[37] S.M. Csicsery, Catalysis by shape selective zeolites-science and technology, Pure and Applied Chemistry, 58 (1986) 841-856.

[38] P.B. Weisz, Molecular shape selective catalysis, Pure and Applied Chemistry, 52 (1980) 2091-2103.

[39] M.J. Climent, A. Corma, S. Iborra, Heterogeneous Catalysts for the One-Pot Synthesis of Chemicals and Fine Chemicals, Chemical Reviews, 111 (2011) 1072-1133.

[40] A. Corma, A. Martinez, Zeolites and zeotypes as catalysts, Advanced Materials, 7 (1995) 137-144.

[41] J. Čejka, G. Centi, J. Perez-Pariente, W.J. Roth, Zeolite-based materials for novel catalytic applications: Opportunities, perspectives and open problems, Catalysis Today, 179 (2012) 2-15.

[42] G. Busca, Acid catalysts in industrial hydrocarbon chemistry, Chemical Reviews, 107 (2007) 5366-5410.

[43] R.M. Barrer, Zeolites and their synthesis, Zeolites, 1 (1981) 130-140.

[44] R. Barrer, Chemical nomenclature and formulation of compositions of synthetic and natural zeolites, Pure and Applied Chemistry, 51 (1979) 1091-1100.

[45] R.M. Milton, Molecular sieve adsorbents, in, US Patent No 2,882,244. Washington, DC. U.S. Patent and Trademark Office, 1959.

[46] R.M. Barrer, D.A. Ibbitson, Occlusion of hydrocarbons by chabazite and analcite, Transactions of the Faraday Society, 40 (1944) 195-206.

[47] J.A. Rabo, Unifying Principles in Zeolite Chemistry and Catalysis, Catalysis Reviews, 23 (1981) 293-313.

[48] C.J. Plank, E.J. Rosinski, W.P. Hawthorne, Acidic Crystalline Aluminosilicates. New Superactive, Superselective Cracking Catalysts, I&EC Product Research and Development, 3 (1964) 165-169.

[49] C.D. Chang, A.J. Silvestri, The conversion of methanol and other O-compounds to hydrocarbons over zeolite catalysts, Journal of Catalysis, 47 (1977) 249-259.

[50] U. Olsbye, S. Svelle, M. Bjørgen, P. Beato, T.V.W. Janssens, F. Joensen, S. Bordiga, K.P. Lillerud, Conversion of Methanol to Hydrocarbons: How Zeolite Cavity and Pore Size Controls Product Selectivity, Angewandte Chemie International Edition, 51 (2012) 5810-5831.

[51] G. Kokotailo, J. Schlenker, F. Dwyer, E. Valyocsik, The framework topology of ZSM-22: A high silica zeolite, Zeolites, 5 (1985) 349-351.

[52] J.B. Higgins, R.B. LaPierre, J.L. Schlenker, A.C. Rohrman, J.D. Wood, G.T. Kerr, W.J. Rohrbaugh, The framework topology of zeolite beta, Zeolites, 8 (1988) 446-452.

[53] E.I. Administration, U.S. Energy Information Administration Petroleum Marketing Monthly, in, March 2017.

[54] H. Owen, P.B. Venuto, Conversion of methanol to products comprising gasoline boiling components, in, United States Patent No 3,969,426. Washington, DC. U.S. Patent and Trademark Office, 1976.

[55] Mobil proves gasoline-from-methanol process, Chemical & Engineering News Archive, 56 (1978) 26-28.

[56] C.D. Chang, The New Zealand Gas-to-Gasoline plant: An engineering tour de force, Catalysis Today, 13 (1992) 103-111.

[57] S. Yurchak, Development of Mobil's Fixed-Bed Methanul-to-Gasoline (MTG) Process, in: Studies in Surface Science and Catalysis, Elsevier, 1988, pp. 251-272.

[58] M.W. Erichsen, J.S. Martinez-Espin, F. Joensen, S. Teketel, P. del Campo Huertas, K.P. Lillerud, S. Svelle, P. Beato, U. Olsbye, 14 Syngas to Liquids via Oxygenates, Small-Scale Gas to Liquid Fuel Synthesis, (2015) 441.

[59] J. Topp-Jorgensen, Process for the preparation of catalysts for use in ether synthesis, in, U.S. Patent No 4,536,485. Washington, DC. U.S. Patent and Trademark Office, 1985.

[60] J. Topp-Jørgensen, Topsøe Integrated Gasoline Synthesis – The Tigas Process, in: Studies in Surface Science and Catalysis, Elsevier, 1988, pp. 293-305.

[61] J.Q. Chen, A. Bozzano, B. Glover, T. Fuglerud, S. Kvisle, Recent advancements in ethylene and propylene production using the UOP/Hydro MTO process, Catalysis Today, 106 (2005) 103-107.

[62] H. Koempel, W. Liebner, Lurgi's Methanol To Propylene (MTP®) Report on a successful commercialisation, in: Studies in Surface Science and Catalysis, Elsevier, 2007, pp. 261-267.

[63] A. Avidan, Gasoline and distillate fuels from methanol, Studies in Surface Science and Catalysis, 36 (1988) 307-323.

[64] T. Mokrani, M. Scurrell, Gas Conversion to Liquid Fuels and Chemicals: The Methanol Route-Catalysis and Processes Development, Catalysis Reviews, 51 (2009) 1-145.

[65] C.D. Chang, Methanol conversion to light olefins, Catalysis Reviews Science and Engineering, 26 (1984) 323-345.

[66] C.D. Chang, C.T. Chu, R.F. Socha, Methanol conversion to olefins over ZSM-5: I. Effect of temperature and zeolite SiO2Al2O3, Journal of Catalysis, 86 (1984) 289-296.

[67] C.D. Chang, Hydrocarbons from methanol, Catalysis Reviews Science and Engineering, 25 (1983) 1-118.

[68] U. Olsbye, S. Svelle, K.P. Lillerud, Z.H. Wei, Y.Y. Chen, J.F. Li, J.G. Wang, W.B. Fan, The formation and degradation of active species during methanol conversion over protonated zeotype catalysts, Chemical Society Reviews, 44 (2015) 7155-7176.
[69] N. Chen, W. Reagan, Evidence of autocatalysis in methanol to hydrocarbon reactions over zeolite catalysts, Journal of Catalysis, 59 (1979) 123-129.
[70] W. Song, D.M. Marcus, H. Fu, J.O. Ehresmann, J.F. Haw, An oft-studied reaction that may never have been: Direct catalytic conversion of methanol or dimethyl ether to hydrocarbons on the solid acids HZSM-5 or HSAPO-34, Journal of the American Chemical Society, 124 (2002) 3844-3845.
[71] D.M. Marcus, K.A. McLachlan, M.A. Wildman, J.O. Ehresmann, P.W. Kletnieks, J.F. Haw, Experimental Evidence from H/D Exchange Studies for the Failure of Direct C-C Coupling Mechanisms in the Methanol-to-Olefin Process Catalyzed by HSAPO‐34, Angewandte Chemie, 118 (2006) 3205-3208.
[72] D. Lesthaeghe, V. Van Speybroeck, G.B. Marin, M. Waroquier, Understanding the failure of direct C-C coupling in the zeolite-catalyzed methanol-to-olefin process, Angewandte Chemie International Edition, 45 (2006) 1714-1719.
[73] A.D. Chowdhury, K. Houben, G.T. Whiting, M. Mokhtar, A.M. Asiri, S.A. Al-Thabaiti, S.N. Basahel, M. Baldus, B.M. Weckhuysen, Initial Carbon-Carbon Bond Formation during the Early Stages of the Methanol-to-Olefin Process Proven by Zeolite-Trapped Acetate and Methyl Acetate, Angewandte Chemie International Edition, 55 (2016) 15840-15845.
[74] Y. Liu, S. Müller, D. Berger, J. Jelic, K. Reuter, M. Tonigold, M. Sanchez‐Sanchez, J.A. Lercher, Formation Mechanism of the First Carbon‐Carbon Bond and the First Olefin in the Methanol Conversion into Hydrocarbons, Angewandte Chemie International Edition, 19 (2016) 5723-5726.
[75] Z. Wei, Y.-Y. Chen, J. Li, W. Guo, S. Wang, M. Dong, Z. Qin, J. Wang, H. Jiao, W. Fan, Stability and Reactivity of Intermediates of Methanol Related Reactions and C–C Bond Formation over H-ZSM-5 Acidic Catalyst: A Computational Analysis, The Journal of Physical Chemistry C, 120 (2016) 6075-6087.
[76] X. Wu, S. Xu, W. Zhang, J. Huang, J. Li, B. Yu, Y. Wei, Z. Liu, Revaling the Direct Mechanism of the First Carbon-Carbon Bond Formation in Methanol to Hydrocarbons Process, Angewandte Chemie International Edition, (2017. DOI: 10.1002/anie.201703902).
[77] I. Dahl, S. Kolboe, On the reaction mechanism for propene formation in the MTO reaction over SAPO-34, Catalysis Letters, 20 (1993) 329-336.
[78] I.M. Dahl, S. Kolboe, On the Reaction Mechanism for Hydrocarbon Formation from Methanol over SAPO-34: I. Isotopic Labeling Studies of the Co-Reaction of Ethene and Methanol, Journal of Catalysis, 149 (1994) 458-464.

[79] I.M. Dahl, S. Kolboe, On the Reaction Mechanism for Hydrocarbon Formation from Methanol over SAPO-34: 2. Isotopic Labeling Studies of the Co-reaction of Propene and Methanol, Journal of Catalysis, 161 (1996) 304-309.

[80] S. Svelle, F. Joensen, J. Nerlov, U. Olsbye, K.P. Lillerud, S. Kolboe, M. Bjørgen, Conversion of methanol into hydrocarbons over zeolite H-ZSM-5: Ethene formation is mechanistically separated from the formation of higher alkenes, Journal of the American Chemical Society, 128 (2006) 14770-14771.

[81] B. Arstad, S. Kolboe, Methanol-to-hydrocarbons reaction over SAPO-34. Molecules confined in the catalyst cavities at short time on stream, Catalysis Letters, 71 (2001) 209-212.

[82] S. Svelle, U. Olsbye, F. Joensen, M. Bjørgen, Conversion of Methanol to Alkenes over Medium- and Large-Pore Acidic Zeolites: Steric Manipulation of the Reaction Intermediates Governs the Ethene/Propene Product Selectivity, The Journal of Physical Chemistry C, 111 (2007) 17981-17984.

[83] Ø. Mikkelsen, P.O. Rønning, S. Kolboe, Use of isotopic labeling for mechanistic studies of the methanol-to-hydrocarbons reaction. Methylation of toluene with methanol over H-ZSM-5, H-mordenite and H-beta, Microporous and Mesoporous Materials, 40 (2000) 95-113.

[84] M. Bjorgen, S. Svelle, F. Joensen, J. Nerlov, S. Kolboe, F. Bonino, L. Palumbo, S. Bordiga, U. Olsbye, Conversion of methanol to hydrocarbons over zeolite H-ZSM-5: On the origin of the olefinic species, Journal of Catalysis, 249 (2007) 195-207.

[85] R. Dessau, On the H-ZSM-5 catalyzed formation of ethylene from methanol or higher olefins, Journal of Catalysis, 99 (1986) 111-116.

[86] R. Dessau, R. LaPierre, On the mechanism of methanol conversion to hydrocarbons over HZSM-5, Journal of Catalysis, 78 (1982) 136-141.

[87] B.E. Langner, Reactions of methanol on zeolites with different pore structures, Applied Catalysis, 2 (1982) 289-302.

[88] T. Mole, G. Bett, D. Seddon, Conversion of methanol to hydrocarbons over ZSM-5 zeolite: An examination of the role of aromatic hydrocarbons using 13carbon-and deuterium-labeled feeds, Journal of Catalysis, 84 (1983) 435-445.

[89] T. Mole, J.A. Whiteside, D. Seddon, Aromatic co-catalysis of methanol conversion over zeolite catalysts, Journal of Catalysis, 82 (1983) 261-266.

[90] D. Lesthaeghe, A. Horré, M. Waroquier, G.B. Marin, V. Van Speybroeck, Theoretical Insights on Methylbenzene Side-Chain Growth in ZSM-5 Zeolites for Methanol-to-Olefin Conversion, Chemistry – A European Journal, 15 (2009) 10803-10808.

[91] J.F. Haw, W. Song, D.M. Marcus, J.B. Nicholas, The mechanism of methanol to hydrocarbon catalysis, Accounts of chemical research, 36 (2003) 317-326.

[92] P.W. Goguen, T. Xu, D.H. Barich, T.W. Skloss, W. Song, Z. Wang, J.B. Nicholas, J.F. Haw, Pulse-quench catalytic reactor studies reveal a carbon-pool mechanism in methanol-to-gasoline chemistry on zeolite HZSM-5, Journal of the American Chemical Society, 120 (1998) 2650-2651.

[93] J.F. Haw, P.W. Goguen, T. Xu, T.W. Skloss, W. Song, Z. Wang, In situ NMR investigations of heterogeneous catalysis with samples prepared under standard reaction conditions, Angewandte Chemie International Edition, 37 (1998) 948-949.

[94] J.F. Haw, J.B. Nicholas, W. Song, F. Deng, Z. Wang, T. Xu, C.S. Heneghan, Roles for cyclopentenyl cations in the synthesis of hydrocarbons from methanol on zeolite catalyst HZSM-5, Journal of the American Chemical Society, 122 (2000) 4763-4775.

[95] T. Xu, D.H. Barich, P.W. Goguen, W. Song, Z. Wang, J.B. Nicholas, J.F. Haw, Synthesis of a benzenium ion in a zeolite with use of a catalytic flow reactor, Journal of the American Chemical Society, 120 (1998) 4025-4026.

[96] J.F. Haw, Zeolite acid strength and reaction mechanisms in catalysis, Physical Chemistry Chemical Physics, 4 (2002) 5431-5441.

[97] B. Arstad, S. Kolboe, The Reactivity of Molecules Trapped within the SAPO-34 Cavities in the Methanol-to-Hydrocarbons Reaction, Journal of the American Chemical Society, 123 (2001) 8137-8138.

[98] W.G. Song, J.F. Haw, J.B. Nicholas, C.S. Heneghan, Methylbenzenes are the organic reaction centers for methanol-to-olefin catalysis on HSAPO-34, Journal of the American Chemical Society, 122 (2000) 10726-10727.

[99] M. Hunger, M. Seiler, A. Buchholz, In situ MAS NMR spectroscopic investigation of the conversion of methanol to olefins on silicoaluminophosphates SAPO-34 and SAPO-18 under continuous flow conditions, Catalysis Letters, 74 (2001) 61-68.

[100] M. Seiler, U. Schenk, M. Hunger, Conversion of methanol to hydrocarbons on zeolite HZSM‐5 investigated by in situ MAS NMR spectroscopy under flow conditions and on‐line gas chromatography, Catalysis Letters, 62 (1999) 139-145.

[101] M. Seiler, W. Wang, A. Buchholz, M. Hunger, Direct evidence for a catalytically active role of the hydrocarbon pool formed on zeolite H-ZSM-5 during the methanol-to-olefin conversion, Catalysis Letters, 88 (2003) 187-191.

[102] M. Bjørgen, U. Olsbye, D. Petersen, S. Kolboe, The methanol-to-hydrocarbons reaction: insight into the reaction mechanism from [12 C] benzene and [13 C] methanol coreactions over zeolite H-beta, Journal of Catalysis, 221 (2004) 1-10.

[103] A. Sassi, M.A. Wildman, H.J. Ahn, P. Prasad, J.B. Nicholas, J.F. Haw, Methylbenzene chemistry on zeolite HBeta: Multiple insights into methanol-to-olefin catalysis, The Journal of Physical Chemistry B, 106 (2002) 2294-2303.

[104] S. Ilias, R. Khare, A. Malek, A. Bhan, A descriptor for the relative propagation of the aromatic- and olefin-based cycles in methanol-to-hydrocarbons conversion on H-ZSM-5, Journal of catalysis, 303 (2013) 135-140.

[105] R. Khare, D. Millar, A. Bhan, A mechanistic basis for the effects of crystallite size on light olefin selectivity in methanol-to-hydrocarbons conversion on MFI, Journal of Catalysis, 321 (2015) 23-31.

[106] R. Khare, A. Bhan, Mechanistic studies of methanol-to-hydrocarbons conversion on diffusion-free MFI samples, Journal of Catalysis, 329 (2015) 218-228.

[107] M. Bjørgen, F. Joensen, K.-P. Lillerud, U. Olsbye, S. Svelle, The mechanisms of ethene and propene formation from methanol over high silica H-ZSM-5 and H-beta, Catalysis Today, 142 (2009) 90-97.

[108] W. Song, H. Fu, J.F. Haw, Supramolecular Origins of Product Selectivity for Methanol-to-Olefin Catalysis on HSAPO-34, Journal of the American Chemical Society, 123 (2001) 4749-4754.

[109] B.P. Hereijgers, F. Bleken, M.H. Nilsen, S. Svelle, K.-P. Lillerud, M. Bjørgen, B.M. Weckhuysen, U. Olsbye, Product shape selectivity dominates the Methanol-to-Olefins (MTO) reaction over H-SAPO-34 catalysts, Journal of catalysis, 264 (2009) 77-87.

[110] M. Bjørgen, S. Akyalcin, U. Olsbye, S. Benard, S. Kolboe, S. Svelle, Methanol to hydrocarbons over large cavity zeolites: Toward a unified description of catalyst deactivation and the reaction mechanism, Journal of Catalysis, 275 (2010) 170-180.

[111] S. Teketel, S. Svelle, K.-P. Lillerud, U. Olsbye, Shape-Selective Conversion of Methanol to Hydrocarbons Over 10-Ring Unidirectional-Channel Acidic H-ZSM-22, ChemCatChem, 1 (2009) 78-81.

[112] S. Teketel, U. Olsbye, K.-P. Lillerud, P. Beato, S. Svelle, Selectivity control through fundamental mechanistic insight in the conversion of methanol to hydrocarbons over zeolites, Microporous and Mesoporous Materials, 136 (2010) 33-41.

[113] S. Teketel, W. Skistad, S. Benard, U. Olsbye, K.P. Lillerud, P. Beato, S. Svelle, Shape Selectivity in the Conversion of Methanol to Hydrocarbons: The Catalytic Performance of One-Dimensional 10-Ring Zeolites: ZSM-22, ZSM-23, ZSM-48, and EU-1, ACS Catalysis, 2 (2012) 26-37.

[114] S. Teketel, U. Olsbye, K.P. Lillerud, P. Beato, S. Svelle, Co-conversion of methanol and light alkenes over acidic zeolite catalyst H-ZSM-22: Simulated recycle of non-gasoline range products, Applied Catalysis A: General, 494 (2015) 68-76.

[115] X. Sun, S. Müller, H. Shi, G.L. Haller, M. Sanchez-Sanchez, A.C. van Veen, J.A. Lercher, On the impact of co-feeding aromatics and olefins for the methanol-to-olefins reaction on HZSM-5, Journal of Catalysis, 314 (2014) 21-31.

[116] X. Sun, S. Müller, Y. Liu, H. Shi, G.L. Haller, M. Sanchez-Sanchez, A.C. van Veen, J.A. Lercher, On reaction pathways in the conversion of methanol to hydrocarbons on HZSM-5, Journal of Catalysis, 317 (2014) 185-197.

[117] I. Yarulina, S. Bailleul, A. Pustovarenko, J.R. Martinez, K.D. Wispelaere, J. Hajek, B.M. Weckhuysen, K. Houben, M. Baldus, V. Van Speybroeck, Suppression of the Aromatic Cycle in Methanol-to-Olefins Reaction over ZSM-5 by Post-Synthetic Modification Using Calcium, ChemCatChem, 8 (2016) 3057-3063.

[118] M. Westgård Erichsen, S. Svelle, U. Olsbye, The influence of catalyst acid strength on the methanol to hydrocarbons (MTH) reaction, Catalysis Today, 215 (2013) 216-223.

[119] M. Westgård Erichsen, S. Svelle, U. Olsbye, H-SAPO-5 as methanol-to-olefins (MTO) model catalyst: Towards elucidating the effects of acid strength, Journal of Catalysis, 298 (2013) 94-101.

[120] H. Schulz, “Coking” of zeolites during methanol conversion: Basic reactions of the MTO-, MTP- and MTG processes, Catalysis Today, 154 (2010) 183-194.

[121] M. Guisnet, L. Costa, F.R. Ribeiro, Prevention of zeolite deactivation by coking, Journal of Molecular Catalysis A: Chemical, 305 (2009) 69-83.

[122] S.M.T. Almutairi, B. Mezari, E.A. Pidko, P.C.M.M. Magusin, E.J.M. Hensen, Influence of steaming on the acidity and the methanol conversion reaction of HZSM-5 zeolite, Journal of Catalysis, 307 (2013) 194-203.

[123] M. Nielsen, R.Y. Brogaard, H. Falsig, P. Beato, O. Swang, S. Svelle, Kinetics of Zeolite Dealumination: Insights from H-SSZ-13, ACS Catalysis, (2015) 7131-7139.

[124] T.V.W. Janssens, A new approach to the modeling of deactivation in the conversion of methanol on zeolite catalysts, Journal of Catalysis, 264 (2009) 130-137.

[125] T.V.W. Janssens, S. Svelle, U. Olsbye, Kinetic modeling of deactivation profiles in the methanol-to-hydrocarbons (MTH) reaction: A combined autocatalytic–hydrocarbon pool approach, Journal of Catalysis, 308 (2013) 122-130.

[126] S. Müller, Y. Liu, M. Vishnuvarthan, X. Sun, A.C. van Veen, G.L. Haller, M. Sanchez-Sanchez, J.A. Lercher, Coke formation and deactivation pathways on H-ZSM-5 in the conversion of methanol to olefins, Journal of Catalysis, 325 (2015) 48-59.

[127] F.L. Bleken, K. Barbera, F. Bonino, U. Olsbye, K.P. Lillerud, S. Bordiga, P. Beato, T.V.W. Janssens, S. Svelle, Catalyst deactivation by coke formation in microporous and desilicated zeolite H-ZSM-5 during the conversion of methanol to hydrocarbons, Journal of Catalysis, 307 (2013) 62-73.

[128] F. Schmidt, C. Hoffmann, F. Giordanino, S. Bordiga, P. Simon, W. Carrillo-Cabrera, S. Kaskel, Coke location in microporous and hierarchical ZSM-5 and the impact on the MTH reaction, Journal of Catalysis, 307 (2013) 238-245.

[129] D.M. Bibby, N.B. Milestone, J.E. Patterson, L.P. Aldridge, Coke formation in zeolite ZSM-5, Journal of Catalysis, 97 (1986) 493-502.
[130] P.L. Benito, A.G. Gayubo, A.T. Aguayo, M. Olazar, J. Bilbao, Deposition and characteristics of coke over a H-ZSM5 zeolite-based catalyst in the MTG process, Industrial & Engineering Chemistry Research, 35 (1996) 3991-3998.
[131] M. Kaarsholm, F. Joensen, J. Nerlov, R. Cenni, J. Chaouki, G.S. Patience, Phosphorous modified ZSM-5: Deactivation and product distribution for MTO, Chemical Engineering Science, 62 (2007) 5527-5532.
[132] J.F. Haw, D.M. Marcus, Well-defined (supra)molecular structures in zeolite methanol-to-olefin catalysis, Topics in Catalysis, 34 (2005) 41-48.
[133] D.S. Wragg, M.G. O'Brien, F.L. Bleken, M. Di Michiel, U. Olsbye, H. Fjellvag, Watching the methanol-to-olefin process with time- and space-resolved high-energy operando X-ray diffraction, Angewandte Chemie International Edition, 51 (2012) 7956-7959.
[134] F. Bleken, W. Skistad, K. Barbera, M. Kustova, S. Bordiga, P. Beato, K.P. Lillerud, S. Svelle, U. Olsbye, Conversion of methanol over 10-ring zeolites with differing volumes at channel intersections: comparison of TNU-9, IM-5, ZSM-11 and ZSM-5, Physical Chemistry Chemical Physics, 13 (2011) 2539-2549.
[135] M. Guisnet, P. Magnoux, D. Martin, Roles of acidity and pore structure in the deactivation of zeolites by carbonaceous deposits, in: Studies in Surface Science and Catalysis, Elsevier, 1997, pp. 1-19.
[136] F. Bleken, M. Bjørgen, L. Palumbo, S. Bordiga, S. Svelle, K.-P. Lillerud, U. Olsbye, The effect of acid strength on the conversion of methanol to olefins over acidic microporous catalysts with the CHA topology, Topics in Catalysis, 52 (2009) 218-228.
[137] J.S. Martinez-Espin, M. Morten, T.V.W. Janssens, S. Svelle, P. Beato, U. Olsbye, New insights into catalyst deactivation and product distribution of zeolites in the methanol-to-hydrocarbons (MTH) reaction with methanol and dimethyl ether feeds, Catalysis Science & Technology, (2017 DOI: 10.1039/C7CY00129K).
[138] J. Kim, M. Choi, R. Ryoo, Effect of mesoporosity against the deactivation of MFI zeolite catalyst during the methanol-to-hydrocarbon conversion process, Journal of Catalysis, 269 (2010) 219-228.
[139] I. Yarulina, J. Goetze, C. Gucuyener, L. van Thiel, A. Dikhtiarenko, J. Ruiz-Martinez, B.M. Weckhuysen, J. Gascon, F. Kapteijn, Methanol-to-olefins process over zeolite catalysts with DDR topology: effect of composition and structural defects on catalytic performance, Catalysis Science & Technology, 6 (2016) 2663-2678.
[140] M. Bjørgen, U. Olsbye, S. Kolboe, Coke precursor formation and zeolite deactivation: mechanistic insights from hexamethylbenzene conversion, Journal of Catalysis, 215 (2003) 30-44.

[141] R. Khare, Z. Liu, Y. Han, A. Bhan, A mechanistic basis for the effect of aluminum content on ethene selectivity in methanol-to-hydrocarbons conversion on HZSM-5, Journal of Catalysis, 348 (2017) 300-305.
[142] R. Wei, C. Li, C. Yang, H. Shan, Effects of ammonium exchange and Si/Al ratio on the conversion of methanol to propylene over a novel and large partical size ZSM-5, Journal of Natural Gas Chemistry, 20 (2011) 261-265.
[143] Z. Wan, W. Wu, G.K. Li, C. Wang, H. Yang, D. Zhang, Effect of SiO 2/Al 2 O 3 ratio on the performance of nanocrystal ZSM-5 zeolite catalysts in methanol to gasoline conversion, Applied Catalysis A: General, 523 (2016) 312-320.
[144] S. Wilson, P. Barger, The characteristics of SAPO-34 which influence the conversion of methanol to light olefins, Microporous and Mesoporous Materials, 29 (1999) 117-126.
[145] I.M. Dahl, H. Mostad, D. Akporiaye, R. Wendelbo, Structural and chemical influences on the MTO reaction: a comparison of chabazite and SAPO-34 as MTO catalysts, Microporous and Mesoporous Materials, 29 (1999) 185-190.
[146] L.-T. Yuen, S.I. Zones, T.V. Harris, E.J. Gallegos, A. Auroux, Product selectivity in methanol to hydrocarbon conversion for isostructural compositions of AFI and CHA molecular sieves, Microporous Materials, 2 (1994) 105-117.
[147] G.J. Hutchings, F. Gottschalk, R. Hunter, Comments on" kinetic model for methanol conversion to olefins" with respect to methane formation at low conversion, Industrial & Engineering Chemistry Research, 26 (1987) 635-637.
[148] J. Perez-Ramirez, C.H. Christensen, K. Egeblad, C.H. Christensen, J.C. Groen, Hierarchical zeolites: enhanced utilisation of microporous crystals in catalysis by advances in materials design, Chemical Society Reviews, 37 (2008) 2530-2542.
[149] M. Bjørgen, F. Joensen, M. Spangsberg Holm, U. Olsbye, K.-P. Lillerud, S. Svelle, Methanol to gasoline over zeolite H-ZSM-5: Improved catalyst performance by treatment with NaOH, Applied Catalysis A: General, 345 (2008) 43-50.
[150] J.C. Groen, J.C. Jansen, J.A. Moulijn, J. Pérez-Ramírez, Optimal aluminum-assisted mesoporosity development in MFI zeolites by desilication, The Journal of Physical Chemistry B, 108 (2004) 13062-13065.
[151] J.C. Groen, W. Zhu, S. Brouwer, S.J. Huynink, F. Kapteijn, J.A. Moulijn, J. Pérez-Ramírez, Direct demonstration of enhanced diffusion in mesoporous ZSM-5 zeolite obtained via controlled desilication, Journal of the American Chemical Society, 129 (2007) 355-360.
[152] J.C. Groen, L.A. Peffer, J.A. Moulijn, J. Pérez-Ramírez, Mechanism of Hierarchical Porosity Development in MFI Zeolites by Desilication: The Role of Aluminium as a Pore-Directing Agent, Chemistry-A European Journal, 11 (2005) 4983-4994.

[153] J.C. Groen, J.A. Moulijn, J. Pérez-Ramírez, Desilication: on the controlled generation of mesoporosity in MFI zeolites, Journal of Materials Chemistry, 16 (2006) 2121-2131.
[154] K. Barbera, F. Bonino, S. Bordiga, T.V.W. Janssens, P. Beato, Structure-deactivation relationship for ZSM-5 catalysts governed by framework defects, Journal of Catalysis, 280 (2011) 196-205.
[155] P. Magnoux, P. Roger, C. Canaff, V. Fouche, N.S. Gnep, M. Guisnet, New technique for the characterization of carbonaceous compounds responsible for zeolite deactivation, Studies in Surface Science and Catalysis, 34 (1987) 317-330.
[156] L. Palumbo, F. Bonino, P. Beato, M. Bjørgen, A. Zecchina, S. Bordiga, Conversion of methanol to hydrocarbons: spectroscopic characterization of carbonaceous species formed over H-ZSM-5, The Journal of Physical Chemistry C, 112 (2008) 9710-9716.
[157] J.W. Park, G. Seo, IR study on methanol-to-olefin reaction over zeolites with different pore structures and acidities, Applied Catalysis A: General, 356 (2009) 180-188.
[158] D. Mores, E. Stavitski, M.H. Kox, J. Kornatowski, U. Olsbye, B.M. Weckhuysen, Space-and Time-Resolved In-situ Spectroscopy on the Coke Formation in Molecular Sieves: Methanol-to-Olefin Conversion over H-ZSM‐5 and H-SAPO‐34, Chemistry‐A European Journal, 14 (2008) 11320-11327.
[159] C. Vogt, B.M. Weckhuysen, J. Ruiz-Martinez, Effect of Feedstock and Catalyst Impurities on the Methanol-to-Olefin Reaction over H-SAPO-34, ChemCatChem, 9 (2017) 183-194.
[160] E. Borodina, F. Meirer, I. Lezcano-González, M. Mokhtar, A. Asiri, S. Al-Thabaiti, S. Basahel, J. Ruiz-Martinez, B. Weckhuysen, Influence of the Reaction Temperature on the Nature of the Active and Deactivating Species during Methanol to Olefins Conversion over H-SSZ-13, ACS catalysis, 5 (2015) 992-1003.
[161] T. Liang, J. Chen, Z. Qin, J. Li, P. Wang, S. Wang, G. Wang, M. Dong, W. Fan, J. Wang, Conversion of methanol to olefins over H-ZSM-5 zeolite: reaction pathway is related to the framework aluminum siting, ACS Catalysis, 6 (2016) 7311-7325.
[162] P. Beato, E. Schachtl, K. Barbera, F. Bonino, S. Bordiga, Operando Raman spectroscopy applying novel fluidized bed micro-reactor technology, Catalysis Today, 205 (2013) 128-133.
[163] R.F. Howe, E.K. Gibson, C.R.A. Catlow, A. Hameed, J. McGregor, P. Collier, S.F. Parker, D. Lennon, An assessment of hydrocarbon species in the methanol-to-hydrocarbon reaction over a ZSM-5 catalyst, Faraday Discussions, 197 (2017) 447-471.
[164] J.P. Hofmann, D. Mores, L.R. Aramburo, S. Teketel, M. Rohnke, J. Janek, U. Olsbye, B.M. Weckhuysen, Large Zeolite H-ZSM-5 Crystals as Models for the Methanol-to-Hydrocarbons Process: Bridging the Gap between Single-Particle Examination and Bulk Catalyst Analysis, Chemistry-A European Journal, 19 (2013) 8533-8542.

[165] D. Chen, K. Moljord, T. Fuglerud, A. Holmen, The effect of crystal size of SAPO-34 on the selectivity and deactivation of the MTO reaction, Microporous and Mesoporous Materials, 29 (1999) 191-203.

[166] M. Castilla, A.G. Gayubo, A.T. Aguayo, J.M. Arandes, J. Bilbao, Simulation and optimization of methanol transformation into hydrocarbons in an isothermal fixed-bed reactor under reaction-regeneration cycles, Industrial & Engineering Chemistry Research, 37 (1998) 2383-2390.

[167] D. Chen, A. Grønvold, K. Moljord, A. Holmen, Methanol Conversion to Light Olefins over SAPO-34: Reaction Network and Deactivation Kinetics, Industrial & Engineering Chemistry Research, 46 (2007) 4116-4123.

[168] F.L. Bleken, T.V.W. Janssens, S. Svelle, U. Olsbye, Product yield in methanol conversion over ZSM-5 is predominantly independent of coke content, Microporous and Mesoporous Materials, 164 (2012) 190-198.

[169] S. Teketel, M. Westgard Erichsen, F. Lonstad Bleken, S. Svelle, K. Petter Lillerud, U. Olsbye, Chapter 6 Shape selectivity in zeolite catalysis. The Methanol to Hydrocarbons (MTH) reaction, in: Catalysis: Volume 26, The Royal Society of Chemistry, 2014, pp. 179-217.

[170] N.V. Scarlett, I.C. Madsen, Quantification of phases with partial or no known crystal structures, Powder Diffraction, 21 (2006) 278-284.

[171] S. Brunauer, P.H. Emmett, E. Teller, Adsorption of Gases in Multimolecular Layers, Journal of the American Chemical Society, 60 (1938) 309-319.

[172] S. Brunauer, Adsorption of gases and vapors, (1943).

[173] J. Rouquerol, P. Llewellyn, F. Rouquerol, Is the BET equation applicable to microporous adsorbents?, Studies in Surface Science and Catalysis, 160 (2007) 49-56.

[174] B.C. Lippens, J. De Boer, Studies on pore systems in catalysts: V. The t method, Journal of Catalysis, 4 (1965) 319-323.

[175] B. Lippens, B. Linsen, J. De Boer, Studies on pore systems in catalysts I. The adsorption of nitrogen; apparatus and calculation, Journal of Catalysis, 3 (1964) 32-37.

[176] S. Lowell, J.E. Shields, M.A. Thomas, M. Thommes, Surface Area Analysis from the Langmuir and BET Theories, in: Characterization of Porous Solids and Powders: Surface Area, Pore Size and Density, Springer Netherlands, Dordrecht, 2004, pp. 58-81.

[177] E. Selli, L. Forni, Comparison between the surface acidity of solid catalysts determined by TPD and FTIR analysis of pre-adsorbed pyridine, Microporous and Mesoporous Materials, 31 (1999) 129-140.

[178] A. Damin, M. Signorile, F. Bonino, S. Bordiga, R. Disa, submitted, n. 102015000069819, in, Italy, 2015.

[179] M. Signorile, In situ and operando characterization of zeolite-based catalysts by means of Raman spectroscopy, in, University of Turin, 2017.
[180] M.M. Mertens, in: 2009/117186 (Ed.), World Patent Office 2009.
[181] Y.T. Chua, P.C. Stair, An ultraviolet Raman spectroscopic study of coke formation in methanol to hydrocarbons conversion over zeolite H-MFI, Journal of Catalysis, 213 (2003) 39-46.
[182] C. Li, P.C. Stair, Ultraviolet Raman spectroscopy characterization of coke formation in zeolites, Catalysis Today, 33 (1997) 353-360.
[183] A.C. Ferrari, J. Robertson, Interpretation of Raman spectra of disordered and amorphous carbon, Physical Review B, 61 (2000) 14095.
[184] M.S. Dresselhaus, G. Dresselhaus, R. Saito, A. Jorio, Raman spectroscopy of carbon nanotubes, Physics Reports, 409 (2005) 47-99.
[185] A.C. Ferrari, J. Meyer, V. Scardaci, C. Casiraghi, M. Lazzeri, F. Mauri, S. Piscanec, D. Jiang, K. Novoselov, S. Roth, Raman spectrum of graphene and graphene layers, Physical Review Letters, 97 (2006) 187401.
[186] A. Ferrari, J. Robertson, Resonant Raman spectroscopy of disordered, amorphous, and diamondlike carbon, Physical Review B, 64 (2001) 075414.
[187] M. Zokaie, D.S. Wragg, A. Grønvold, T. Fuglerud, J.H. Cavka, K.P. Lillerud, O. Swang, Unit cell expansion upon coke formation in a SAPO-34 catalyst: A combined experimental and computational study, Microporous and Mesoporous Materials, 165 (2013) 1-5.
[188] J. Li, G. Xiong, Z. Feng, Z. Liu, Q. Xin, C. Li, Coke formation during the methanol conversion to olefins in zeolites studied by UV Raman spectroscopy, Microporous and Mesoporous Materials, 39 (2000) 275-280.
[189] M.A. Bañares, Operando methodology: combination of in situ spectroscopy and simultaneous activity measurements under catalytic reaction conditions, Catalysis Today, 100 (2005) 71-77.
[190] M. Signorile, F. Bonino, A. Damin, S. Bordiga, UV-Raman Fingerprint of Brønsted Sites in MFI Zeolites: A Useful Marker in Dealumination Detection, The Journal of Physical Chemistry C, 120 (2016) 18088-18092.
[191] S. Asher, C. Johnson, Raman spectroscopy of a coal liquid shows that fluorescence interference is minimized with ultraviolet excitation, Science, 225 (1984) 311-313.
[192] J. Peng, D.L. Cedeño, C. Manzanares, Cis-and trans-3-hexene: infrared spectrum in liquid argon solution, ab initio calculations of equilibrium geometry, normal coordinate analysis, and vibrational assignments, Journal of Molecular Structure, 440 (1998) 265-288.
[193] M. Signorile, F. Bonino, A. Damin, S. Bordiga, In Situ Resonant UV-Raman Spectroscopy of Polycyclic Aromatic Hydrocarbons, The Journal of Physical Chemistry C, 119 (2015) 11694-11698.

[194] P. del Campo, W.A. Slawinski, R. Henry, M.W. Erichsen, S. Svelle, P. Beato, D. Wragg, U. Olsbye, Time- and space-resolved high energy operando X-ray diffraction for monitoring the methanol to hydrocarbons reaction over H-ZSM-22 zeolite catalyst in different conditions, Surface Science, 648 (2016) 141-149.
[195] E.W. Thiele, Relation between catalytic activity and size of particle, Industrial & Engineering Chemistry, 31 (1939) 916-920.
[196] B.-T. Bleken, D. Wragg, B. Arstad, A. Gunnæs, J. Mouzon, S. Helveg, L. Lundegaard, P. Beato, S. Bordiga, U. Olsbye, S. Svelle, K. Lillerud, Unit cell thick nanosheets of zeolite H-ZSM-5: Structure and activity, Topics in Catalysis, 56 (2013) 558-566.
[197] W. Haag, Catalysis by zeolites–science and technology, Studies in Surface Science and Catalysis, 84 (1994) 1375-1394.

Appendices

A.1. Additional results

Table A-1. Summary of the zeolite catalysts used throughout the thesis

Topology	Channel Dimensionality	Sample	Commercial (C) Home made (hm)	Si/Al
MFI	3D -10MR 5.1 x 5.6Å 5.3 x 5.6 Å	MFI-27	C	14
		Pentasil	C	46
		PZ-2-100H	C	59
		PZ-2-25H	C	13
		CBV-8014	C	42
		CBV-8014-S	C	45
		ZSM-5-hm	hm	52
MOR	1D - 12MR 6.5 x 7.0 Å	Mordenite 14-386	C	11
		CBV-21A	C	11
TON	1D -10 MR 5.7 x 4.6 Å	ZSM-22	C	45
		ZSM-22-hm	hm	41
BEA	3D-12MR 6.6 x 7.7 Å 5.6 x 5.6 Å	Beta-CP806	C	17
		Beta-CP7119	C	13
		Beta-CP814E	C	14
CHA	3D -12 MR cages & 8 MR channels	SAPO-34	hm	11*
MTT	1D 10MR 4.5 x 5.2 Å	ZSM-23-hm	hm	28
IMF	3D - 10MR 5.5 x 5.6 Å / 5.3 x 5.4 Å 5.3 x 5.9 / 4.8 x 5.4 Å 5.1 x 5.3 Å	IM-5-hm	hm	15
ITH	3D- 9 & 10 MR 4.0 x 4.8 Å 4.8 x 5.3 Å / 4.8 x 5.1	ITQ-13	hm	50

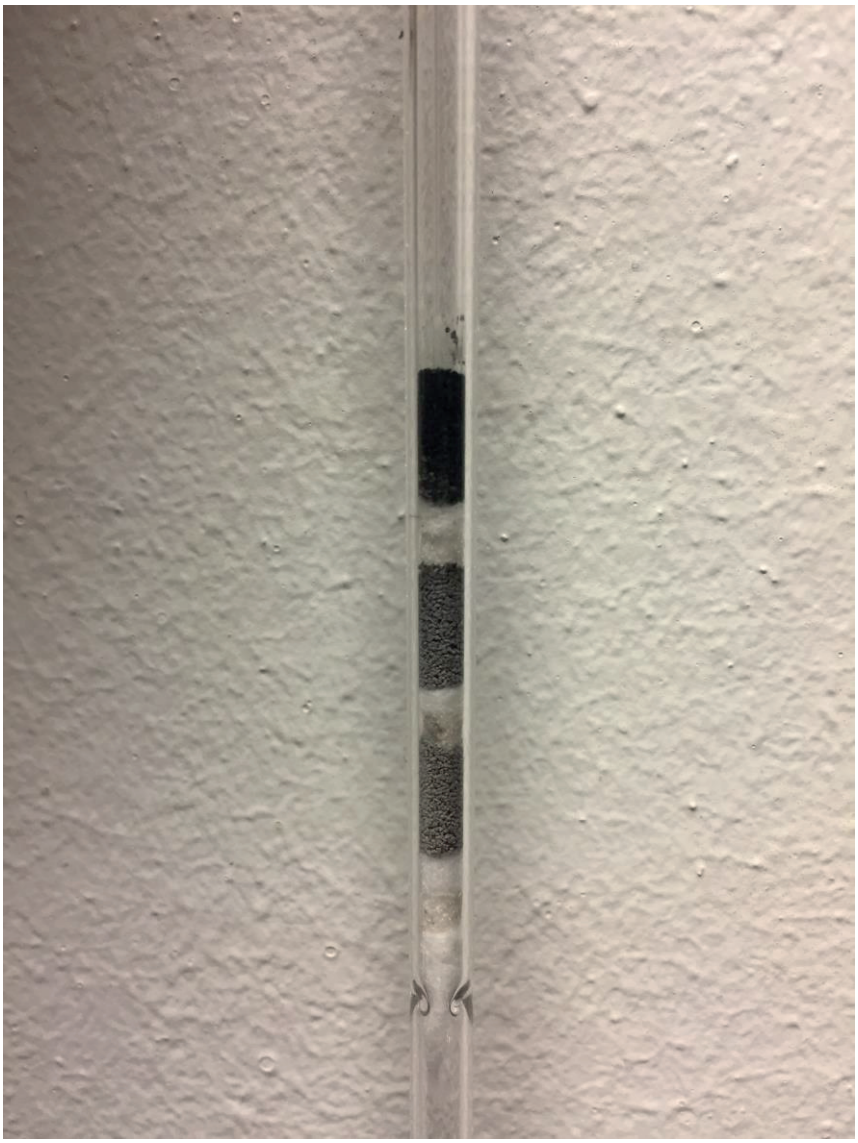

Figure A-1. Photograph of the ZSM-5-MFI-27 bed after running the MTH reaction at 400 °C, WHSV = 2 g_{MeOH} g_{cat}^{-1} h^{-1} and P_{atm} for 7 hours. The black area corresponds to the top layer, the dark grey zone is the middle layer, and the light grey area corresponds to the bottom layer.

A.2 Paper I

I

A.3 Paper II

II

A.4 Paper III

III

A.5 Paper IV

IV